

This figure "fig11_1.jpg" is available in "jpg" format from:

<http://arxiv.org/ps/astro-ph/0207401v4>

This figure "fig20_1.jpg" is available in "jpg" format from:

<http://arxiv.org/ps/astro-ph/0207401v4>

This figure "fig22_1.jpg" is available in "jpg" format from:

<http://arxiv.org/ps/astro-ph/0207401v4>

TABLE 1
MORPHOLOGICAL PARAMETERS

IRAS FSC (1)	NS kpc (2)	TL kpc (3)	IC (4)	ST (5)	IRAS FSC (1)	NS kpc (2)	TL kpc (3)	IC (4)	ST (5)
00091-0738	2.1	12	IIIb	HII	12359-0725	22.9	16	IIIa	L
00188-0856			V	L	12447+3721			IVa	HII
00397-1312			V	HII	12540+5708		14	IVb	S1
00456-2904	20.7	9	IIIa	HII	13106-0922		82	IVa	L
00482-2721	6.7	15	IIIb	L	13218+0552			V	S1
01004-2237			V	HII	13305-1739			V	S2
01166-0844	9.8	7	IIIb	HII	13335-2612	3.2	14	IIIb	L
01199-2307	20.3		IIIa	HII	13342+3932		8	IVb	S1
01298-0744		9	IVb	HII	13428+5608		31	IVb	S2
01355-1814	5.8		IIIb	HII	13443+0802			Tpl	S2
01494-1845			IVa		13451+1232	4.0	35	IIIb	S2
01569-2939		55	IVa	HII	13454-2956	15.8	10	IIIa	S2
01572+0009		46	IVb	S1	13469+5833	4.3	56	IIIb	HII
02021-2103			IVa		13509+0442		15	IVb	HII
02411+0353	7.1		IIIb	HII	13539+2920	7.0		IIIb	HII
02480-3745		27	IVa		14053-1958	1.5	11	IIIb	S2
03209-0806		61	IVb	HII	14060+2919		9	IVa	HII
03250+1606			IVb	L	14070+0525			V	S2
03521+0028	3.5		IIIb	L	14121-0126	9.1	22	IIIb	L
04074-2801		28	IVa	L	14197+0813			V	
04103-2838		8	IVb	L	14202+2615	14.8	19	IIIa	HII
04313-1649		59	IVa		14252-1550	8.3		IIIb	L
05020-2941		8	IVa	L	14348-1447	4.8	12	IIIb	L
05024-1941		12	IVa	S2	14394+5332		35	Tpl	S2
05156-3024		10	IVb	S2	14485-2434			IVb	
05189-2524		20	IVb	S2	15001+1433			Tpl	S2
07599+6508			IVb	S1	15043+5754	5.1		IIIb	HII
08201+2801		25	IVa	HII	15130-1958		14	IVb	S2
08474+1813			V		15206+3342			IVb	HII
08559+1053		18	IVb	S2	15225+2350		31	IVa	HII
08572+3915	5.7	5	IIIb	L	15327+2340	0.4	11	IIIb	L
08591+5248			V		15462-0450		8	IVb	S1
09039+0503		24	IVa	L	16090-0139			IVa	L
09116+0334	15.8	12	IIIa	L	16156+0146	7.5		IIIb	S2
09463+8141		76	IVa	L	16300+1558			V	L
09539+0857			V	L	16333+4630	13.1		IIIa	L
10035+2740		54	IVa		16468+5200	7.8	14	IIIb	L
10091+4704		29	IVa	L	16474+3430	6.5	11	IIIb	HII
10190+1322	5.5		IIIb	HII	16487+5447	5.4		IIIb	L
10378+1108			IVb	L	17028+5817	23.3		IIIa	L
10485-1447	20.0	56	IIIa	L	17044+6720		8	IVb	L
10494+4424		12	IVb	L	17068+4027			Tpl	HII
10594+3818	4.4	90	IIIb	HII	17179+5444		7	IVb	S2
11028+3130		5	IVa	L	20414-1651			IVb	HII
11095-0238		14	IVb	L	21208-0519	14.1	14	IIIa	HII
11119+3257		25	IVb	S1	21219-1757			V	S1
11130-2659		21	IVa	L	21329-2346		49	IVa	L
11180+1623	21.8	22	IIIa	L	21477+0502			Tpl	L
11223-1244	87.9	35	IIIa	S2	22088-1831	4.3		IIIb	HII
11387+4116			V	HII	22206-2715	7.7		IIIb	HII
11506+1331			IVb	HII	22491-1808	2.2		IIIb	HII
11582+3020			V	L	22541+0833	18.5		IIIa	S2
11598-0112		12	IVb	S1	23060+0505		22	IVb	S2
12018+1941			IVb		23129+2548		11	IVa	L
12032+1707	12.0		IIIa	L	23233+2817			Iso.	S2
12072-0444		28	IVb	S2	23234+0946	7.4	18	IIIb	L
12112+0305	3.8	8	IIIb	L	23327+2913	22.7	7	IIIa	L
12127-1412	21.9		IIIa	L	23389+0300	4.9		IIIb	S2
12265+0219			IVb	S1	23498+2423	12.7	17	IIIa	S2

Col 1: IRAS name

Col 2: Nuclear Separation in kpc unit

Col 3: Tail length in kpc unit

Col 4: Morphological class

Col 5: Spectral type: HII = H II region galaxy, L = LINER, S2 = Seyfert 2, S1 = Seyfert 1

This figure "fig11_2.jpg" is available in "jpg" format from:

<http://arxiv.org/ps/astro-ph/0207401v4>

This figure "fig20_2.jpg" is available in "jpg" format from:

<http://arxiv.org/ps/astro-ph/0207401v4>

This figure "fig22_2.jpg" is available in "jpg" format from:

<http://arxiv.org/ps/astro-ph/0207401v4>

TABLE 2
PARAMETERS OF SURFACE BRIGHTNESS PROFILES

IRAS FSC	PSF (%)		χ_r^2 value				Best Fit	r_e (kpc)		μ_e (mag/as ²)		Host Galaxy(mag)	
	R	K'	R(DP)	R(EP)	K'(DP)	K'(EP)		R	K'	R	K'	M _R	M _{K'}
(1)	(2)	(3)	(4)	(5)	(6)	(7)	(8)	(9)	(10)	(11)	(12)	(13)	(14)
00091-0738	5.2	2.2	27.2	11.0	E	3.2	...	21.0	...	-21.37	-24.37
00188-0856	...	53	0.8	0.4	8.3	0.7	E	3.2	1.8	20.4	16.2	-21.81	-24.90
00397-1312	0.3	1.6	0.5	1.0	E/D	4.2	...	21.0	...	-21.94	-25.53
00456-2904	1.2	1.5	4.2	0.5	E	3.5	...	20.5	...	-22.08	-25.17
00482-2721	22.9	16.2	7.1	7.8	A	-21.17	-24.08
01004-2237	71	50	0.8	0.2	0.4	1.0	E/D	2.8	...	21.7	...	-19.52	-24.05
01166-0844	21.7	63.3	37.3	52.5	A	-21.60	-24.49
01199-2307	0.4	1.8	0.4	0.4	E/D	4.3	...	21.5	...	-21.99	-24.14
01298-0744	...	76	23.1	52.1	1.5	1.9	A	-21.18	-23.70
01355-1814	51.2	58.2	36.0	24.9	A	-21.43	-24.21
01494-1845	5.6	1.9	9.2	6.7	E	6.2	...	22.2	...	-21.54	-25.23
01569-2939	5.5	30.1	5.9	2.7	A	-21.46	-24.48
01572+0009	...	66	8.7	1.0	17.6	3.1	E	4.5	...	20.0	...	-23.85	-26.27
02021-2103	7.1	1.9	13.5	1.4	E	7.0	...	19.5	-25.67
02411+0353	18.7	61.1	18.4	28.6	A	-22.62	-25.35
02480-3745	16.7	8.6	10.6	11.6	A	-21.15	-24.51
03209-0806	...	62	29.7	15.9	0.7	1.1	A	-22.22	-24.41
03250+1606	...	64	2.3	0.1	7.8	2.9	E	5.1	...	21.2	...	-21.98	-24.91
03521+0028	11.5	15.1	5.9	12.6	A	-20.62	-25.02
04074-2801	45.0	23.9	0.9	3.4	A	-21.94	-24.69
04103-2838	...	64	9.3	19.8	25.7	10.3	A	-22.05	-24.71
04313-1649	8.6	6.9	4.2	3.9	E/D	6.2	5.3	21.8	19.0	-22.01	-24.54
05020-2941	2.7	1.7	0.0	0.0	E/D	5.8	...	22.0	...	-21.35	-24.14
05024-1941	2.3	0.8	8.8	3.5	E/D	4.7	4.2	20.8	17.2	-22.42	-25.68
05156-3024	...	61	2.4	6.5	7.8	3.2	E/D	5.2	...	21.1	...	-22.04	-24.75
05189-2524	47	74	25.9	5.9	51.0	13.6	E	4.3	...	21.3	...	-21.48	-24.72
07599+6508	...	46	28.2	4.2	142.1	18.4	E	3.5	2.2	17.8	13.5	-24.76	-27.85
08201+2801	9.3	9.3	1.4	0.3	A	-21.49	-24.80
08474+1813	...	54	14.6	28.8	0.7	1.6	E/D	4.1	...	21.7	...	-20.44	-23.30
08559+1053	...	55	10.3	2.8	20.3	2.7	E	6.2	3.1	21.5	16.4	-22.51	-25.87
08572+3915	4.6	20.0	33.7	38.2	A	-21.68	-23.93
08591+5248	...	70	3.1	5.4	4.5	1.9	E/D	4.1	4.1	20.6	17.7	-21.83	-25.05
09039+0503	16.7	14.7	13.8	9.9	A	-21.35	-24.75
09116+0334	64	64	4.5	2.3	13.9	2.9	E	4.1	...	20.7	...	-22.11	-26.16
09463+8141	9.2	11.2	3.8	6.9	A	-21.83	-25.08
09539+0857	26	61	1.1	3.1	0.7	1.3	E/D	3.1	...	20.9	...	-20.54	-23.56
10035+2740	12.4	12.1	5.4	17.2	A	-22.15	-25.43
10091+4704	19.6	6.7	3.6	0.6	E	9.8	...	22.2	...	-22.31	-25.38
10190+1322	11.2	21.1	13.0	45.7	A	-21.79	-25.45
10378+1108	...	76	2.8	5.5	21.9	7.9	E/D	6.1	...	21.8	...	-22.15	-24.66
10485-1447 E	3.9	11.2	2.0	1.4	A	-20.53	-22.72
10485-1447 W	2.7	2.8	1.9	1.1	E/D	5.4	...	22.0	...	-20.91	-23.90
10494+4424	...	33	11.3	1.6	11.3	7.6	E	4.2	...	21.2	...	-21.23	-24.38
10594+3818	21.3	2.9	4.9	8.9	E	4.6	...	20.5	...	-22.27	-25.17
11028+3130	0.8	2.1	3.0	2.7	E/D	4.7	4.2	21.7	19.1	-21.03	-24.13
11095-0238	32.7	11.3	2.2	6.3	A	-21.03	-24.19
11119+3257	...	37	2.9	0.6	5.5	1.1	E	2.6	1.7	19.2	14.0	-22.71	-27.14
11130-2659	14.5	6.7	1.9	0.8	A	-21.74	-24.41
11180+1623 E	5.9	0.6	3.5	4.4	E	4.6	...	21.4	...	-21.45	-24.65
11223-1244	29.1	14.3	13.9	16.1	A	-22.93	-26.01
11387+4116	...	68	4.6	18.8	1.9	1.3	E/D	3.5	3.0	20.5	17.4	-21.52	-24.66
11506+1331	...	59	11.3	16.4	11.4	17.4	A	-21.41	-24.37
11582+3020	0.9	0.8	0.3	0.7	E/D	7.1	...	22.5	...	-21.53	-24.88
11598-0112	...	69	2.8	8.2	15.6	8.4	E/D	4.2	3.0	20.3	16.8	-22.69	-25.41
12018+1941	3.1	0.9	1.0	0.7	E/D	4.6	...	21.1	...	-21.80	-24.86
12032+1707	11.2	24.9	15.0	13.1	A	-22.22	-25.79
12072-0444	...	55	23.7	7.2	19.8	3.4	E	6.3	...	21.4	...	-22.30	-24.92
12112+0305	6.2	3.8	17.7	11.5	A	-21.51	-24.71
12127-1412	4.1	2.2	3.0	0.5	E/D	4.9	...	21.5	...	-21.08	-25.63
12265+0219	68	53	7.9	3.2	28.8	2.6	E	2.5	2.0	16.1	12.9	-25.22	-28.41
12359-0725 N	2.2	0.5	3.7	2.8	E/D	3.4	...	21.5	...	-20.56	-23.87
12359-0725 S	10.9	3.2	0.0	0.0	E	4.6	...	22.3	...	-20.54	-22.86
12447+3721	5.2	12.5	0.7	0.5	A	-21.00	-23.90
12540+5708	61	58	55.6	7.9	29.9	3.5	E	3.3	...	19.8	...	-22.52	-25.85
13106-0922	0.8	5.3	2.0	2.5	E/D	6.4	...	21.4	...	-21.61	-24.39
13218+0552	5.3	0.7	12.6	0.7	E	5.4	4.0	21.3	15.5	-22.07	-27.35
13305-1739	44.3	8.7	0.8	1.8	E	3.9	...	19.4	...	-22.76	-25.82
13335-2612	0.5	0.1	5.9	7.8	A	-21.74	-24.80
13342+3932	...	44	7.8	1.5	4.3	3.6	E	6.0	5.2	21.1	17.9	-22.96	-26.43
13428+5608	28	38	76.7	14.8	4.8	0.6	E	4.3	...	20.4	...	-22.33	-24.67
13443+0802 NE	14.7	36.1	16.8	27.5	A	-22.51	-25.93
13443+0802 SW	0.9	0.1	1.1	2.6	E/D	4.3	...	21.7	...	-21.16	-23.64
13451+1232	36.3	15.7	6.0	15.0	A	-23.32	-25.87
13454-2956 N	1.2	0.6	1.0	0.1	E	6.9	...	22.2	...	-21.26	-25.18
13454-2956 S	2.2	1.0	0.4	0.4	E/D	6.8	...	22.2	...	-21.23	-25.26
13469+5833	65.0	14.5	7.5	14.3	A	-21.95	-25.14
13509+0442	...	57	16.8	17.6	2.0	1.0	A	-21.02	-24.70
13539+2920	7.4	18.8	11.1	8.0	A	-21.47	-25.02
14053-1958	15.1	7.1	1.3	1.7	E/D	6.3	...	22.0	...	-21.39	-24.64
14060+2919	9.8	16.5	7.2	1.5	E/D	5.7	...	21.0	...	-21.98	-25.21

TABLE 2—Continued

IRAS FSC (1)	PSF (%)		χ^2_r value				Best Fit (8)	r_e (kpc)		μ_e (mag/as ²)		Host Galaxy (mag)	
	R (2)	K' (3)	R(DP) (4)	R(EP) (5)	K'(DP) (6)	K'(EP) (7)		R (9)	K' (10)	R (11)	K' (12)	M _R (13)	M _{K'} (14)
14070+0525	0.8	2.3	0.7	1.3	E/D	6.1	...	21.5	...	-22.25	-25.78
14121-0126	31.8	47.8	24.2	24.8	A	-21.79	-25.51
14197+0813	...	71	9.2	25.7	0.2	0.2	A	-22.21	-24.60
14202+2615	9.7	5.1	5.2	2.4	A	-22.31	-25.80
14252-1550	9.6	19.9	15.3	22.3	A	-21.33	-24.98
14348-1447	5.7	14.5	10.7	12.9	A	-22.36	-25.34
14394+5332 E	23	23	23.4	6.5	8.3	2.8	E	3.2	...	20.1	...	-21.77	-25.23
14394+5332 W	3.4	6.4	1.8	3.1	D	-21.25	-23.91
14485-2434	...	73	9.7	2.1	2.9	1.1	E	5.0	...	21.1	...	-21.46	-24.45
15001+1433	14.1	26.4	23.1	7.2	A	-22.64	-25.68
15043+5754	17.1	60.0	10.5	23.4	A	-21.21	-25.67
15130-1958	18.1	3.8	5.2	2.1	E	2.9	...	20.6	...	-20.94	-25.23
15206+3342	48	53	4.6	1.1	6.5	14.9	E/D	2.9	...	19.9	...	-21.99	-24.82
15225+2350	...	62	25.3	4.0	1.3	0.7	A	-21.47	-24.35
15327+2340	10.8	23.6	11.3	3.1	E	4.9	2.1	20.8	17.1	-21.39	-24.41
15462-0450	74	43	2.4	2.9	2.5	4.7	E/D	4.7	1.5	21.6	15.8	-20.96	-25.04
16090-0139	2.4	4.6	6.4	1.1	E/D	5.2	...	21.3	...	-21.95	-25.25
16156+0146	23.3	51.8	21.0	21.8	A	-20.87	-23.91
16300+1558	5.2	1.0	1.9	8.5	E/D	7.2	5.8	21.5	18.0	-22.63	-25.82
16333+4630	16.2	22.1	40.2	38.9	A	-22.11	-25.42
16468+5200	37.5	90.6	4.2	7.2	A	-21.51	-24.32
16474+3430	68.8	114.6	10.2	19.2	A	-22.07	-25.34
16487+5447	13.8	27.6	20.6	45.0	A	-21.87	-24.69
17028+5817 W	3.2	2.1	7.9	1.5	E/D	5.3	...	22.0	...	-21.07	-24.63
17028+5817 E	31	31	4.3	1.5	2.3	8.2	E/D	3.1	...	21.1	...	-20.58	-23.82
17044+6720	...	70	0.8	4.2	5.5	2.1	E/D	5.2	...	21.8	...	-21.81	-24.23
17068+4027 E	15.7	9.5	2.9	7.7	A	-21.47	-24.80
17179+5444	...	65	12.4	5.4	4.0	0.7	E/D	5.4	...	21.2	...	-22.35	-25.05
20414-1651	13	64	11.4	3.7	0.1	1.8	E/D	3.6	...	21.0	...	-21.01	-23.91
21208-0519	34.9	78.7	79.2	130.0	A	-22.55	-25.65
21219-1757	91	63	18.0	2.8	14.9	0.5	E	4.1	...	20.4	...	-22.17	-26.06
21329-2346	4.6	1.8	3.6	1.6	E	6.7	...	22.5	...	-21.66	-24.52
21477+0502 E	15.7	15.6	5.3	14.6	A	-21.86	-24.94
21477+0502 W	2.6	1.2	3.6	5.3	E/D	4.6	...	23.1	...	-20.37	-23.42
22088-1831	16.1	1.9	2.2	3.8	A	-22.18	-25.21
22206-2715	32.9	77.9	25.7	33.1	A	-22.18	-25.21
22491-1808	21.6	26.4	5.3	1.1	A	-21.90	-24.56
22541+0833 NW	9.9	2.5	4.9	1.2	E	3.3	2.4	21.0	16.7	-21.44	-24.96
22541+0833 SE	60	60	6.1	2.3	2.2	3.2	E	3.3	...	21.5	...	-20.34	-23.56
23060+0505	...	81	1.8	2.1	9.8	0.1	E	6.2	4.6	21.0	16.8	-22.92	-25.29
23129+2548	2.8	9.6	0.9	1.0	E/D	4.3	...	21.5	...	-21.63	-24.68
23233+2817	...	76	4.1	12.1	2.7	8.1	D	-22.02	-24.89
23234+0946	31.4	96.0	16.9	14.2	A	-21.84	-25.25
23327+2913 S	4.4	3.4	2.5	3.4	E/D	4.9	...	21.5	...	-21.71	-24.60
23327+2913 N	12.5	3.7	3.9	8.3	E	5.9	...	22.5	...	-21.35	-24.08
23389+0300	15.7	37.9	8.7	21.4	A	-20.99	-24.50
23498+2423	13.7	9.2	36.4	21.2	A	-22.52	-26.65

Col 1: Object name. See text for details.

Col 2: R-band % of PSF relative to the galaxy.

Col 3: K'-band % of PSF relative to the galaxy.

Col 4: R-band reduced χ^2 value fitted to the exponential profile.

Col 5: R-band reduced χ^2 value fitted to the de Vaucouleurs's $r^{1/4}$ law profile.

Col 6: K'-band reduced χ^2 value fitted to the exponential profile.

Col 7: K'-band reduced χ^2 value fitted to the de Vaucouleurs's $r^{1/4}$ law profile.

Col 8: Best fitted profile (A: ambiguous, E: elliptical-like, D: disk-like, E/D: border-line object between E and D.)

Col 9: R-band seeing-deconvolved half-light (effective) radius r_e for E and E/D objects.

Col 10: K'-band seeing-deconvolved half-light (effective) radius r_e for E and E/D objects.

Col 11: R-band effective surface brightness μ_e , not corrected for cosmological dimming.

Col 12: K'-band effective surface brightness μ_e , not corrected for cosmological dimming.

Col 13: Absolute R magnitude for the host galaxy.

Col 14: Absolute K' magnitude for the host galaxy.

OPTICAL AND NEAR-INFRARED IMAGING OF THE IRAS 1-JY SAMPLE OF ULTRALUMINOUS INFRARED GALAXIES. II. THE ANALYSIS

S. VEILLEUX^{1,2}, D.-C. KIM^{3,4}, AND D. B. SANDERS^{2,5}

ABSTRACT

An R & K' atlas of the *IRAS* 1-Jy sample of 118 ultraluminous infrared galaxies (ULIGs) was presented in a companion paper (Kim, Veilleux, & Sanders 2002; Paper I). The present paper discusses the results from the analysis of these images supplemented with new spectroscopic data obtained at Keck. All but one object in the 1-Jy sample show signs of a strong tidal interaction/merger. Multiple mergers involving more than two galaxies are seen in no more than 5 of the 118 (< 5%) systems. None of the 1-Jy sources is in the first-approach stage of the interaction, and most (56%) of them harbor a single disturbed nucleus and are therefore in the later stages of a merger. Seyfert galaxies (especially those of type 1), warm ULIGs ($f_{25}/f_{60} > 0.2$) and the more luminous systems ($> 10^{12.5} L_{\odot}$) all show a strong tendency to be advanced mergers with a single nucleus.

The individual galaxies in the binary systems of the 1-Jy sample show a broad distribution in host magnitudes (luminosities) with a mean of -21.02 ± 0.76 mag. ($0.85 \pm_{0.43}^{0.86} L^*$) at R and -23.98 ± 1.25 mag. ($0.90 \pm_{0.61}^{1.94} L^*$) at K' , and a R - or K' -band luminosity ratio generally less than ~ 4 . Single-nucleus ULIGs also show a broad distribution in host magnitudes (luminosities) with an average of -21.77 ± 0.92 mag. ($1.69 \pm_{0.97}^{2.25} L^*$) at R and -25.03 ± 0.94 mag. ($2.36 \pm_{1.38}^{3.24} L^*$) at K' . These distributions overlap considerably with those of quasars. The same statement applies to $R-K'$ colors in ULIG and quasar hosts.

An analysis of the surface brightness profiles of the host galaxies in single-nucleus sources reveals that about 73% of the R and K' surface brightness profiles are fit adequately by an elliptical-like $R^{1/4}$ -law. These elliptical-like 1-Jy systems have luminosity and R -band axial ratio distributions that are similar to those of normal (inactive) intermediate-luminosity ellipticals and follow with some scatter the same $\mu_e - r_e$ relation, giving credence to the idea that some of these objects may eventually become intermediate-luminosity elliptical galaxies if they get rid of their excess gas or transform this gas into stars. These elliptical-like hosts are most common among merger remnants with Seyfert 1 nuclei (83%), Seyfert 2 optical characteristics (69%) or mid-infrared (*ISO*) AGN signatures (80%). The mean half-light radius of these ULIGs is 4.80 ± 1.37 kpc at R and 3.48 ± 1.39 kpc at K' , typical of intermediate-luminosity ellipticals. These values are in excellent agreement with recent quasar measurements obtained at H with *HST*, but are systematically lower than other *HST* measurements derived at R . The reason for this discrepancy between the two quasar datasets is not known.

In general, the results from the present study are consistent with the merger-driven evolutionary sequence “cool ULIGs \rightarrow warm ULIGs \rightarrow quasars.” However, many exceptions appear to exist to this simple picture (e.g., 46% of the 41 advanced mergers show no obvious signs of Seyfert activity). This underlines the importance of using a large homogeneous sample like the 1-Jy sample to draw statistically meaningful conclusions; the problems of small sample size and/or inhomogeneous selection criteria have plagued many studies of luminous infrared galaxies in the past.

Subject headings: galaxies: active – galaxies: interactions – galaxies: Seyfert – galaxies: starburst – infrared: galaxies

1. INTRODUCTION

Local ultraluminous infrared galaxies (ULIGs; $\log [L_{\text{IR}}/L_{\odot}] \geq 12$; $H_0 = 75 \text{ km s}^{-1} \text{ Mpc}^{-1}$ and $q_0 = 0$) represent some of the best laboratories to study in detail the violent aftermaths of galaxy collisions and their possible connection with quasars and normal (inactive) elliptical galaxies. Recent deep surveys with the Infrared Space Observatory (*ISO*) and sub-mm ground-based facilities have revealed several distant ($z \approx 0.5 - 4.0$) infrared-luminous galaxies which appear to share many of the properties of local ULIGs (*ISO*: Kawara et al. 1998; Puget et al. 1999; Matsuhara et al. 2000; Efstathiou et al. 2000; Serjeant et al. 2001; Sanders et al. 2002, in prep.; *SCUBA*: Smail, Ivi-

son, & Blain 1997; Hughes et al. 1998; Blain et al. 1999; Eales et al. 1999; Barger, Cowie, & Sanders 1999). This extragalactic population of high- z infrared bright galaxies appears to dominate the far-infrared extragalactic background and is probably a major contributor to the overall star formation and metal enrichment history of the universe (e.g., Smail et al. 1997; Hughes et al. 1998; Barger et al. 1998; Genzel & Cesarsky 2000; Rupke, Veilleux, & Sanders 2002; Blain et al. 2002).

Two crucial questions need to be answered to properly address the issue of the origin and evolution of ULIGs: (1) What is the dominant energy source in ULIGs: Starbursts or active galactic nuclei (AGNs)? (2) Is the dominant energy source a

¹ Department of Astronomy, University of Maryland, College Park, MD 20742; E-mail: veilleux@astro.umd.edu

² Visiting Astronomer, W. M. Keck Observatory, jointly operated by the California Institute of Technology and the University of California

³ Institute of Astronomy and Astrophysics, Academia Sinica, P.O. Box 1-87, Nankang, Taipei, 115 Taiwan

⁴ Current address: School of Earth and Environmental Sciences (BK21), Seoul National University, Seoul, Korea; E-mail: dckim@astro.snu.ac.kr

⁵ Institute for Astronomy, University of Hawaii, 2680 Woodlawn Drive, Honolulu, HI 96822, and Max-Planck Institut für Extraterrestrische Physik, D-85740, Garching, Germany; E-mail: sanders@ifa.hawaii.edu

function of the interaction/merger phase in these systems? Considerable progress has been made in recent years in answering the first of these questions. Ground-based optical and near-infrared spectroscopic survey of the 1-Jy sample has shown that at least 25 – 30% of ULIGs show genuine signs of AGN activity (Kim, Veilleux, & Sanders 1998; Veilleux, Kim, & Sanders 1999a; Veilleux, Sanders, & Kim 1997, 1999b; see also Goldader et al. 1995; Murphy et al. 2001b). This fraction increases to 35 – 50% among the objects with $\log [L_{\text{IR}}/L_{\odot}] \geq 12.3$. Comparisons of the dereddened emission-line luminosities of the BLRs detected at optical or near-infrared wavelengths in the ULIGs of the 1-Jy sample with those of optical quasars indicate that the AGN/quasar in ULIGs is the main source of energy in at least 15 – 25% of all ULIGs in the 1-Jy sample. This fraction is closer to 30 – 50% among ULIGs with $L_{\text{IR}} > 10^{12.3} L_{\odot}$. These results are compatible with those from recent mid-infrared spectroscopic surveys carried out with *ISO* (e.g., Genzel et al. 1998; Lutz et al. 1998; Rigopoulou et al. 1999; Tran et al. 2001). Indeed, a detailed object-by-object comparison of the optical and mid-infrared classifications shows an excellent agreement between the two classification schemes (Lutz, Veilleux, & Genzel 1999). These results suggest that strong nuclear activity, once triggered, quickly breaks the obscuring screen at least in certain directions, thus becoming detectable over a wide wavelength range.

Much of the research effort now focusses on answering the second, more difficult question of a possible dependence of the energy source on the interaction/merger phase. A large dataset already exists in the literature on the morphology of luminous and ultraluminous infrared galaxies. Optical studies have shown that the fraction of strongly interacting/merger systems increases with increasing infrared luminosities, reaching > 95% among the ultraluminous systems (e.g., Sanders et al. 1988a; Melnick & Mirabel 1990; Murphy et al. 1996; Clements et al. 1996; although see Lawrence et al. 1989; Zou et al. 1991; Leech et al. 1994). The improved angular resolution and lower optical depth in the near-infrared as compared to the optical provides a cleaner view of the nuclear stellar distribution of ULIGs. The infrared morphologies of ULIGs often look significantly different from the optical images (e.g., Carico et al. 1990; Graham et al. 1990; Eales et al. 1990; Majewski et al. 1993). Over the past few years, high-resolution imaging with *HST* has contributed significantly to our knowledge of ULIGs (e.g., Surace et al. 1998; Zheng et al. 1999; Scoville et al. 2000; Borne et al. 2000; Cui et al. 2001; Farrah et al. 2001; Colina et al. 2001; Bushouse et al. 2002). These studies have had great success characterizing the central cores and massive stellar clusters in these objects, but the images often do not reach faint enough flux limits to fully characterize the host galaxies and associated tidal features. Adaptive optics imaging with ground-based telescopes offers a promising new way to acquire deep high-resolution of ULIGs, but this technique has so far been used for only a limited number of objects (e.g., Surace & Sanders 1999, 2000; Surace, Sanders, & Evans 2000, 2001).

In Kim, Veilleux, & Sanders (2002; Paper I), we presented an R & K' atlas of the *IRAS* 1-Jy sample of 118 ULIGs. This large and homogeneous dataset on the nearest (median redshift = 0.145) and brightest such objects in the universe is particularly well suited to address the issue of the origin and evolution of ULIGs (see Kim 1995 and Kim & Sanders 1998 for a detailed description of the 1-Jy sample; note that Galactic ex-

inction is negligible for the 1-Jy sample since $|b| > 30^\circ$ for all these sources). Results derived from the 1-Jy sample should serve as a good local baseline for studies on distant luminous infrared galaxies planned in the years to come with *SIRTF*, *SOFIA*, and other ground-based infrared and submm facilities. In the present paper, we analyze these images and combine the results of this analysis with those derived from our optical and near-infrared spectroscopic data to look for possible trends with optical and near-infrared morphological and spectrophotometric parameters. When possible, the results from our analysis of the ground-based data on the 1-Jy sample are combined with published results obtained at other wavelengths and compared with the quickly growing set of high-quality data on optical and infrared-bright QSOs (e.g., McLure et al. 1999; Márquez et al. 2000; McLeod & McLeod 2001; Canalizo & Stockton 2000a, 2000b, 2001; Surace et al. 2001; Dunlop et al. 2002 and references therein; see Stockton 1999 for a review of the data before 1999). Given the high frequency of mergers among ULIGs, the data on the 1-Jy sample also allow us to examine the disk-disk merger scenario for elliptical galaxy formation (e.g., Toomre 1977; Schweizer 1982; Wright et al. 1990; Scoville et al. 1990; Stanford & Bushouse 1991; Kormendy & Sanders 1992; Doyon et al. 1994; Genzel et al. 2001). The results of our analysis are described in §§2 – 4. These results are then used in §5 to discuss the origin and evolution of ULIGs and their possible evolutionary link with quasars and elliptical galaxies. A summary is presented in §6. Each object in the 1-Jy sample is described in detail in an Appendix. Preliminary results of this study were presented in Veilleux (2001).

We adopt $H_0 = 75 \text{ km s}^{-1} \text{ Mpc}^{-1}$ and $q_0 = 0.0$ throughout this paper and have converted the results from published papers to this cosmology to facilitate comparisons. We also compare our absolute magnitudes with the magnitudes corresponding to a L^* galaxy in a Schechter function description of the local field galaxy luminosity function. The reader should be cautious when comparing luminosities from various papers as they may be based on different definitions of L^* . The values of the absolute magnitudes of a L^* galaxy in various bands, M^* , are now better constrained than in the past thanks to large-scale surveys such as the 2dF Galaxy Redshift Survey (2dFGRS). Here we adopt $M_R^* = -21.2 \text{ mag.}$ and $M_{K'}^* = -24.1 \text{ mag.}$ The value of M_R^* was derived using a L^* magnitude of $M_r = -20.9 \text{ mag.}$ based on the results from the Las Campanas Redshift Survey (Lin et al. 1996) and assuming a typical $r-R = 0.3 \text{ mag.}$ for a moderately old stellar population at $z \approx 0.1$ (Surace 2002, private communication). A similar value for M_R^* is derived using $M_B^* = -20.1 \text{ mag.}$ (e.g. Mobasher et al. 1993; Zucca et al. 1997; Ratcliffe et al. 1998; Folkes et al. 1999) and adopting $B-R \approx 1.0 \text{ mag.}$ for typical field galaxies at $z \approx 0.1$ (e.g. Fukugita et al. 1995), but keeping in mind that this color term is strongly dependent on morphological type and more specifically on the level of star formation activity in the galaxy. The K' magnitude is based directly on the results of Cole et al. (2001) from an infrared-selected subsample of the 2dFGRS. These results are also consistent to within $\pm \sim 0.2 \text{ mag.}$ with the numbers quoted from optically selected samples (e.g., Mobasher, Sharples, & Ellis 1993; Loveday 2000) and from the K-band surveys by Glazebrook et al. (1995) and Gardner et al. (1997), after taking into account the various k - and photometric corrections mentioned in Table 3 of Cole et al. (2001).

2.1. Absolute Magnitudes

The integrated (nucleus + host) R and K' absolute magnitudes and $R-K'$ colors of the 1-Jy ULIGs were discussed briefly in Paper I (§3.3). Figure 1 presents the global and nuclear (4-kpc diameter) color – magnitude diagrams of the 1-Jy sample. As mentioned in Paper I, the galaxies in our sample show a broad range of integrated R and K' luminosities $\sim 0.4 - 120 L^*$. There is no significant trend between global or nuclear R magnitudes and $R-K'$ colors, although there is a slight tendency for the redder objects to have brighter K' magnitudes especially when considering the nuclear quantities (Fig. 1). The more luminous 1-Jy objects at R and K' show a tendency to have warm $IRAS\ 25\ \mu\text{m}/60\ \mu\text{m}$ colors ($f_{25}/f_{60} \geq 0.2$) and to present Seyfert/AGN characteristics at optical and mid-infrared wavelengths (Fig. 2). There also appears to be a weak positive correlation between infrared luminosities and the global R or K' luminosities (see Figs. 2*g* and 2*h*). Note, however, that the 1-Jy sample is flux limited and is therefore subject to luminosity-dependent distance biases: systems with $L_{\text{IR}} > 10^{12.3} L_{\odot}$ are more distant on average ($\langle z \rangle = 0.183 \pm 0.053$) than ULIGs with $L_{\text{IR}} \leq 10^{12.3} L_{\odot}$ ($\langle z \rangle = 0.132 \pm 0.029$). Consequently one should not be surprised to find trends between global luminosities and infrared luminosities. No trends are seen between global R or K' luminosities and the $IRAS\ 60\ \mu\text{m}/100\ \mu\text{m}$ colors or the strengths (equivalent widths) of the stellar $H\beta$ and Mg Ib features.

The ULIGs in the 1-Jy sample are on average less luminous at R than the quasars in the sample of Dunlop et al. (2002; see also Taylor et al. 1996; McLure et al. 1999), although there is considerable overlap between the two samples. Adopting $H-K' \approx 0.8$ for typical low-redshift quasars (e.g., PG QSOs; Surace 2002, private communication), we find that 1-Jy ULIGs are a better match in terms of total K' luminosities to the set of “low-luminosity” quasars of McLeod & Rieke (1994a; $-23.2 \leq M_B \leq -22.1$ mag. for our adopted H_0) than the “high-luminosity quasars” of McLeod & Rieke (1994b) and McLeod & McLeod (2001) with $M_B \leq -23.2$ mag. However, we note in §4.2 that the situation is reversed when considering only the magnitudes of the host galaxies instead of the integrated magnitudes.

2.2. Colors

The (nuclei of the) 1-Jy ULIGs are (significantly) redder than normal galaxies [median $R-K'$ and $(R-K')_4 = 3.25$ and 4.27 mag., respectively, versus 2.62 ± 0.34 mag. for normal galaxies; see §3.3 in Paper I]. These colors are also redder than those of the PG QSOs ($R-K' = 2.7$ mag. on average if redshifted to $z \approx 0.1$ to match the average redshift of the 1-Jy ULIGs; Surace 2002, private communication). The red ULIGs with integrated $R-K' \gtrsim 4$ mag. or nuclear $(R-K')_4 \gtrsim 5$ mag. have a tendency to host Seyfert nuclei and have warm $IRAS\ 25\ \mu\text{m}/60\ \mu\text{m}$ colors (Fig. 3). There is no significant correlation between the integrated or nuclear $R-K'$ colors and the infrared luminosities, $IRAS\ 60\ \mu\text{m}/100\ \mu\text{m}$ colors, and strengths of the stellar absorption features. Ten single-nucleus objects in the sample have $(R-K')_4 > 5$ mag. and would therefore be considered extremely red objects (EROs; Elston, Rieke, & Rieke 1988) if it were not for the circumnuclear emission (which presumably would not be detected at slightly higher redshifts; neglecting k -corrections). Of these ten objects, only two (F11119+3257 and F13218+0552) have *integrated* colors which meet the ERO criterion; both of these objects are optically classified Seyfert 1

galaxies.

2.3. Compactness

The compactness is defined as the ratio of the luminosity from the inner 4 kpc to the total luminosity. This quantity is physically meaningful only for single-nucleus systems. In Paper I, we mentioned that the mean compactness of our galaxies at K' (0.36 ± 0.17) is significantly higher than at R (0.14 ± 0.09). We find no significant trend between K' compactness and the infrared luminosity or $IRAS\ f_{60}/f_{100}$ color within the 1-Jy sample. However, Figure 4*b* shows that compact objects with $(L_{K'})_4/L_{K'} \geq \frac{1}{3}$ host most of the optically identified Seyfert galaxies in our sample. Given the well-known correlations between warm $IRAS\ 25\ \mu\text{m}$ -to- $60\ \mu\text{m}$ color, the presence of an AGN, and small equivalent widths of Mg Ib (especially in Seyfert 1s; e.g., Veilleux et al. 1995, 1999a), it is not surprising to find a tendency for these compact objects to also have $f_{25}/f_{60} > 0.2$ and $\text{EW}(\text{Mg Ib}) \leq 1\ \text{\AA}$. The trends with f_{25}/f_{60} and $\text{EW}(\text{Mg Ib})$ are weaker than the trend with optical spectral type so it appears that the presence of a Seyfert nucleus is the key factor determining the value of the K' compactness. Similar trends are found when considering the R compactness. These results may reflect the fact that Seyfert nuclei contribute significantly to the emission at R and K' or that the host galaxies of Seyfert nuclei are more compact than those of other galaxies. Our data on host galaxy properties appear to rule out this last possibility (see §4.5).

3. MORPHOLOGICAL EVIDENCE FOR GALAXY INTERACTIONS

3.1. Frequency of Multiple Mergers

A careful inspection of the images in the 1-Jy atlas (Fig. 1 in Paper I) combined with Keck spectroscopy of field galaxies (described in detail in Appendix A) indicates that nearly 100% of the objects in 1-Jy sample show signs of a strong tidal interaction/merger in the form of distorted or double nuclei, tidal tails, bridges, and overlapping disks. The only possible exception is F23233+2817 (see Appendix A). Nearly all of these objects are involved in the interaction/merger of two, and no more than two, galaxies. At most five systems out of 118 ($\lesssim 5\%$) are comprised of more than two interacting systems: F13443+0802, F14394+5332, F15001+1433, F17068+4027, and F21477+0502. In all five cases, triplets appear to be involved although the physical connection between the various components of the triplets have not all been confirmed. The fraction (number) of multiple (> 2) nuclei, double/pair mergers, and single-nucleus merger remnants in the 1-Jy sample is 4% (5), 39% (46), and 56% (66, excluding F23233+2817), respectively.

The general lack of multiple (> 2) systems in the 1-Jy sample is not consistent with the relatively large fraction ($\sim 20\%$) of multiple systems claimed by Borne et al. (2000) and Cui et al. (2001) from an optical *HST* dataset. Part of the discrepancy may be in the sample selection. Very few objects in the *HST* sample are also part of the 1-Jy sample. It is possible, though probably not very likely, that the *HST* sample studied by both Borne et al. and Cui et al. just happens to include a larger fraction of multiple systems. Other sources of uncertainties will affect the measured fraction of multiple systems. The criteria for interaction differ slightly from one study to the next due to different observational parameters (e.g., high spatial

resolution will favor the detection of compact nuclei *and* stellar clusters; deep surface brightness limits will favor the detection of faint tidal features) and the subjective nature of deciding if an interaction is indeed taking place without accurate spectroscopy of all galaxies in the system. In our study, galaxies are said to be interacting only if they show convincing signs of large-scale tidal tails and/or present distorted outer isophotes. In many cases, Keck long-slit spectra of the galaxies in the systems were obtained to confirm the interaction and to reject a few stellar sources or foreground/background galaxies. Some of the systems are accompanied by one or two galaxies at the same redshift as the *IRAS* sources but with no convincing signs of interaction. These galaxies are labeled “G” in Figure 1 of Paper I; they may be part of the same group of galaxies as the *IRAS* source but they do not appear to be interacting with it (see Appendix A).

Another source of discrepancy is the definition of a galactic nucleus. Cui et al. define nuclei as having $M_I < -17$ mag. The *HST* study by Surace et al. (1998) of 12 warm ULIGs has found several genuine stellar superclusters with $M_I < -17$ mag. These would be misclassified as nuclei according to the criterion of Cui et al. For comparison, all of the galaxies in the present paper have global $M_R < -20.1$ mag. or $M_I \lesssim -20.7$ mag. if we assume a typical $R-I \approx 0.6$ mag. (e.g., Fukugita et al. 1995).

Finally, the waveband sampled by the observations is an important consideration when comparing the results from different studies. The *HST* data in Borne et al. and Cui et al. were obtained in the *I*-band while our observations are taken at *R* and *K'*. The near-infrared data are particularly useful to reduce the effects of obscuration and thus to reveal the true stellar morphology of these galaxies. This is made obvious when we compare our data with those of Cui et al. for the few objects that we have in common. Five of these objects (F13539+2920, F14060+2919, F14202+2615, F22206–2715, F22491–1808) are part of the group of 17 multiple systems of Cui et al. In all cases except F14202+2615, *K'* images reveal the presence of only one or two galactic nuclei (in F14202+2615, the third galaxy shows no signs of interaction with the northern pair; see Appendix A). In all four of these cases, bright star-forming knots which were apparent in the *R*-band images disappear when observed at *K'*, indicating the lack of an obvious old stellar population in these clusters.

A recent *HST H*-band imaging study by Bushouse et al. (2002; see also Colina et al. 2001) of a subset of objects from the sample of Borne et al. (2002) and Cui et al. (2001) confirm our conclusions on the frequency of multiple systems. Out of 27 ULIGs, Bushouse et al. find only one candidate for multiple merging (IRAS 18580+6527; see their Table 1), or $\sim 4\%$ of their sample. This fraction is virtually identical to that found from our sample. This excellent agreement emphasizes the importance of imaging galaxies at near-infrared wavelengths rather than in the optical when trying to determine the stellar distribution in these objects. We refer the reader to Appendix A for a discussion of the four 1-Jy ULIGs (F11095–0238, F13469+5833, F20414–1651, and F22206–2715) which were also observed by Bushouse et al. (2002).

In the rest of this section, we use the *R* and *K'* images of the 1-Jy sample to look for possible trends in the properties of ULIGs along the merger sequence. In the discussion below, three morphological parameters are used to trace the merger sequence: the observed (projected) nuclear separation, the length

of tidal tail(s), and the overall morphology of the system.

3.2. Apparent Nuclear Separations

Numerical simulations of merging disk systems indicate that the nuclear separation between the two galaxies in the system is not simply a monotonically decreasing function of time. The system often goes through a “pre-merger phase” (Mihos 1999 calls it the “hanging out” phase) characterized by two distinct galaxies with well-developed tidal tails and bridges as a result of the first close encounter (e.g., Barnes & Hernquist 1992; Mihos & Hernquist 1996; Gerritsen 1997; Bekki et al. 1999). This result complicates the interpretation of the measured (projected) nuclear separations (*NS*) in the 1-Jy sample of galaxies since, without kinematic information, we cannot tell if the two galaxies are pre- or post-apgalacticon (farthest approach). The measurements are listed in Table 1 and shown in Figure 5. An excellent agreement is found between our measurements and those of Surace (1998; adjusted to $q_0 = 0$). The distribution of nuclear separations is highly peaked at small values but also presents a significant tail at high values. The median separation of the sample is below the seeing limit ($\lesssim 1'' \sim 3$ kpc). More than 70% (60%) of the objects in the 1-Jy sample have nuclear separations of less than 5.0 (2.5) kpc, but 16% (7%) of the objects have separations in excess of 10 (20) kpc. These widely separated pairs may be difficult to explain in the standard ULIGs scenario, where the main activity is triggered in the late phase of the galaxy merger (e.g., Mihos & Hernquist 1996), unless the ULIG phase was triggered by an earlier merger event which is not evident at the present epoch. This issue is discussed in more detail in §5.1.

We have looked for possible correlations between the measured *NS* and the optical spectral type, infrared luminosity, *IRAS* 25 $\mu\text{m}/60 \mu\text{m}$ and 60 $\mu\text{m}/100 \mu\text{m}$ colors within the 1-Jy sample. We find a significant tendency for the Seyfert 1 galaxies and, to a lesser extent, the Seyfert 2 galaxies to have small nuclear separations. This is shown in Figure 6a. 100% (68%) of the Seyfert 1s (2s) have $NS \leq 2.5$ (5.0) kpc. Similar trends are observed with *IRAS* f_{25}/f_{60} colors (Fig. 6b): 79% of the 14 warm objects with $f_{25}/f_{60} \gtrsim 0.2$ have nuclear separations of 2.5 kpc or less (all of them have a nuclear separation of less than 10 kpc).

The trend between *NS* and AGN activity is confirmed when we use the *ISO* spectral classification of Lutz et al. (1999). Twenty-five objects are in common with our sample. Of the 10 objects classified as AGN-dominated according to *ISO*, all of them have $NS \leq 2.5$ kpc. In contrast, starburst-dominated galaxies show a broad range of nuclear separation.

No obvious trends are observed between the measured nuclear separations and the equivalent widths of the $H\beta$ and Mg Ib stellar absorption features, two traditional indicators of the starburst age (Veilleux et al. 1995, 1999a).

As shown in Figure 7, single-nucleus sources and close pairs are more common in the highest infrared luminosity bin (83% of the sources with $\log [L_{\text{IR}}/L_{\odot}] \geq 12.5$ have $NS \leq 2.5$ kpc versus 58% at $\log [L_{\text{IR}}/L_{\odot}] < 12.24$). This trend appears to extend to lower infrared luminosities: In a recent study of 56 galaxies with $\log [L_{\text{IR}}/L_{\odot}] = 11.10 - 11.99$, Ishida (2002) finds that only about a third of the objects with $\log [L_{\text{IR}}/L_{\odot}] \geq 11.5$ are advanced mergers with a single nucleus.

3.3. Lengths of Tidal Tails

The strength and length of tidal tails in galaxy mergers are strong functions of the encounter geometry and the merger phase. A strong resonance between the orbital and rotational motions of stars and gas produces strong tidal tails in prograde disks (e.g., Toomre & Toomre 1972; Mihos & Hernquist 1996). The lack of resonance in retrograde disks inhibits the formation of extended tidal tails, but still results in the formation of tidally induced spiral arms, central bars, and diffuse tidal debris (e.g., Mihos & Hernquist 1996). Systems in the pre-merger phase, where the two galaxies are still distinct but have gone through the first encounter, are expected to have well-developed tidal features. As the final merger takes place, the tidal tails gradually disappear as the material in the tails is accreted back onto the remnant or escapes the system altogether (e.g., Mihos, Dubinski, & Hernquist 1998; Hibbard & van Gorkom 1996).

In an attempt to further constrain the phase of the interaction in 1-Jy ULIGs, we have measured the total projected lengths of the tidal tails from our R -band images (the K' images are less sensitive to these faint features, so they were not used for this analysis). The measurements were done along each tail down to a constant R surface brightness of 24 magnitudes per square arcsecond. The results are listed in Table 1 and shown in Figure 8. Slightly more than half of the objects in the 1-Jy sample have tail lengths of 10 kpc or less, indicating an advanced merger. There is no obvious correlation between tail lengths and optical spectral types, infrared luminosities, and $IRAS\ 25\ \mu\text{m}/60\ \mu\text{m}$ and $60\ \mu\text{m}/100\ \mu\text{m}$ colors. Note, however, that 70% of the objects with $f_{25}/f_{60} \geq 0.2$ have tail lengths of 10 kpc or less. This fraction is 60%, 36%, 52%, and 66% when considering Seyfert 1s, Seyfert 2s, LINERs, and H II galaxies, respectively.

3.4. Interaction Classification

Using a classification scheme first proposed by Surace (1998) and based on the results of published numerical simulations (e.g., Barnes & Hernquist 1992; Mihos & Hernquist 1996; Gertsen 1997), we have classified each object in the 1-Jy sample (except for the five triplet candidates and F23233+2817, which is an isolated spiral galaxy) according to their morphology:

- I. *First Approach*. This phase refers to the earliest stage of the interaction, prior to the first close passage of the galaxies, when the galaxy disks remain relatively unperturbed and separate and hence do not show evidence for tidal tails or bridges.
- II. *First Contact*. At this stage, the disks overlap but strong bars and tidal tails have not yet formed. These are the primary morphological differences between this phase and the early merger phase (Phase IV below).
- III. *Pre-Merger*. This stage is characterized by two identifiable nuclei with well-developed tidal tails and bridges. While our imaging observations cannot prove that the double-nucleus systems will necessarily merge, the presence of ultraluminous activity combined with the prevalence of mergers in ultraluminous galaxies, as well as the presence of tidal tails and other structure interconnecting the nuclei in every case, would seem to strongly indicate eventual merger. Within this category the systems were further divided into two subclasses based on their projected separations:
 - IIIa. *Wide Binary*. Systems with apparent separation > 10 kpc.
 - IIIb. *Close Binary*. Systems with apparent separation ≤ 10 kpc.

Note that these subclasses are an approximation only to the merger phase since without detailed kinematic information for many of these systems, we cannot tell if the two galaxies are pre- or post-apgalacticon (farthest approach).

IV. *Merger*. This stage occurs after the nuclei have apparently coalesced. These systems have prominent tidal features, but only one nucleus can be detected at optical and near-infrared wavelengths. Additionally, the sole galaxy core is often noticeably extended and tends to be cut by many dust lanes. Following Surace (1998), we further subdivide this class into two categories:

IVa. *Diffuse Merger*. Systems with $(L_{K'})_4/L_{K'} < \frac{1}{3}$.

IVb. *Compact Merger*. Systems with $(L_{K'})_4/L_{K'} \geq \frac{1}{3}$.

Objects in class IVa consists of systems that have diffuse, extended central regions typically composed of several smaller extended emission region which appear to be cut by dust lanes. Objects in class IVb are dominated, particularly at long wavelengths (K'), by a single point source. As pointed out by Surace (1998), there is no a priori reason to believe that the stage IVb systems are any older than the stage IVa systems, other than the fact that stage IVa resembles stage III, and stage IVb resembles stage V, and that stage V is older than stage III based on the appearance of tidal structure.

V. *Old Merger*. These are systems which do not show any direct *unmistakable* signs of tidal tails, yet have disturbed central morphologies similar to those of the merger stage IV systems, particularly those with knots of star formation. At this stage, the surface brightness of the tidal features in the system has fallen below our detection limit, leaving nothing but the high surface brightness relaxed merger remnant core visible.

The results of the classification are given in Table 1. The distribution is shown in Figure 9. None of the 1-Jy sources appears to be in the early stage of the interaction (I and II). Systems comprised of two distinct objects all show prominent tidal features. Most (56%) of the ULIGs harbor a single nucleus and are therefore in the later stages of the merger. This is a very significant result: the ULIG phase is triggered only after the first close encounter between the two galaxies and generally when the two galaxies have coalesced into a single object. The fraction of singles to doubles in the 1-Jy sample varies with infrared luminosity, increasing steeply for the most extreme ULIGs with $\log [L_{IR}/L_{\odot}] > 12.5$ (Fig. 10a). This fraction seems to decrease when considering lower luminosity systems with $\log [L_{IR}/L_{\odot}] = 11.00 - 11.99$ (Ishida 2002). This class of objects is generally comprised of two distinct galaxies often widely separated and sometimes showing no obvious tidal features. Many of these luminous infrared galaxies (i.e. LIGs: $\log [L_{IR}/L_{\odot}] = 11 - 11.99$) therefore fall into interaction classes I – III.

Figure 10b shows that the interaction class is a strong function of the optical spectral type. We find that all ten Seyfert 1s are advanced mergers (class IVb or V) and that half (50%) of the Seyfert 2s are early or advanced mergers (class IVa, IVb, or V). This is consistent with the results of our analysis of their nuclear separations (§3.2). On the other hand, LINERs and H II region-like galaxies show no preference in interaction class

(other than to avoid classes I and II). A strong correlation is also found when we consider the warm objects with $f_{25}/f_{60} > 0.2$ (Fig. 10c): Nearly 80% of these systems (11 objects out of 14) are advanced mergers (class IVb or V).

We find no obvious trend between the interaction class and IRAS 60 $\mu\text{m}/100 \mu\text{m}$ color. The strengths of the H β or Mg Ib stellar features measured in the nuclei of the 1-Jy objects (either considering all the objects in the sample or only in systems optically identified as starburst galaxies) show no correlation with interaction class. This negative result indicates that traditional nuclear indicators of the starburst age are *not* particularly good indicators of the merger phase or the epoch of the merger event. Detailed studies of star clusters in merger-induced starbursts confirm the existence of a broad range of stellar age which reflects the complex star formation history of these systems (e.g., Surace et al. 1998; Whitmore et al. 1999; Gallagher et al. 2001; Zhang, Fall, & Whitmore 2001, and references therein).

4. PROPERTIES OF THE HOST GALAXIES

4.1. Surface Brightness Profiles

In an attempt to characterize the brightness distribution of the host galaxies in the ULIGs of the 1-Jy sample, we have performed the following isophotal analysis. First, a central point source was removed from the centers of the objects with obvious central excess emission. For this procedure, a stellar source within the field of view of the detector was shifted and scaled appropriately in intensity to produce a smooth and monotonic profile in the central regions of the galaxies. Ellipses were then fitted to the residuals using the standard Fourier expansion (e.g., Binney & Merrifield 1998)

$$\delta(\phi) = \bar{\delta} + \sum_{n=1}^4 [A_n \cos(n\phi) + B_n \sin(n\phi)], \quad (1)$$

where $\delta(\phi) \equiv R_i(\phi) - R_e(\phi)$ is the distance at position angle ϕ between the radii of the corresponding points on the ellipse and on the isophote, and A_n and B_n are the coefficients of the Fourier expansion. The typical error for the ellipse fitting is estimated to be less than 0.1 mag. arcsec⁻². Unless otherwise noted, the error bars on the various quantities derived from these fits are equivalent to 1-sigma values and were directly derived from the IRAF routines (see the IRAF help page and in particular Jedrezejewski 1987 and Busko 1996 for a more detailed discussion of the error analysis).

The R and K' surface brightness profiles derived from the ellipse fitting (not corrected for cosmological dimming) are presented in Figure 11 using two different scales on the horizontal axis: a logarithmic scale on the left and a linear^{1/4} scale on the right. An exponential disk and an elliptical-like object with a de Vaucouleurs profile would produce straight lines in the left and right panels, respectively. A vertical arrow in each panel represents the size of the seeing disk. Least-square fits to the profiles were carried out to determine whether an exponential or de Vaucouleurs profile best fits the observed profile at R and K' . To avoid complications due to the seeing, the least-squares fit was applied to the data points only at radii larger than twice the seeing disk. The value of the reduced chi-square is indicated in the upper right hand corner of each panel in Figure 11. The results from the fits are summarized in Table 2. In the calculation of the reduced chi-square, the number of degrees of freedom is the number of data points in the observed radial profile minus the number of free parameters in the fit (= 2 for both

the exponential and de Vaucouleurs profiles). A reduced chi-square of order unity indicates a good fit. If the chi-square is much larger than unity, then the fit is poor. If the reduced chi-square is much less than unity, then there is not enough data points to carry out the fit and the parameters derived from the fit are not reliable.

Figure 12a shows the fraction of single-nucleus objects (i.e. merger remnants with interaction class IV or V) in the 1-Jy sample with pure disk-like (D: 2%), pure elliptical-like (E: 35%), elliptical/disk-like (E/D: 38%), and ambiguous (A: 26%) radial profiles. ‘‘E/D’’ profiles are defined as being equally well fit by an exponential or de Vaucouleurs profile, while neither fits galaxies with ‘‘ambiguous’’ profiles. Both E/D and A profiles are quite common among ULIGs. The large number of E/D galaxies in our sample probably reflects the limitations of our data: images with a larger dynamical range in surface brightness (i.e. higher spatial resolution to probe the nuclear region and fainter surface brightness limits to map the outer portions of the galaxies) would help rule out one type of profile over the other. The large fraction of ambiguous profiles probably reflects the residual effects of the galaxy interaction on the morphology of the merger remnants. If we combine the E and E/D galaxies, we find that 73% of the single-nucleus objects are fit adequately by a de Vaucouleurs profile.

The fraction of ambiguous profiles among double-nucleus systems (Fig. 12b) is significantly larger than among single-nucleus systems. Several binaries show obvious tidal tails and bridges which distort the radial profile. Among the other binaries, we find that the fraction of elliptical-like galaxies is slightly larger than disk-like hosts, perhaps an indication that the progenitor galaxies generally have strong spheroidal components (e.g., bulges).

Strong correlations are found between the type of host galaxy profile and the nuclear and global properties of single-nucleus systems. In the following analysis, we take the conservative approach to double-count each E/D object as an E object *and* a D object (it is conservative because it has the effect of smoothing out possibly stronger trends with host galaxy profiles). Figure 13a shows that the hosts of most merger remnants with Seyfert 1 (83%) or Seyfert 2 (69%) optical characteristics are E-like. This preponderance of E-like hosts among AGN mergers is also seen when using the *ISO* classification (Fig. 13b; 8 out of 10 or 80% of *ISO* AGNs are E-like). A similar trend is seen among warm objects (10 out of the 13 objects with $f_{25}/f_{60} \geq 0.2$ or 77% are E-like; Fig. 13c). Starburst and LINER systems, on the other hand, show no preference between disk-like and E-like hosts.

The nature of the host does not seem to depend strongly on the infrared luminosity, the 60 $\mu\text{m}/100 \mu\text{m}$ ratio, or the strengths of the stellar H β and Mg Ib features. But, as expected in the merger scenario for elliptical galaxy formation, E- and E/D profiles are more common in the later phases of interaction [class V (27%) and especially class IVb (49%); Fig. 13d], while ambiguous profiles are more often seen in early mergers (IVa, 59%), a sign perhaps that many of these systems are still showing the damages caused by the recent merger event.

4.2. Absolute Magnitudes

The absolute R and K' magnitudes of the host galaxies in the 1-Jy sample are listed in the last two columns of Table 2. Median and mean values are listed in Table 3. The distributions for double- and single-nucleus systems are shown separately in

Figure 14. The median and mean R -band luminosities of the individual galaxies involved in binaries are 0.86 and $0.85 \pm \begin{smallmatrix} 0.86 \\ 0.43 \end{smallmatrix} L^*$ (1σ), respectively. At K' , the median and mean for these objects are 0.91 and $0.90 \pm \begin{smallmatrix} 1.94 \\ 0.61 \end{smallmatrix} L^*$. For single-nucleus systems, the median and mean R -band luminosities are 1.69 and $1.69 \pm \begin{smallmatrix} 2.25 \\ 0.97 \end{smallmatrix} L^*$, and the median and mean K' -band luminosities are 1.92 and $2.36 \pm \begin{smallmatrix} 3.24 \\ 1.38 \end{smallmatrix}$. Previous studies have obtained similar host galaxy magnitudes: $\sim 2.5 L_B^*$ (Armus, Heckman, & Miley 1990), $\sim 3 L_r^*$ (ranging from $\sim 1 - 24 L_r^*$) for the ULIGs in the 2-Jy sample (Murphy et al. 1996), $\sim 2.4 L_H^*$ for warm ULIGs from the *IRAS* BGS sample (Surace & Sanders 1999), and $\sim 1 - 2.5 L_H^*$ for cool ULIGs from the BGS and 1-Jy samples (Surace, Sanders, & Evans 2000). Colina et al. (2001) derive noticeably fainter, sub- L^* , host galaxy magnitudes ($\langle M_H \rangle = -23.5 \pm 0.7$ mag. scaled down to our cosmology) for 27 mostly cool ULIGs. The H -band *HST/WFPC2* data used for this analysis are shown in Bushouse et al. (2002). Direct comparisons with our data for the four objects in common with the 1-Jy sample indicate that much of the diffuse low surface brightness features in our data are not visible in the snapshot images of Bushouse et al. (2002). This underestimate of the light contribution from the host galaxies explains the fainter host galaxy magnitudes derived by Colina et al. (2001).

The large number of galaxies in the 1-Jy sample allows us to look for trends between host galaxy luminosities and infrared luminosities, optical spectral types, and *IRAS* colors. Focussing on single-nucleus systems, there appears to be a tendency to find luminous hosts in the most infrared luminous systems of the 1-Jy sample (see Fig. 15a and Table 3). This is due to the fact noted in §2.1 that systems with $L_{\text{IR}} > 10^{12.3} L_{\odot}$ are more distant on average ($\langle z \rangle = 0.183 \pm 0.053$) than ULIGs with $L_{\text{IR}} \leq 10^{12.3} L_{\odot}$ ($\langle z \rangle = 0.132 \pm 0.029$).

Figure 15 and Table 3 indicate that the most luminous hosts also tend to be found in systems with warm *IRAS* 25 $\mu\text{m}/60 \mu\text{m}$ colors (≥ 0.2) and AGN characteristics. The hosts of the warm objects are $0.6 - 0.7$ magnitudes brighter on average than the hosts of the cool objects, although both distributions overlap considerably. In this case, the difference in mean host luminosity cannot be attributed to a difference in redshift since both classes of objects have virtually the same median redshift ($= 0.148$). The same is true when comparing the Seyfert and non-Seyfert populations ($\langle z \rangle = 0.143 \pm 0.056$ and 0.150 ± 0.041 , respectively), yet the host galaxies of Seyferts are brighter by about $0.8 - 1.0$ mag. on average at both R and K' than the hosts of LINERs and H II region-like galaxies. K-S tests between the distributions of Seyferts vs non-Seyferts and warm vs cool ULIGs confirm these differences ($P[\text{null}] < 10^{-5}$ and 10^{-2} , respectively). These results can be attributed to real differences in the host luminosities of AGNs vs non-AGNs, or may be due to a prominent starbursting population in warm Seyferts contributing significantly at R and K' .

One should be cautious when interpreting these results, however. An object-by-object comparison with the H -band data of Surace & Sanders (1999) suggests that the host luminosities measured in a few of the warm Seyferts appear to be slightly higher than those measured from AO imaging (assuming $H - K' \lesssim 0.5$ for the host; see below). This may indicate that we are slightly underestimating the contribution from the central point source in some of these objects (the possibility that the AO imaging of Surace & Sanders is underestimating the host luminosities appears less likely because the exposure times for these observations were fairly long and therefore the

surface brightness limits of the data were fairly deep). The PSF subtraction in our data is more difficult in the warm, highly nucleated systems of the 1-Jy sample than in the cooler, more diffuse systems; this may introduce a slight bias which may account for the weak trends between host luminosities, *IRAS* colors and spectral types. These issues are discussed in more detail in §§4.5, 5.2, and 5.3.

Next we compare the host magnitudes of ULIGs with the results from studies of quasar host galaxies. At R , the host galaxies in ULIGs appear slightly less luminous on average than the HST measurements of Dunlop et al. (2002) on radio-quiet quasars (-22.35 ± 0.15 mag., adjusted to $H_0 = 75 \text{ km s}^{-1} \text{ Mpc}^{-1}$) and radio-loud quasars (-22.85 ± 0.10 mag.). Note, however, that ULIG hosts span a broad range in luminosity so there is considerable overlap between ULIGs and the other classes of objects. Given the correlations between host luminosities, infrared luminosities, *IRAS* 25 $\mu\text{m}/60 \mu\text{m}$ colors, and optical spectral types discussed in the previous paragraphs, we find that if we focus our analysis on the subset of objects with $\log [L_{\text{IR}}/L_{\odot}] \geq 12.3$, $f_{25}/f_{60} \geq 0.2$, and with Seyfert characteristics at optical wavelengths, the apparent shift in host galaxy R magnitudes between these ULIGs and the quasar dataset of Dunlop et al. disappears.

To directly compare our data with the ground-based results of McLeod & Rieke (1994a, 1994b) and HST/NICMOS data of McLeod & McLeod (2001) on quasars, we need to transform the H -band magnitudes listed in these papers into K' magnitudes. For an old stellar population at $z = 0$, $H - K' = 0.16$ (Surace 1998), but $H - K' \approx 0.3 - 0.4$ if $\langle z \rangle = 0.1 - 0.2$ (e.g., Lilly & Longair 1984). Given these corrections, the low-luminosity sample of quasars of McLeod & Rieke (1994a) have an average K' host magnitude $M_{K'} \approx -24.3 \pm 0.6$, while the high-luminosity quasars have $M_{K'} \approx -25.1 \pm 0.7$. The host galaxies in the 1-Jy ULIGs are therefore comparable in luminosity to those of the *high*-luminosity quasars. So even though we found in §2.1 that the 1-Jy ULIGs have lower *integrated* K' luminosities than the high-luminosity quasars of McLeod & Rieke (1994b), we find that they have host galaxies with similar K' luminosities. This good agreement is also found in the more recent analysis of the high-luminosity sample by McLeod & McLeod (2001).

The claim by McLeod & Rieke (1994a, 1994b; ground-based H -band data) and McLeod, Rieke, & Storrie-Lombardi (1999; HST/NICMOS data) of a trend between nuclear and host galaxy luminosities in quasars has recently come under question. The R -band results of Dunlop et al. (2002) do not seem to confirm this trend. A recent K -band ground-based study of 14 very high luminosity ($M_V \lesssim -25$) radio-quiet quasars with $0.26 \geq z \geq 0.46$ by the same group (Percival et al. 2001) find $\langle M_K \rangle \approx -24.3 \pm 0.04$, a value closer to the host galaxy magnitudes of the *low*-luminosity quasar sample of McLeod & McLeod (1994a) and significantly *less* luminous on average than the host galaxies of the 1-Jy ULIGs. However, as stated for instance by Dunlop et al. (2002) when discussing the study of Taylor et al. (1996), the results from ground-based studies of quasars beyond $z = 0.15$ like that of Percival et al. should be treated with caution given the technical difficulties involved in removing the nuclear PSF to characterize the underlying host galaxy of these objects (see also discussion in §4.5).

Adaptive optics imaging of quasars alleviates the problems associated with PSF subtraction in ground-based data. The recent study by Surace et al. (2001) of 18 PG quasars with strong

far-infrared excesses finds H -band host galaxy luminosities that range from 0.5 to 7.5 L^* , with a mean of 2.3 L^* , consistent with the average K' host galaxy luminosity of 1-Jy ULIGs measured in the present study and similar to that found by McLeod & McLeod (2001) among quasars.

4.3. Luminosity Ratios in Binary Systems

The mass ratio of a binary system of galaxies is an important parameter in predicting the amount of “damage” incurred in the interaction. Minor mergers comprised of objects with mass ratios of order ~ 10 are predicted to have only benign effects on the main component of the system (e.g., Walker, Mihos, & Hernquist 1996; Bendo & Barnes 2000; Naab & Burkert 2001). Major mergers with mass ratio of ~ 3 or less appear to be needed to create a ULIG (e.g., Mihos & Hernquist 1996). The kinematic properties of ULIGs also appear consistent with this scenario (e.g., Genzel et al. 2001). Given our lack of detailed kinematic data, we have no reliable way to determine the total mass of each galaxy in our binary systems. We make the assumptions that the total masses scale linearly with the stellar masses and that the stellar masses scale with the R or K' luminosities of the host galaxies. Figure 16 shows the distributions of $\Delta M(R)$ and $\Delta M(K')$ (equivalent to luminosity ratios) of the Class III systems in the 1-Jy sample for which we were able to reliably separate each galaxy (i.e. most of them are Class IIIa). Most systems have a magnitude difference of less than 1.5 or a luminosity ratio of less than 4, in general agreement with the predictions from numerical simulations of galaxy mergers if mass indeed scales linearly with luminosity. The magnitude difference is slightly larger at K' than at R . The two objects with the largest K' magnitude differences are F00456–2904 and F12127–1412.

4.4. Colors

In Figure 17, we find no significant correlation between the nuclear color and the underlying galaxy color $(R-K')_{\text{host}}$ ($P[\text{null}] > 0.01$ for H II, LINER, and Seyfert galaxies). In contrast to the nuclear colors, the median color of the underlying galaxies of ULIGs is only slightly redder than that of normal galaxies or the host galaxies of quasars [$(R-K')_{\text{host}} = 3.0$ for either H II galaxies, LINERs, or Seyfert 2 galaxies compared to 2.6 and 2.5 for normal galaxies and quasars, respectively; de Vaucouleurs & Longo 1988; Dunlop et al. 2002]. This result confirms that the obscuring gas and dust is preferentially concentrated within the inner 4 kpc of ULIGs (e.g., Scoville et al. 2000). The slightly redder colors of Seyfert 1 hosts [with median $(R-K')_{\text{host}}$ of 3.4] may be due to contamination at K' by hot dust emission from the AGN or residuals from the bright central source subtraction procedure. The colors of ULIG hosts are similar to those found by Surace et al. (2001) among infrared-excess PG quasars.

4.5. Half-Light Radii and Surface Brightnesses

The seeing-deconvolved half-light radii, r_e , of the elliptical-like host galaxies in our sample are listed in Table 2 and plotted in Figure 18. The median and mean of r_e at R are 4.60 kpc and 4.80 ± 1.37 kpc (1σ), while at K' we find 3.55 kpc and 3.48 ± 1.39 kpc (1σ). These half-light radii are virtually indistinguishable from those measured at H by McLeod & McLeod (2001) in the eight E-like “high-luminosity” quasars of their sample ($\langle r_e \rangle = 3.39 \pm 1.90$ kpc; Fig. 18b). On the other hand, the values measured by Dunlop et al. (2002) among

high-luminosity radio-quiet quasars (7.63 ± 1.11 kpc adjusted to $H_0 = 75 \text{ km s}^{-1} \text{ Mpc}^{-1}$) and radio-loud quasars (7.82 ± 0.71 kpc) appear to be significantly larger than those measured in the 1-Jy ULIGs, although there is some overlap between the two distributions. We do not try to compare our results with the half-light radii measured by Taylor et al. (1996) at K because these data have proven to be unreliable: An object-by-object comparison between the data of Taylor et al. (1996) and Dunlop et al. (2002) reveal discrepancies of up to a factor of nearly ~ 25 (e.g., 1549+203) in r_e , which cannot be attributed to color gradients ($R-K'$) but rather are probably due to incorrect PSF subtraction in the ground-based data of Taylor et al. Similar technical difficulties are likely to affect to some extent the ground-based data of Percival et al. (2001), given the relatively high redshifts of their sources.

Combining measurements of the half-light radius and mean R -band surface brightness within half-light radius, μ_e , Dunlop et al. (2002) have argued that the host galaxies of luminous quasars follow the same $\mu_e - r_e$ relation as that of normal (inactive) ellipticals. The surface brightnesses of ULIGs listed in Table 2 have been corrected for cosmological dimming [$\propto (1+z)^4$] and are compared with those of elliptical galaxies and quasars in Figure 19a. The elliptical-like (E and E/D) host galaxies of the 1-Jy ULIGs have slightly brighter R -band surface brightnesses than the hosts of the quasars studied by Dunlop et al. Nevertheless, the elliptical-like host galaxies of ULIGs appear to follow the $\mu_e - r_e$ relation of normal ellipticals, although with considerable scatter. In this figure, we used the fit of Hamabe & Kormendy (1989) and shifted it in magnitude by $V - R = 0.5$ mag (keeping the slope constant). Seyfert 1 galaxies show a tendency to fall slightly above the data for non-Seyfert 1s. The source of this tendency is discussed below.

Interpretation of our data at K' is more difficult because r_e and μ_e have been measured reliably in only 18 ULIGs of our sample (this analysis was carried out only when the K' images were deep enough to reliably measure the surface brightness profiles out to a radius comparable to the optical radius). The results are presented in Figure 19b. A weak anti-correlation is found between apparent surface brightnesses and galaxy sizes. This anti-correlation is stronger if we exclude Seyfert 1 galaxy hosts from the fit (solid line in Fig. 19b). The data for the Seyfert 1s should be considered with caution since they are significantly more sensitive to our PSF subtraction procedure than for the other objects. The bright μ_e of the three Seyfert 1 host galaxies near the top of Figure 19b may be due to positive residuals from the AGN.

We first compare our K' results with the V -band $\mu_e - r_e$ relation of Hamabe & Kormendy (1987) for normal ellipticals and find a generally good agreement with the non-Seyfert 1 data if we assume a constant color $V - K' = 3.7$ mag. This color term is slightly redder than that of normal elliptical galaxies (e.g., Nolan et al. 2001; Fukugita et al. 1995), possibly because the hosts of ULIGs are dustier than elliptical galaxies and star formation (red supergiants) contributes at K' . [We did not use the B -band data of Bender, Burstein, & Faber (1992) and Faber et al. (1997) for this comparison to avoid the even larger color correction.] We also compare our results with the K -band data of Pahre (1999). The slope of the $\mu_e - r_e$ relation derived from these data (dotted line in Fig. 19b) is shallower than that of Hamabe & Kormendy (1987). Unfortunately, a comparison with quasar hosts is not possible because of the lack of reliable quasar host data in the near-infrared (McLeod & McLeod 2001

list r_e but not μ_e in their paper, and the data of Taylor et al. are not considered reliable for the reasons discussed in the first paragraph of this section).

There is no obvious correlation of the R -band r_e (or μ_e) with $IRAS\ 25\ \mu\text{m}/60\ \mu\text{m}$ and $60\ \mu\text{m}/100\ \mu\text{m}$ colors, infrared luminosities, optical and mid-infrared spectral types, and the strengths of the stellar $H\beta$ and $Mg\ \text{Ib}$ absorption features. There are too few measurements of r_e at K' to search for statistically significant trends with this parameter. Recall, however, the existence of correlations between the host galaxy R and K' luminosities ($\propto \mu_e r_e^2$) and infrared luminosities, $IRAS\ 25\ \mu\text{m}/60\ \mu\text{m}$ colors, and AGN characteristics noted in §4.2 (Fig. 15 and Table 3).

4.6. Bars, Axial Ratios, and Boxiness

The $\sim 1''$ spatial resolution of our images prevents us from studying in detail the cores of ULIGs on scales smaller than a few kpc. However, a few statements can be made on galactic structures seen beyond the seeing disk. Only three objects in our sample, F14394+5332 W (triplet), F23233+2817 (isolated spiral), and F23327+2913 S (widely separated pair), show evidence for bar-like structures which extend 8 kpc (P.A. = 90°), 12 kpc (20°), and 11 kpc (120°), respectively. None of the single-nucleus merger remnants shows a strong large-scale bar.

Our ellipse-fitting routine of the surface brightness distribution provides quantitative information on the axial ratio (b/a) of the host galaxies on scales larger than twice the seeing disk. Figure 20 shows the radial dependence of the axial ratio for the 58 single-nucleus mergers of our sample with ‘‘E’’ or ‘‘E/D’’ profiles (F23233+2817 is not included in this subset of objects because it is an isolated spiral galaxy). In the majority of cases, the axial ratio is constant with radius to within ± 0.15 . We plot in Figure 21 the distribution of b/a measured at $3 \times r_e$. The median and mean of this quantity are 0.77 and 0.75 ± 0.15 ($1\ \sigma$), respectively. This is similar to the average values measured in normal elliptical galaxies (e.g., Ryden 1992) and in the hosts of quasars (Dunlop et al. 2002).

Surface photometry of elliptical galaxies often shows isophotes that deviate slightly from a perfect ellipse. The departure of the isophotes from a perfect ellipse is measured by the A_4 coefficient of the $\cos 4\phi$ term in equation (1). Typical values for ellipticals normalized to the major-axis length, a , range from -0.02 to $+0.03$ (e.g., Bender et al. 1989), where the negative values indicate boxy isophotes and positive values indicate disk-like isophotes. Ellipticals with boxy isophotes are generally luminous (massive) radio-loud ellipticals with X-ray halos, very slow stellar rotation and a distinct cuspy core, whereas ellipticals with disk-like isophotes are low-to-moderate luminosity (mass) lenticular and elliptical galaxies which are generally radio-quiet, show little or no X-ray emission, and exhibit significant rotational support and a power-law surface brightness profile on small scales (e.g., Kormendy & Bender 1996; Faber et al. 1997; Pahre, de Carvalho & Djorgovski 1998 and references therein).

The radial profiles of the normalized R -band boxiness parameter in the single-nucleus ULIGs of our sample are shown in Figure 22. Several of these galaxies have large absolute values of A_4/a (generally from -0.05 to $+0.05$) compared to normal ellipticals. Significant A_4/a gradients are seen in many objects. Thus it is hard to attribute a single boxiness value to each galaxy. The distributions of A_4/a measured at $2 \times r_e$ and $3 \times r_e$ in elliptical-like (E and E/D) ULIGs are presented in Figure 23.

There is no clear preference between positive and negative boxiness values. The median and mean of A_4/a at $2 \times r_e$ are -0.002 and -0.001 ± 0.036 , and $+0.005$ and $+0.014 \pm 0.059$ at $3 \times r_e$. The broad range of boxiness values in ULIG hosts probably reflects the residual effects of the violent merger that took place in these galaxies.

5. DISCUSSION

In this section, the results from our imaging survey are combined with those from other published studies on ULIGs, quasars, and normal elliptical galaxies to attempt to answer the following questions: (1) What is the nature of ultraluminous infrared galaxies?; (2) Are ultraluminous infrared mergers elliptical galaxies in formation? (3) Are ultraluminous infrared galaxies quasars in formation?

5.1. What is the Nature of Ultraluminous Infrared Galaxies?

What types of galaxies make up ultraluminous infrared systems? What conditions are needed to trigger their quasar-like infrared luminosities? Answers to these two questions would go a long way in clarifying the nature of ULIGs. There is now a consensus among researchers in this field concerning the frequency of interactions in ULIGs and the number of galaxies involved in these interactions. The results from the present survey (§3.1) show convincingly that the great majority of ULIGs ($\sim 95\%$) are involved in the interaction of two, and no more than two, galaxies. The recent HST results of Bushouse et al. (2002) also support this conclusion. The higher frequency of multiple mergers claimed earlier by Borne et al. (2001) and Cui et al. (2001) has now been shown to be due primarily to the presence of several star-forming super star clusters which mimic low-luminosity nuclei at optical wavelengths. Near-infrared observations reveal the true nature of these clusters, ruling out genuine galactic nuclei. Follow-up spectroscopy of apparent neighbors to ULIG systems also reveals in some cases that they are not physically associated with the ULIGs (see Appendix A).

Our detailed morphological analysis of the 1-Jy sample provides new statistical evidence that most (56%) ULIGs are involved in the late phase of a merger where the two nuclei have merged into a single object. This frequency does not seem to depend strongly on spatial resolution since the *HST* data of Scoville et al. (2000), Colina et al. (2001), and Bushouse et al. (2002) reveal very few double-nucleus systems that were not already known from arcsecond-resolution ground-based data like ours. As described in §3.2, the frequency of advanced mergers is a function of infrared luminosity, increasing dramatically above $\sim 10^{12.5} L_\odot$ and decreasing among luminous infrared galaxies with $\log [L_{\text{IR}}/L_\odot] = 11.50 - 11.99$. So not only can we say that the ultraluminous infrared phase is generally triggered when the individual galaxies in the merger have lost their individual identity and the nuclei have fused into a single entity, but also that the extreme environment during the final phases of a merger appears to be a *necessary* condition to produce the most extreme examples of ULIGs.

Another $\sim 39\%$ of the ULIGs in the 1-Jy sample harbor two distinct nuclei but always show tidal tails at R , evidence that the ultraluminous infrared phase here was triggered *after* the first close passage of the two interacting galaxies. These results are at least qualitatively consistent with the simulations of Mihos & Hernquist (1996) where two merging galaxies go through two distinct episodes of enhanced star formation activity (and therefore large infrared luminosity; note that Mihos

& Hernquist do not try to model AGN activity) with the first peak taking place shortly ($\sim 1 - 2 \times 10^8$ yr) after the first close encounter, when the two galaxies are still widely separated, and the second peak taking place during the final merger of the galaxies, $\sim 10^9$ yr after the first encounter. Our results indicate that in quite a few cases the star formation activity triggered during the first passage is sufficient to reach the ULIG threshold (although we have no high-resolution maps in the infrared to determine whether the FIR-emitting region in these widely spaced ULIG systems is a kpc-scale ring, as predicted by the simulations of Mihos & Hernquist). The detailed kinematic study of four ULIGs (including F10190+1322 from the 1-Jy sample) by Murphy et al. (2001a) confirms that the ULIG phase may sometimes take place well before the final merger.

In the simulations of Mihos & Hernquist, the relative amplitude of the peaks of enhanced star formation activity is only weakly dependent on the initial orientation of the merging galaxies but depends strongly on the morphological properties of these galaxies, particularly their bulge-to-disk mass ratio. Unfortunately, reliable profile decomposition to determine this ratio in our sample of binary galaxies requires sub-kpc resolution and therefore cannot be done with the present data. Nevertheless, our data analysis provides some constraints on the type of galaxies involved in the interactions. Our crude profile classification in §4.1 suggests that an important fraction of these binary galaxies have a prominent spheroidal component (possibly a bulge). As discussed in §4.2 (and in more detail in §5.2 and §5.3 below), the host galaxies of single-nucleus ULIGs span a broad range in luminosities with average of order $\sim 2 L^*$. Binary systems involve two $\sim 0.9 L^*$ (on average) galaxies with luminosity ratio generally less than 4. This is evidence that mergers between small galaxies or minor mergers involving the accretion of small satellite galaxies by larger ones do not provide the conditions necessary to trigger an ultraluminous infrared phase. Large torques appear needed to produce enough “damage” to the galaxies involved in the interaction so that gas transfer to the inner portions of the galaxies is sufficient to trigger a strong episode of star formation and/or AGN activity and reach the ULIG phase. These results are qualitatively consistent with numerical simulations of unequal mass mergers (e.g., Mihos & Hernquist 1996; Walker, Mihos, & Hernquist 1996; Bendo & Barnes 2000; Naab & Burkert 2001) and the recent kinematic data of Genzel et al. (2001).

There are interesting exceptions to the merger scenario for ULIGs. Among these is F23233+2817, the only spiral galaxy in the 1-Jy sample which does not seem to be involved in any galactic interaction. The infrared luminosity of this object lies on the boundary between luminous and ultraluminous infrared galaxies ($\log [L_{\text{IR}}/L_{\odot}] = 12.00$), so it may be that the Seyfert 2 nucleus in this object (or unsuspected circumnuclear starburst) is sufficiently powerful to heat enough dust to reach the ultraluminous threshold without the need for refueling from a major merger. Eight ULIGs in the 1-Jy sample appear to involve interacting galaxies that are widely (> 20 kpc) separated (see Table 1 and Fig. 5; one of these objects, F11223–1244, hosts a Seyfert 2 nucleus). All of these objects show tidal features indicative of a pre-merger phase (i.e. after first contact; this seems to rule out the possibility that these objects are observed *before* first contact, as suggested by Dinh-V-Trung et al. 2001). It would therefore appear that an ultraluminous infrared phase can also be triggered when two galaxies in a pair are near apogalacticon (farthest approach after first passage). This is difficult to recon-

cile with the predictions of the merger scenario. A way out of this uncomfortable situation is to suppose that the ULIG phase was triggered by an earlier merger event which is not evident at the present epoch. One should also be cautious when interpreting the data on these eight ULIGs since the physical connection between the galaxies in most of these pairs has not yet been confirmed through detailed spectroscopy (see Appendix A).

5.2. Are Ultraluminous Infrared Mergers Elliptical Galaxies in Formation?

Among the 66 single-nucleus mergers in the 1-Jy sample, 48 (73%) of them are fit adequately by a de Vaucouleurs profile at R and K' (§4.1). This fraction is uncertain, however, since the relatively modest dynamical range of our data (especially at K') prevents us from deciding if a de Vaucouleurs profile is a better fit than an exponential disk in 25 (38%) of these objects (these are the so-called E/D galaxies in Table 2 and Fig. 12). Nevertheless, we can state with confidence that elliptical-like hosts are observed in the majority ($> 50\%$) of late mergers of the 1-Jy sample. This result supports the conclusions from previous studies that were based on smaller samples of ULIGs (e.g., Wright et al. 1990; Stanford & Bushouse 1991; Doyon et al. 1994; Scoville et al. 2000; Cui et al. 2001), and is at least qualitatively consistent with the scenario that ULIGs evolve into ellipticals through merger-induced, dissipative collapse (Kormendy & Sanders 1992). In the rest of this section, we further explore the predictions of this scenario by comparing the properties of the elliptical-like hosts found in the 1-Jy sample with those of nearby spiral bulges, lenticular (S0) galaxies, and ellipticals, while taking into account the various sources of errors in our analysis of the ULIGs.

In §4.2, the elliptical-like (E and E/D) hosts in the 1-Jy sample were found to have a median and average luminosities at R of 1.77 and $1.66 \pm {}_{0.77}^{1.45} L^*$, and 2.00 and $1.98 \pm {}_{0.86}^{1.52} L^*$ at K' . Residuals from AGNs and compact circumnuclear starbursts may affect (overestimate) slightly the luminosities of some of these hosts – this effect appears to be more important at K' than at R and more frequent among Seyfert 1s than among Seyfert 2s (§4.2 and §4.5). The results at R are thus considered more reliable, even though the effects associated with dust extinction may be more significant here than at near-infrared wavelengths. Assuming $V - R \approx 0.6$ mag for typical ellipticals (Fukujita et al. 1995), the average V -band absolute magnitude of the elliptical-like hosts in the 1-Jy sample is $\sim -21.1 \pm 0.7$ mag. The elliptical-like hosts of ULIGs therefore span the intermediate luminosity range between the low-luminosity ($\lesssim 1.0 L^*$) “power-law galaxies” and high-luminosity ($\gtrsim 3.5 L^*$) “core galaxies” of Faber et al. (1997).

The distribution of axial ratios among elliptical-like hosts in the 1-Jy sample resembles that of elliptical galaxies (§4.6). The surface brightness profiles of ULIG hosts also follow the $\mu_e - r_e$ projection of the fundamental plane of nearby ellipticals, but considerable scatter is present (§4.5; Fig. 19). The average r_e of the 1-Jy ULIGs (4.80 ± 1.37 kpc at R and 3.48 ± 1.39 kpc at K') are fairly typical of intermediate-luminosity ellipticals (e.g., Kormendy & Djorgovski 1989; Bender et al. 1992; Faber et al. 1997). We mentioned in §4.5 that residuals from the PSF subtraction may artificially increase the values of the average surface brightness within half-light radius (the half-light radius may also be slightly *underestimated*). This effect is likely to be at the origin of some of the scatter in Figure 19 and may also explain why some Seyfert 1 hosts in our sample lie signif-

icantly above the $\mu_e - r_e$ relation of ellipticals. Dust extinction and emission and circumnuclear star formation are other likely sources of scatter in this diagram.

Given the recent violent merger events in ULIGs, it is perhaps surprising to find that *any* of these galaxies follow the $\mu_e - r_e$ of ellipticals. This result brings support to numerical simulations which show that violent relaxation in dissipative gas-rich merger systems is very efficient. A general rule of thumb pointed out by Mihos (1999) is that “violent relaxation and/or dynamical mixing occurs on a few rotation periods *at the radius in question*.” This time scale is only $\sim 10^8$ yrs in the central (\lesssim kpc) regions of the mergers, but exceeds 10^9 yrs in the outer (\gtrsim a few r_e) regions. Indeed, while the central regions of many ULIG hosts appear to mimic those of elliptical galaxies, the effects of the mergers still appear to be visible beyond a few r_e as illustrated by the broad range of boxiness values measured in ULIG elliptical-like hosts of the 1-Jy sample (§4.6; Fig. 23). The large fraction (26%) of ULIG hosts which are not fit adequately by either an exponential or de Vaucouleurs profile is another indication that the light distribution in several objects may still be showing the effects of the recent mergers (patchy dust distribution could also explain these results).

It will be important in the future to obtain deep high-resolution ($\lesssim 100$ pc) images of the 1-Jy ULIGs in both the visible and near-infrared domains to improve on our AGN/PSF subtraction and determine if the ULIG host galaxies are power-law or core galaxies with properties that are consistent with the photometric portion ($\mu_e - r_e$) of the core and global fundamental planes of early-type galaxies (e.g., Faber et al. 1997). Multi-color maps combined with detailed radiative transfer models will be particularly useful in these objects to help disentangle the effects of dust extinction and emission and circumnuclear star formation on this scale (see, for instance, Regan, Vogel, & Teuben 1995). ULIGs are known to have sub-kpc nuclear concentrations of molecular gas with mean surface densities similar to the stellar densities measured in the cores of ellipticals (a few $\times 10^4 M_\odot \text{ pc}^{-2}$; e.g., Bryant & Scoville 1999; Downes & Solomon 1998). If *post*-ULIG hosts are indeed genuine ellipticals, one might therefore expect the hosts of current star-forming ULIGs to have *lower* stellar densities than the core densities of classical ellipticals. This effect could be significant since the star formation rates of ULIGs are \sim few $\times 100 M_\odot \text{ yr}^{-1}$ and the ULIG phase may last $10^7 - 10^8$ years. The effect at large radii should be less important because most of the star formation (and AGN) activity in ULIGs is concentrated well within the central kpc (e.g., Soifer et al. 2000, 2001).

Given that merger systems are expected to reach their equilibrium values of light distribution and kinematics on a short time scale (e.g., Mihos 1999; Bendo & Barnes 2000), the kinematic properties of ULIGs should also follow the fundamental plane of ellipticals. Considerable efforts have been invested in recent years to constrain the stellar kinematics in the cores of luminous infrared mergers (e.g., Doyon et al. 1994; Shier & Fisher 1998; James et al. 1999; Genzel et al. 2001). The advent of powerful new near-infrared spectrographs on 8-meter class telescopes now allows the radial profiles of the velocity dispersion and rotation velocity to be measured in the brightest systems and compared with those of elliptical galaxies. Most relevant to our study of the 1-Jy ULIGs are the results from Genzel et al. (2001) since they refer to ULIGs while those of Shier & Fisher (1998) and James et al. (1999) refer to systems of lower luminosities. Genzel et al. (2001) find that random

motions dominate the stellar dynamics in the cores of their (12) systems, but that significant rotation is also common. The properties of these galaxies closely resemble those of intermediate-mass ($\sim L^*$), disk ellipticals. These results are consistent with ours in the fact that they rule out giant ($\gtrsim 3.5 L^*$) ellipticals with large cores and little rotation as the hosts of ULIGs. A more quantitative comparison is difficult due the broad range of photometric properties found in the 1-Jy sample and the relatively small size of the kinematic sample of Genzel et al. Recently commissioned three-dimensional spectrographs on large telescopes should provide the sensitivity and two-dimensional spatial coverage needed to derive detailed kinematic maps for several more ULIG hosts, and therefore allow more robust comparisons with our results.

5.3. Are Ultraluminous Infrared Galaxies Quasars in Formation?

The results presented in §2 and §3 indicate clear trends between merger phase, *IRAS* colors, and the importance of AGN activity in ULIGs (in addition to the trend between infrared luminosity and merger phase, which has already been discussed in §5.1). Objects with warm quasar-like infrared colors (as measured by the *IRAS* 25 $\mu\text{m}/60 \mu\text{m}$ flux ratio) present strong signs of AGN-dominated activity at both optical and mid-infrared (*ISO*) wavelengths and are generally found in advanced mergers (based not only on the apparent nuclear separation but also on the overall morphology of the system including the shape and compactness of the nuclear core and the strengths and lengths of the tidal tails). These trends are consistent with an evolutionary sequence in which cool starburst-dominated ULIGs transform into warm AGN-dominated ULIGs as the merger of the two $\sim 0.9 L^*$ galaxies takes place.

It is clear that exceptions to these general trends with merger phase abound in the 1-Jy sample. For instance, 46% of the 41 advanced mergers (classes IVb and V in §3.4) in our sample show no obvious signs of Seyfert activity (see Fig. 10). There are also seven Seyfert 2 nuclei (but no Seyfert 1s) among the 45 pre-mergers (classes IIIa and IIIb). The cases of an isolated AGN with a spiral galaxy host and a widely separated pair with an AGN were mentioned in §5.1. Although merger phase appears to be an important factor in determining the relative importance of star formation and AGN activity in ULIGs, it is not the only one (see the discussion in Farrah et al. 2001). Star formation activity depends on the molecular gas supply and the efficiency to transform this gas into stars (which is a complicated function of density, metallicity, magnetic field strength, local gas kinematics, etc.). On the other hand, the level of AGN activity in ULIGs depends linearly on the local mass accretion rate onto the supermassive black holes that are presumed to exist in these objects, and the efficiency of the system to transform the gravitational energy into radiation that can escape the system and be detected by our instruments. One only needs an accretion rate of $\sim 1 M_\odot \text{ yr}^{-1}$ to produce the infrared (bolometric) luminosity of a ULIG (assuming a radiative efficiency of 10% in rest-mass units). Given the complexity of the star formation and AGN phenomena it is not surprising to see large scatter in the correlations between merger phase and AGN activity. Note, however, that a late merger phase appears to be a necessary condition to trigger powerful Seyfert 1 (= quasar) activity. Our results emphasize the importance of studying a large and homogeneous set of ULIGs like the 1-Jy sample to draw statistically meaningful conclusions on these objects. The

problems of small sample sizes and/or inhomogeneous selection criteria have plagued many studies of luminous infrared galaxies in the past.

The natural end-result of the merger sequence described in the first paragraph is an object with quasar-like colors and luminosities that shows only slight residual effects from the merger. This object has several properties in common with nearby quasars. A summary of the properties of quasar host galaxies is beyond the scope of this paper. Suffice it to say that evidence for galaxy interactions and mergers is seen in some but not all nearby quasars (see, e.g., Hutchings & Neff 1992; Hutchings et al. 1994; Disney et al. 1995; Bahcall et al. 1997; Stockton 1999; Dunlop et al. 2002 and references therein). The present discussion focusses on the so-called infrared-excess quasars since they are particularly good candidates for transition objects which have just gone through a ULIG phase and are now in the process of settling in to become optical quasars. These objects show morphological evidence for recent mergers (e.g., Surace et al. 2001 and references therein), contain large quantities of molecular gas (e.g., Evans et al. 2001 and references therein), and sometimes present spectroscopic evidence for substantial gas outflows (e.g., BAL phenomenon, Lipari, Colina, & Macchetto 1994). The host galaxies of these infrared-excess quasars have luminosities and colors which are similar to those of the 1-Jy ULIGs (§4.2 and §4.3). In a series of papers, Canalizo & Stockton (2000a, 2000b, 2001) have shown that these “transition” quasars show strong recent star-forming activity, which in most case is directly related to the tidal interaction. The ages they derive for the starburst populations range from currently active star formation in some objects to poststarburst ages ~ 300 Myr in others. They argue for a direct connection between interactions, starbursts, and QSO activity.

The issue of the hosts in ULIGs and quasars is important and deserves further attention. If these two classes of objects are indeed related, then they should have similar host galaxy properties, modulo possible evolutionary effects. In §4.2, we found good agreement between the host luminosities of the 1-Jy ULIGs and those of infrared-excess quasars (Surace et al. 2001) and optical quasars from the sample of McLeod & Rieke (1994b; McLeod & McLeod 2001), but less so when comparing with the sample of radio-quiet and radio-loud quasars of Dunlop et al. (2002). Morphological classification of the hosts in ULIGs indicates a preponderance of elliptical-like hosts among single-nucleus systems (§4.1 and §5.2), a result which is at least qualitatively consistent with the conclusions of Dunlop et al. (2002; note that the conclusions of McLeod & McLeod 2001 are ambiguous in this respect). We also found that the half-light radii of the 1-Jy ULIG hosts are similar to those found by McLeod & McLeod (2001), but significantly smaller than those measured by Dunlop et al. (2002). The half-light surface brightnesses of ULIG hosts at R also appear to be slightly brighter than those measured by Dunlop et al. (McLeod & McLeod 2001 do not tabulate this quantity in their paper).

It is not clear at present whether the differences found between our results and those of Dunlop et al. are significant. Many effects may complicate the interpretation of our data. Excess R -band emission from circumnuclear starbursts, known to be common in ULIGs (e.g., Veilleux et al. 1995) but less so among classical quasars, could explain the brighter μ_e in ULIG hosts but may have difficulties explaining the $\sim 50\%$ difference in r_e between the ULIG hosts and the quasar hosts of Dunlop et al. (2002). As discussed in §5.2, residuals from the AGN

subtraction may also artificially brighten the half-light surface brightnesses and decrease the half-light radii in our sample but this effect is not thought to be sufficient to reconcile our results with those of Dunlop et al. (2002). The apparent lack of agreement between McLeod & McLeod (2001) and Dunlop et al. (2002) in terms of the half-light radii suggests that the quasar results may depend on sample selection (although these two samples have similar mean redshifts, $\langle z \rangle = 0.2$, and luminosities) or the methods of observations (R -band versus H -band HST imaging). On-going adaptive optics imaging studies of quasar hosts (e.g., Guyon 2002, in prep.) will increase the sample size and will span a broader range in quasar properties; the results from these studies should settle this issue within the next few years.

In §4.2, we mentioned the existence in our data of slight trends between host luminosities, $IRAS\ 25\ \mu m/60\ \mu m$ colors, and nuclear optical spectral types. The most straightforward explanation for these trends is that quasar activity generally requires the mergers of massive ($\gtrsim L^* + L^*$) progenitors. However, this scenario has difficulties explaining the fact that the trends appear to be stronger at K' than at R . Given the presence of circumnuclear starbursts in many of these objects (e.g., Veilleux et al. 1995; Kim et al. 1998), it is possible that these starbursts contribute significantly to the host luminosities, perhaps more so in warm Seyfert galaxies than in the cooler objects. If the effect is to be more significant at K' than at R , then the starburst age has to be \gtrsim a few $\times 10^7$ yrs at which point the K' luminosity is dominated by young, red supergiants (Bruzual & Charlot 1993; Leitherer et al. 1999). Another possible explanation, also discussed in §4.2, is that the trends are due to errors in the PSF subtraction, which are more likely to affect the warm highly nucleated Seyferts than the cooler more diffuse LINERs and H II region galaxies, and are more severe at K' than at R . An object-by-object comparison with the H -band adaptive-optics results of Surace & Sanders (1999) was carried out in §4.2 and seems to indicate a slight luminosity offset for the few warm Seyferts in common between the two samples. Needless to say, it will be important to expand the sample of warm ULIGs observed with adaptive optics or with HST to refine the measurements of the host luminosities in these objects and verify the trends detected in our data.

6. CONCLUSIONS

An R - and K' -band atlas of the $IRAS$ 1-Jy sample of 118 ULIGs was presented in a companion paper (Kim, Veilleux, & Sanders 2002). The present paper discusses the results from the analysis of these images and combines them with the results from published spectroscopic studies of ULIGs at optical, near-infrared, and mid-infrared wavelengths as well as new Keck spectroscopy. The results on the 1-Jy sample are compared with those from optical and near-infrared studies of quasars and normal ellipticals. The main conclusions are as follows:

1. All but one object in the 1-Jy sample show signs of a strong tidal interaction/merger in the form of distorted or double nuclei, tidal tails, bridges, and overlapping disks. Interactions involving more than two galaxies are seen in only 5 (4%) of the 118 systems. These results confirm those of previous studies.
2. Objects with red $R-K'$ colors and large nuclear-to-total luminosity ratios show a tendency to host Seyfert nu-

- clei, have warm *IRAS* 25 $\mu\text{m}/60 \mu\text{m}$ colors and be AGN-dominated according to the *ISO* classification scheme.
3. Using a classification scheme first proposed by Surace (1998) and based on the results of published numerical simulations of the mergers of two galaxies, we classified the 1-Jy sources according to their overall morphology and apparent nuclear separations. None of the 1-Jy sources appears to be in the early stages (first approach or first contact) of a merger. Most (56%) of them harbor a single disturbed nucleus with and without tidal tails; they are therefore in the late stages of a merger. The fraction of advanced mergers with a single nucleus increases above infrared luminosities of $10^{12.5} L_{\odot}$ and decreases below $10^{12} L_{\odot}$.
 4. The strengths of the $H\beta$ and Mg Ib stellar features measured in the nuclei of ULIGs are not particularly good indicators of the merger phase or epoch of the merger event.
 5. All Seyfert 1s and most of the Seyfert 2s are advanced mergers, either based on their overall morphology or their small (< 5 kpc) nuclear separations. A similar result is found when we consider the warm objects with $f_{20}/f_{60} > 0.2$ or the AGN-dominated objects based on *ISO* classification. LINERs and H II region-like galaxies show no preference between pre-merger and advanced merger phases.
 6. The individual galaxies making up the binary systems of the 1-Jy sample show a broad distribution in host absolute magnitudes (luminosities) with a mean of -21.02 ± 0.76 mag. ($0.85 \pm_{0.43}^{0.86} L^*$) at R and -23.98 ± 1.25 mag. ($0.90 \pm_{0.61}^{1.94} L^*$) at K' , and a luminosity ratio at R or K' generally less than ~ 4 . The hosts of single-nucleus ULIGs have mean absolute magnitudes (luminosities) of -21.77 ± 0.92 mag. ($1.69 \pm_{0.97}^{2.25} L^*$) at R and -25.03 ± 0.94 mag. ($2.36 \pm_{1.38}^{3.24} L^*$) at K' . These magnitudes are similar to those found in previous studies of ULIGs, except those derived from shallow *HST* snapshots which underestimate the contribution from low surface brightness features. Correlations are observed between host galaxy luminosity and infrared luminosity, *IRAS* 25 $\mu\text{m}/60 \mu\text{m}$ color, and optical spectral type. The trend with infrared luminosity is due to a redshift bias. There is considerable overlap between the host galaxy luminosity distribution of single-nucleus ULIGs and that of quasars, although the hosts of the quasars studied by Dunlop et al. (2002) are slightly more luminous on average than the 1-Jy ULIG hosts. This luminosity shift is not observed when comparing with the results of McLeod & McLeod (2001) and Surace et al. (2001). The $R-K'$ colors of ULIG hosts are similar to those of quasars.
 7. An analysis of the surface brightness profiles of the host galaxies in single-nucleus ULIGs reveals that about 35% and 2% of the R and K' surface brightness profiles are fit adequately by an elliptical-like $R^{1/4}$ -law and an exponential disk, respectively. Another 38% are equally well fit by either an exponential or an elliptical-like profile. The remainder (26%) of the single-nucleus sources cannot be fit with either one of these profiles. Combining these results, we find that a de Vaucouleurs profile is an adequate fit to $\sim 73\%$ of the single-nucleus ULIGs in the 1-Jy sample. These elliptical-like hosts are most common in merger remnants with Seyfert 1 nuclei (83%), Seyfert 2 characteristics (60%) or mid-infrared (*ISO*) AGN signatures (80%).
 8. The hosts of ULIGs have half-light radii ($\langle r_e \rangle = 4.80 \pm 1.37$ kpc at R and $\langle r_e \rangle = 3.48 \pm 1.39$ kpc at K') which are similar to those measured by McLeod & McLeod (2001) in quasar hosts, but are significantly smaller than the quasar hosts studied by Dunlop et al. (2002). The origin of this apparent discrepancy between the two quasar datasets is not clear at present. The hosts of 1-Jy systems follow with some scatter the $\mu_e - r_e$ relation of normal ellipticals (especially if Seyfert 1s are excluded from the analysis due to possible AGN residuals). The distributions of luminosities, R -band axial ratios, and half-light radii in single-nucleus ULIGs are also similar to those of normal ellipticals of intermediate luminosities. The results at K' are more uncertain because of the smaller sample size and possible PSF subtraction residuals. Elliptical-like hosts in the 1-Jy sample show a broader range of boxiness values than normal ellipticals.
 9. Results #7 and #8 provide strong support to the idea that some of the ultraluminous infrared mergers in the 1-Jy sample may eventually become intermediate-luminosity elliptical galaxies under the condition that they get rid of their excess gas or transform this gas into stars. The significant fraction of single-nucleus ULIGs with ambiguous surface brightness profiles or with large boxiness parameters indicate that these objects are still feeling the effects of the recent mergers. These results confirm the predictions of numerical simulations that violent relaxation is very efficient at the center of the merger but less so in the outer regions.
 10. The results from this study are generally consistent with the evolutionary scenario in which ULIGs are the results of a merger of two gas-rich galaxies which first goes through a starburst-dominated pre-merger phase when the system is seen as a binary, next reaches a dust-enshrouded AGN-dominated merger phase once the two nuclei have merged into one, and then finally ends up as an optical (post-ULIG) AGN where the host is elliptical-like and shows only limited signs of the merger. However, our results also indicate that many ULIGs in the 1-Jy sample may not follow this exact scenario. For instance, approximately 46% of the 41 advanced mergers in the 1-Jy sample show no obvious signs of Seyfert activity, while seven of the 45 pre-mergers already show Seyfert 2 (but not Seyfert 1) activity. The possible correlations between host luminosities, *IRAS* 25 $\mu\text{m}/60 \mu\text{m}$ color, and optical spectral types may add another twist to the merger scenario, suggesting that merger-induced quasar activity may require the merger of massive ($\gtrsim L^* + L^*$) galaxies. These trends may also be due to a brightening of the circumnuclear starburst in the hosts of the warm Seyfert ULIGs. However, one needs to be cautious when interpreting these apparent trends because of the difficulty associated with removing the contribution of the central AGN in some of the warm Seyfert ULIGs.

Deep near-infrared *HST* and adaptive-optics imaging of ULIGs and quasars will help further clarify the nature of their host galaxies. These observing techniques should be applied to a large sample of warm ULIGs to refine the PSF subtraction in these objects and verify the possible trends with host luminosities reported in the present paper. The spatial resolution of the data presented here is not sufficient to determine the core properties of the elliptical-like ULIG hosts and the bulge-to-disk ratio of the galaxies in the pre-merger phase. Both high spatial resolution and large dynamic range will be needed to fully characterize the host galaxies of these ULIGs. A similar program should be carried out on the classical quasars to help us understand the apparent inconsistencies between the various quasar datasets. Finally, three-dimensional spectrographs on large telescopes will provide the sensitivity and two-dimensional spatial coverage needed to derive detailed kinematic maps in several elliptical-like ULIG hosts. Comparisons with data on normal old (low- z) and young (high- z) ellipticals will help quantify the similarities and differences between these two classes of objects.

We acknowledge the help from Jim Deane, Aaron Evans, Cathy Ishida, and Joe Jensen in acquiring some of the images presented in the companion paper. The authors thank Jason Surace for many useful discussions, comments, and suggestions which have greatly improved this paper. We also thank Dave Rupke who carried out the reduction of the Keck/ESI spectra. Helpful conversations with Reinhard Genzel, Richard Green, John Kormendy, and Tod Lauer are also acknowledged. We thank the anonymous referee for a prompt and thorough review. S.V. is grateful for partial support of this research by NASA/LTSA grant NAG 56547. D.C.K. acknowledges financial support from the Academia Sinica in Taipei and the BK21 project of the Korean Government. D.B.S. gratefully acknowledges the hospitality of the Max-Planck Institut for Extraterrestrische Physik and is grateful for support from a senior award from the Alexander von Humboldt-Stiftung and from NASA JPL contract 961566. This work has made use of NASA's Astrophysics Data System Abstract Service and the NASA/IPAC Extragalactic Database (NED), which is operated by the Jet Propulsion Laboratory, California Institute of Technology, under contract with the National Aeronautics and Space Administration.

Appendix A: Notes on Individual Objects

In this Appendix, we briefly discuss the rationale behind the interaction classification of the 1-Jy sample presented in Table 1 and discussed in §3.4. For this task, we used the R and K' images presented in Figure 1 of Paper I and new long-slit spectra obtained on 2000 March 30 – 31 and 2001 January 22 – 23 using Keck II with the Echellette Spectrograph and Imager (ESI) in the prism mode. This configuration produces 4000 – 9000 Å spectra with a dispersion that ranges from 50 to 300 km s⁻¹ pix⁻¹. Accurate wavelength calibration was derived by fitting a 9th-order Chebychev polynomial to the line positions of xenon and mercury-neon lamps observed with the same setup as that of the objects. The redshifts derived from these data are generally accurate to within ± 0.001 (1σ). This is not accurate enough to allow us to make any statement about the relative motion of galaxies in a system but it allows us to determine companionship and group membership. The exposure times were typically 10 minutes for each slit position. Systems for which we obtained long-slit ESI spectra are indicated by an asterisk.

- *F00091–0738* (IIIb): This system is a close pair with apparent nuclear separation of only 2.1 kpc. The two nuclei are more easily visible in the K' image.

- *F00188–0856** (V): This is a single-nucleus system with slight distortions in the outer isophotes. The bright source south of the nucleus is a star.

- *F00397–1312* (V): This is a single-nucleus system with elongated nuclear isophotes and distorted outer isophotes.

- *F00456–2904* (IIIa): The redshift of the north-east component of this pair is unknown. A broad tidal tail is apparent on the north-east galaxy and a shorter one extending to the north-west is apparent on the main galaxy.

- *F00482–2721* (IIIb): This is a relatively close pair with apparent nuclear separation of 6.7 kpc. The “wisp” to the south-west is barely apparent in the K' image and appears to be unrelated to the pair. The redshift of this feature is unknown.

- *F01004–2237* (V): This is a highly nucleated source with slight distortions in the outer isophotes (see *HST* image of Surace et al. 1998).

- *F01166–0844* (IIIb): This is a classic looking pair with a moderately large nuclear separation of 9.8 kpc and a prominent tidal tail extending to the north of the north-west component.

- *F01199–2307** (IIIa): This is a pair of emission-line galaxies separated by 20.3 kpc. The north-east companion has the same redshift as the main component (0.155 versus 0.156, respectively). A faint tidal tail is visible on the west side of the main component, and material also appears to bridge the binary.

- *F01298–0744** (IVb): The *IRAS* source is the distorted object to the north-east. This object harbors two prominent tidal tails, signs of a recent merger. The galaxy to the south-west shows no sign of interaction and has an absorption-line spectrum with a redshift of 0.188 instead of 0.136 for the *IRAS* source.

- *F01355–1814** (IIIb): This object is classified as a close pair based on the separation (5.8 kpc) between the centroid of the bright south-east (SE) component and the fan-like north-west (NW) component. The feature to the south-east of this pair appears to be a star-forming tidal feature based on the fact that it is barely visible at K' . All three features have emission-line redshifts of 0.191 to within ± 0.001 . Deep multi-band imaging or spectroscopy will be needed to confirm the nature of the faint south-east feature; the existence of an old underlying stellar population in this object would require changing the classi-

fication of this system to a triplet.

- *F01494–1845** (IVa): This diffuse single-nucleus source shows a broad tidal feature to the north-west. The faint object to the south-east is a star while the elongated source to the north is an emission-line galaxy at the same redshift as the *IRAS* source. The compact source to the east of the elongated galaxy is a broad-lined quasar with redshift of ~ 1.62 based on the identifications of the C IV $\lambda 1549$, C III] $\lambda 1909$, and Mg II $\lambda 2798$ features.

- *F01569–2939* (IVa): This highly distorted source harbors a narrow tidal tail stretching over 55 kpc. A shorter counter-tail is also probably present on the west side of the object.

- *F01572+0009 = Mrk 1014* (IVb): This single-nucleus source presents two curved tidal features extending 46 kpc (also see Surace et al. 1998).

- *F02021–2103* (IVa): This highly distorted object presents two symmetric tidal features.

- *F02411+0353** (IIIb): This apparently complex system at R is a close (7.1 kpc) pair at K' . The north-east (NE) component presents a fan-like tidal feature extending to the east. Keck spectroscopy has confirmed the physical interaction between the NE and SW components ($z = 0.144$ and 0.143, respectively). The compact source near the western edge of the R -band field appears to display a very faint feature extending to the south and therefore may not be a star.

- *F02480–3745* (IVa): This single-nucleus object presents two symmetric tidal features extending over 27 kpc.

- *F03209–0806* (IVb): This compact object harbors spectacular tidal tails extending over 61 kpc.

- *F03250+1606** (IVb): This object shows weak tidal features to the north and south-east of the nucleus. The faint compact object near the eastern edge of the field of view is a star, and the same also appears to be true for the other compact object west of the star. The compact object (labelled “G”) to the south-west has the same redshift (both emission and absorption lines) as the *IRAS* source, but shows no sign of interaction.

- *FZ03521+0028* (IIIb): This is a close pair separated by only 3.5 kpc.

- *F04074–2801** (IVa): This source is highly distorted. A tidal feature is seen extending ~ 28 kpc north of the nucleus. The two galaxies to the north-west and north-east of the *IRAS* source show no signs of interaction but are at the same emission-line redshift as the *IRAS* source to within the measurement uncertainties.

- *F04103–2838* (IVb): This compact source presents two short curved tidal features extending 8 kpc.

- *F04313–1649* (IVa): This is a classic merger remnant with two large tidal tails extending 59 kpc.

- *F05020–2941** (IVa): The *IRAS* source is the distorted source with short tidal tails to the south and north-west. The bright source to the east is a star. No obvious emission or absorption feature was detected in the faint diffuse object between the star and the *IRAS* source.

- *F05024–1941** (IVa): The *IRAS* source is the distorted source near the center of the image. A tidal feature is clearly visible on the west side of this object. The east source is a bright star.

- *F05156–3024* (IVb): This single-nucleus object presents a short tidal feature to the south.

- *F05189–2524* (IVb): This compact galaxy has a faint curved tidal feature to the north-west (refer to Surace et al. 1998 for a high-resolution *HST* image of this object).

- *F07599+6508* (IVb): The *IRAS* source lies to the south-east in this field, and presents faint tidal features on the west and south sides (more easily visible in the images of Surace 1998). The other bright source in the field is a star.

- *F08201+2801** (IVa): This object harbors a broad tidal tail that extends over 25 kpc. The spectrum of the faint source to the north-west presents faint [O II] $\lambda 3727$ emission at the same redshift as the *IRAS* source, but it is not clear whether the emission really originates in the north-west source; it may be contamination from the diffuse tidal feature surrounding the *IRAS* source. No obvious emission or absorption feature was detected in the southern object.

- *F08474+1813** (V): This apparently complex system comprises the *IRAS* source to the west and two stars to the south-east and north-east of this source. No obvious tidal tail is apparent in the *IRAS* source.

- *F08559+1053** (IVb): A diffuse tidal tail seems to emerge from the south-west side of the bright galaxy. The two galaxies to the west of the brighter source have the same emission-line redshifts as that of the main source to within ± 0.001 , but show no sign of interaction with the main object. This system is therefore classified as a single-nucleus source, and the other two galaxies are considered (non-interacting) group members.

- *F08572+3915* (IIIb): This is a well-known interacting pair separated by 5.7 kpc (e.g., Sanders et al. 1988a,b; Armus et al. 1990; Surace et al. 1998).

- *F08591+5248** (V): The *IRAS* source to the east is a compact object with slightly distorted isophotes but no obvious tidal tails. The source to the west is a faint emission-line galaxy at the same redshift as the *IRAS* source ($z = 0.157$), but it shows no sign of interaction.

- *F09039+0503* (IVa): This is a single-nucleus system with a prominent curved tidal tail extending 24 kpc to the east.

- *F09116+0334** (IIIa): The compact source located east of the bright Seyfert 2 nucleus is a small absorption-line galaxy at the same redshift as the Seyfert galaxy. Tidal features are seen to the east and west of the Seyfert galaxy.

- *F09463+8141* (IVa): This source appears to be a pair at *R* but the *K'* image shows that it is in fact a single nucleus with a prominent tidal tail extending out to 76 kpc to the west.

- *F09539+0857* (V): This compact object has distorted outer isophotes but shows no obvious tidal tails.

- *F10035+2740* (IVa): This object appears to be double at *R* but the *K'* image shows that it is in fact a single nucleus with a prominent tail extending out to 54 kpc to the north. The redshift of the bright galaxy to the south-west is unknown; it shows no obvious sign of interaction with the main object.

- *F10091+4704* (IVa): This highly distorted source presents two complex tidal features to the south and north-west of the nucleus. The southern feature presents a luminous knot at *R* which is not apparent at *K'*.

- *F10190+1322* (IIIb): This is a close (5.5 kpc) pair with weak tidal features. The compact source to the south is star.

- *F10378+1108* (IVb): This single-nucleus source presents broad tidal features extending to the north and south.

- *F10485-1447** (IIIa): Stars complicates the classification of this system. The two brightest stars in the field have been confirmed spectroscopically. The identification of the third one located next to the galaxy labelled “E” is based on its unresolved point spread function. The eastern (absorption-line) and western (emission-line) components have similar redshifts ($z = 0.133$). Tidal features seem to emanate from the western com-

ponent and one of them possibly creates a bridge with the eastern component. This interpretation is not unique, however. It is possible that the eastern component is not interacting with the western component and that the apparent “bridge” is instead a second tidal feature from the western component as a result of an earlier merger.

- *F10494+4424* (IVb): This object presents two peculiar “spikes” to the north which are presumably of tidal origin and a fainter diffuse feature to the south-west.

- *F10594+3818* (IIIb): This close (4.4 kpc) pair shows prominent tidal tails extending out to 90 kpc to the west. The bright source to the west is a star.

- *F11028+3130* (IVa): This single-nucleus source shows a broad tidal feature to the west.

- *F11095-0238* (IVb): A prominent curved tidal tail is visible to the north of this compact source. The high-resolution *H*-band image of Bushouse et al. (2002) reveals an interesting double core in this object. However, as mentioned in their paper, it is not clear whether the double core represents two galactic nuclei or a single nucleus bisected by a dust lane. This is the reason why this object is classified as a late merger (IVb) rather than a close binary (IIIb).

- *F11119+3257* (IVb): This compact source shows an interesting bootlegged tidal feature to the east.

- *F11130-2659* (IVa): This single-nucleus system presents a complex tidal feature to the north-west and a shorter feature to the south-east.

- *F11180+1623** (IIIa): The *IRAS* source is the wide (21.8 kpc) pair of galaxies to the south-east in this field. The emission lines in the spectrum of the western component in this pair are quite faint. No spectrum was obtained of the two galaxies labelled “G”.

- *F11223-1244* (IIIa): This source is conservatively classified as a very widely separated (88 kpc) pair. The redshift of the eastern component is unknown. The signs of interaction in the eastern component are very slight and it is possible that the tidal features of the western component were caused instead by an earlier galaxy merger.

- *F11387+4116* (V): This compact source shows slight outer isophotal distortions. The redshifts of the two faint sources north-west of the nucleus are not available.

- *F11506+1331* (IVb): This is a single-nucleus object with two symmetric tidal tails to the east and west of the nucleus. The nature of the object to the south is unknown, but does not appear to participate in an interaction.

- *F11582+3020* (V): The *IRAS* source is the distorted object on the east in this field. The compact object to the west is a star, and the other two diffuse sources (labelled “G”) are galaxies with redshifts similar to that of the *IRAS* source but they show no sign of interaction with it.

- *FZ11598-0112* (IVb): The *IRAS* source is the object in the middle of the field with two prominent tidal tails extending out to 12 kpc. The redshift of the galaxy to the north is unknown.

- *F12018+1941* (IVb): The *IRAS* source presents two symmetric tidal tails.

- *F12032+1707* (IIIa): The *K'* image of this object reveals the presence of two interacting galaxies separated by 12.0 kpc.

- *F12072-0444* (IVb): This single-nucleus source presents a curved tidal tail to the south and a shorter feature to the north-west (see high-resolution image of Surace et al. 1998).

- *F12112+0305* (IIIb): This peculiar-looking object is a close pair separated by 3.8 kpc. A bright tidal tail is present

in the *R*-band image.

- *F12127–1412** (IIIa): The members of this widely separated (21.9 kpc) pair have similar emission-line redshifts ($z = 0.133$) although the emission lines in the north-east component are considerably stronger than those in the south-west component

- *F12265+0219 = 3C 273* (IVb): This object is highly nucleated, but shows a thick tidal feature towards the north-east and a very faint feature to the north-west (e.g., Tyson, Baum, & Kreidl 1982). The faint linear feature emerging to the south-west is the well-known optical jet in this system (e.g., Bahcall et al. 1995).

- *F12359–0725** (IIIa): This apparent triplet is made of a widely separated pair (labeled “N” and “S”; separated by 22.9 kpc) and of a background galaxy at $z = 0.396$ to the west.

- *F12447+3721* (IVa): This diffuse object shows broad tidal features to the east and north-west.

- *F12540+5708 = Mrk 231* (IVb): This object is made of a compact nucleus surrounded by a diffuse tidal complex (e.g., Surace et al. 1998).

- *F13106–0922** (IVa): The *IRAS* source is the highly distorted source to the north-east in this field with a very long (82 kpc) tidal tail. The source north of the *IRAS* source is a star and so is the source to the west.

- *F13218+0552** (V): This is a highly nucleated source with no obvious tidal tails. The compact object to the south-west of the *IRAS* source appears to be a background absorption-line galaxy at $z = 0.23$ although additional data are needed to confirm this redshift.

- *F13305–1739** (V): This highly nucleated galaxy shows slight isophotal distortions. Our spectrum of the compact source to the north-west is not of sufficient quality to determine the nature and redshift of this object.

- *F13335–2612* (IIIb): The two nuclei in this close (3.2 kpc) pair are more easily visible in the *K'* image.

- *F13342+3932** (IVb): This object is misclassified as an interacting group by Borne et al. (2000). The *IRAS* source is in the middle of the field. The galaxy to the north-east (labelled “G”) has an emission-line redshift of 0.180, very similar to that of the *IRAS* source. However, it shows no sign of interaction with the *IRAS* source. The elongated galaxy to the north-west lies in the foreground at $z = 0.165$. No redshift is available for the other galaxy to the north-west.

- *F13428+5608* (IVb): This merger remnant harbors a spectacular tidal tail which extends out 31 kpc to the south.

- *F13443+0802** (Tpl) All three objects in the field are emission-line galaxies with similar redshifts ($z = 0.135$). A bridge of material may be present between the eastern binary and the south-west component.

- *F13451+1232* (IIIb): This is a well-known pair separated by 4.0 kpc (e.g., Surace et al. 1998; Evans et al. 1999).

- *F13454–2956* (IIIa): A tidal tail appears to emerge south-west of the southern component in this widely separated (15.8 kpc) pair.

- *F13469+5833* (IIIb): This close (4.3 kpc) pair shows prominent curved tidal tails to the north-east and south-west.

- *F13509+0442** (IVb): The *IRAS* source is at the center of the field and shows a prominent tidal tail which extends 15 kpc to the south. The galaxy near the northern edge of the field of view is a background emission-line galaxy at $z = 0.188$. The object to the south-west of the *IRAS* source is a star.

- *F13539+2920* (IIIb): This relatively close (7.0 kpc) pair presents a strong tidal feature to the north which gives the appearance of a third nucleus in the *R*-band image (or *I*-band *HST* image of Cui et al. 2001). This feature is barely apparent in the *K'* image.

- *F14053–1958* (IIIb): This very close (1.5 kpc) pair is barely resolved in the *K'* image and presents two tidal features to the north and south.

- *F14060+2919* (IVa): This is a highly distorted source with a strong linear tidal feature to the north-east surrounded by a diffuse envelope of material. A single nucleus is observed in this object at *K'*. This object is misclassified as multiple (> 2) by Cui et al. (2001).

- *F14070+0525* (V): This compact object shows no obvious tidal features but has disturbed isophotes.

- *F14121–0126* (IIIb): This moderately close (9.1 kpc) pair shows a prominent curved tidal tail to the north-west and a fainter feature which seems to emerge from the southern component. The compact source to the south-west appears to be a star based on its unresolved point spread function.

- *F14197+0813* (V): A star to the north is superposed on the body of this object. There is no evidence for tidal tails in this object.

- *F14202+2615* (IIIa): The *IRAS* source is the pair of galaxies to the north. The redshift of the southern galaxy is unknown but since it shows no obvious sign of interaction with the pair, we classify this system as a pair instead of a triplet (Cui et al. 2001).

- *F14252–1550* (IIIb): This appears to be a moderately close (8.3 kpc) pair with a fairly large luminosity ratio of ~ 8 at *K'*.

- *F14348–1447* (IIIb): This is a close (4.8 kpc) binary with distinct tidal features to the north and south of the galaxies. The compact source near the eastern edge of the field is a star based on its unresolved point spread function.

- *F14394+5332* (Tpl) This system is classified as a triplet because the eastern component has two close (2.6 kpc) nuclei and a prominent tidal feature appears to bridge the eastern and western components. However, we have no confirmation that the two components lie at the same distance.

- *F14485–2434* (IVb): The *IRAS* source lies west of the field center. The redshift of the galaxy to the north-east is unknown; it shows no sign of tidal disturbance.

- *F15001+1433** (Tpl) This object is classified as a triplet because the tidal feature west of the eastern component appears to point towards the other two western sources. One of these (labelled W in Fig. 1 of Paper I) has the same redshift as the main component ($z = 0.162$). The low signal-to-noise of the spectrum for the westernmost (WW) component does not allow us to confirm its physical connection with the other galaxies in the system.

- *F15043+5754* (IIIb): This is a close (5.1 kpc) double with short and stubby tidal features.

- *F15130–1958* (IVb): This single-nucleus source has two tidal features extending to the north and south over 14 kpc.

- *F15206+3342* (IVb): This is a relatively compact source with a distinct tidal feature to the west. *HST* images of this image reveal a complex morphology (Surace et al. 1998). A recent detailed kinematic study of this object by Arribas & Colina (2002) confirms the existence of a single nucleus in this system. The source to the north is a star based on its unresolved point spread function.

- *F15225+2350* (IVa): This merger remnant presents a prominent tidal tail to the south-west and a fainter one to the south-east.

- *F15327+2340 = Arp 220* (IIIb): This system is well known to harbor two near-infrared nuclei separated by $0''.9$ or 0.4 kpc (e.g., Scoville et al. 2000), but these two nuclei are not distinct at the resolution of our images.

- *F15462-0450** (IVb): The *IRAS* source presents tidal tails extending over 8 kpc. The compact source to the south is a spectroscopically confirmed star.

- *F16090-0139* (IVa): This single-nucleus object presents a diffuse tidal feature to the north-east.

- *F16156+0146** (IIIb): The two objects in this pair have emission-line spectra with similar redshifts ($z = 0.133$). The system presents a faint stubby tidal feature to the south and a very faint tail to the north-west. A tidal bridge may also be connecting the two objects in the pair. The compact source near the galaxy pair appears to be a star based on its unresolved point spread function, although underlying continuum emission from the north-west component makes this statement uncertain.

- *F16300+1558* (V): This is a compact object with distorted outer isophotes, but no obvious signs of tidal tails.

- *F16333+4630* (IIIa): This widely separated (13.1 kpc) binary appears to be linked by a tidal bridge. The object to the north-east of the pair is a star based on its unresolved point spread function.

- *F16468+5200* (IIIb): This moderately close (7.8 kpc) pair presents a tidal tail which seems to emerge from the western component and extends 14 kpc to the north.

- *F16474+3430* (IIIb): This object is similar to *F14252-1550* in that it is a moderately close (6.5 kpc) pair with a fairly large *nuclear* luminosity ratio of ~ 5.5 at K' (the components are too close to each other to determine reliably the global luminosity ratio). A prominent tidal tail is visible on the west side.

- *F16487+5447* (IIIb): This close (5.4 kpc) pair appears to be linked by a tidal bridge.

- *F17028+5817** (IIIa): The western component of this widely separated (23.3 kpc) pair presents diffuse tidal features and the isophotes of the eastern component are extended in the direction of the western companion. Both components have the same redshift within the uncertainties ($z = 0.106$ versus 0.107, respectively)

- *F17044+6720* (IVb): The brightest source in the field is a star. The *IRAS* source presents a peculiar tidal feature to the north-west of the nucleus.

- *F17068+4027* (Tpl): This source is tentatively classified as a triplet because of its resemblance with the other triplet candidate *F15001+1433*. The main source (labelled “E”) in the field has a single nucleus but is elongated along the east-west direction, i.e. in the same direction as the two fainter western (W and WW) galaxies. Note that the redshifts of these two galaxies are unknown and that no obvious signs of interaction are visible in these objects. If future observations do not confirm the interaction, the *IRAS* source should be re-classified as a IVa.

- *F17179+5444** (IVb): This single-nucleus source is surrounded by what seems to be tidal material extending asymmetrically to the south-west. The compact source to the south-west is a star based on its unresolved point spread function and its spectrum.

- *F20414-1651** (IVb): The isophotes of this single-nucleus object are highly elongated. The spectra of the two compact

and diffuse sources to the south of the main galaxy are not of sufficient quality to allow us determine the nature of these objects (a faint $H\alpha$ feature at the same redshift as the main galaxy may be present in the spectrum of the compact object, but this feature is very faint and may be due to contaminating emission from the main object). These southern sources may be galaxies in interaction with the main source but the evidence is not sufficiently convincing to classify this system as an interacting pair.

- *F21208-0519* (IIIa): This wide binary is separated by 14.1 kpc and shows distinct tidal features which extend out to 14 kpc.

- *F21219-1757* (V): The isophotes of this compact object are only slightly distorted.

- *F21329-2346* (IVa): This single-nucleus object presents a faint tidal feature to the south and a peculiar bootlegged feature to the north which is also presumably of tidal origin.

- *F21477+0502* (Tpl) This is arguably the best case for a triple system in the 1-Jy sample. A bridge of material appears to connect the western component to the eastern pair.

- *F22088-1831* (IIIb): The members of this pair are separated by 4.3 kpc. The compact source to the north-east is a star based on its unresolved point spread function.

- *F22206-2715* (IIIb): This moderately close (7.7 kpc) binary shows two prominent tidal features to the south-east and north-west. It is misclassified as a multiple (> 2) system by Cui et al. (2001).

- *F22491-1808* (IIIb): This close (2.2 kpc) pair shows two classic tidal tails to the east and north-west. It is misclassified as a multiple (> 2) system by Cui et al. (2001).

- *F22541+0833* (IIIa): This system is tentatively classified a widely separated (18.5 kpc) binary. The outer isophotes of the south-east galaxy are highly elongated in the direction of the north-west companion. Note, however, that the redshift of the south-east galaxy is unknown.

- *F23060+0505* (IVb): This single-nucleus system presents a diffuse tidal feature to the south-west.

- *F23129+2548* (IVa): The *IRAS* source lies north in this field and present tidal features to the south and west. The redshift of the galaxy to the south is unknown. This galaxy shows no sign of interaction with the *IRAS* object.

- *F23233+2817* (Isolated): This source shows a spiral-like pattern surrounding a very compact nucleus. No obvious tail is visible in this object. The point sources directly south and north-east of the nucleus are presumed to be bright H II regions based on their luminosities and colors. This is the only object in the 1-Jy sample with no obvious sign of interaction.

- *F23234+0946* (IIIb): This moderately close (7.4 kpc) pair shows a hook-like tidal feature to the south-east. The nature of the two faint point sources to the south-east and north-west of the pair are unknown. Neither one shows signs of interaction with the *IRAS* source.

- *F23327+2913* (IIIa): Each member of this wide (22.7 kpc) binary presents tidal features and appears to be linked to each other by a bridge of material.

- *F23389+0300* (IIIb): This close (4.9 kpc) binary presents a short tidal feature to the south.

- *F23498+2423* (IIIa): This wide (12.7 kpc) binary source presents prominent tidal tails at R . The compact source west of the binary is a star based on its unresolved point spread function.

REFERENCES

- Armus, L., Heckman, T. M., & Miley, G. K. 1990, *ApJ*, 364, 471
- Arribas, S., & Colina, L. 2002, *ApJ*, 10 July issue, 000
- Bahcall, J. N., Kirhakos, S., Saxe, D. H., & Schneider, D. P. 1997, *ApJ*, 479, 642
- Bahcall, J. N., et al. 1995, *ApJ*, 452, L91
- Barnes, J. E., Hernquist, L. 1992, *ARA&A*, 30, 705
- Barger, A. J., Cowie, L. L., & Sanders, D. B. 1999, *ApJ*, 518, L5
- Bender, R., Burstein, D., & Faber, S. M. 1992, *ApJ*, 399, 462
- Bender, R., Surma, P., Döbereiner, S., Möllenhoff, C., & Madejsky, R. 1989, *A&A*, 217, 35
- Binney, J., & Merrifield, M. 1998, *Galactic Astronomy*, Princeton Series in Astrophysics
- Blain, A. W., Kneib, J.-P., Ivison, R. J., & Smail, I. 1999, *ApJ*, 512, L87
- Blain, A. W., Smail, I., Ivison, R. J., Kneib, J.-P., & Frayer, D. T. 2002, preprint (astro-ph/0202228)
- Borne, K. D., Bushouse, H., Lucas, R. A., & Colina, L. 2000, *ApJ*, 529, L77
- Bruzual, G. A., & Charlot, S. 1993, *ApJ*, 405, 538
- Bryant, P. M., & Scoville, N. Z. 1999, *AJ*, 117, 2632
- Bushouse, H. A., et al. 2002, *ApJS*, 138, 1
- Busko, I. 1996, *Proceedings of the Fifth Astronomical Data Analysis Software and Systems Conference*, Tucson, PASP Conference Series vol. 101, ed. G.H. Jacoby and J. Barnes, p. 139
- Canalizo, G., & Stockton, A. 2000, *AJ*, 120, 1750
- Canalizo, G., & Stockton, A. 2001, *ApJ*, 555, 719
- Carico, D. P., et al. 1990, *ApJ*, 349, L39
- Clements, D. L., Sutherland, W. J., McMahon, R. G., & Saunders, W. 1996, *MNRAS*, 279, 477
- Colina, L., et al. 2001, *ApJ*, 563, 546
- Cui, J., Xia, X.-Y., deng, Z.-G., Mao, S., & Zou, Z.-L. 2001, *AJ*, 122, 63
- De Vaucouleurs, A., & Longo, G. 1988, *Catalog of optical and infrared photometry of galaxies from 0.5 micrometer to 10 micrometer (1965 – 1985)* (Austin: Univ. of Texas)
- Dinh-V-Trung, Lo, K. Y., Kim, D.-C., Gao, Y., & Gruendl, R. A. 2001, *ApJ*, 556, 141
- Disney, M. J., et al. 1995, *Nature*, 376, 150
- Downes, D., & Solomon, P. M. 1998, *apj*, 507, 615
- Doyon, R., Wells, M., Wright, G. S., Joseph, R. D., Nadeau, D., & James, P. A. 1992, *ApJ*, 437, L23
- Dunlop, J. S., et al. 2002, *MNRAS*, in press (astro-ph/0108397)
- Eales, S. A., Becklin, E. E., Hodapp, K. W., Simons, D. A., & Wynn-Williams, C. G. 1990, *ApJ*, 365, 478
- Eales, S., Lilly, S., Gear, W., Dunne, L., Bond, J. R., Hammer, F., Le Fèvre, O., & Crampton, D. 1999, *ApJ*, 515, 518
- Efstathiou, A., et al. 2000, *MNRAS*, 319, 1169
- Elston, R., Rieke, G. H., & Rieke, M. J. 1988, *ApJ*, 331, L77
- Evans, A. S., Frayer, D. T., Surace, J. A., Sanders, D. B. 2001, *AJ*, 121, 1893
- Evans, A. S., Kim, D. C., Mazzarella, J. M., Scoville, N. Z., & Sanders, D. B. 1999, *ApJ*, 521, L107
- Faber, S. M., et al. 1997, *AJ*, 114, 1771
- Farrar, D., et al. 2001, *MNRAS*, 326, 1333
- Gallagher, S. C., Charlton, J. C., Hunsberger, S. D., Zaritsky, D., & Whitmore, B. C. 2001, *AJ*, 122, 163
- Genzel, R., & Cesarsky, C. J. 2000, *ARA&A*, 38, 761
- Genzel, R., et al. 1998, *ApJ*, 498, 579
- Genzel, R., Tacconi, L. J., Rigopoulou, D., Lutz, D., & Tecza, M. 2001, *ApJ*, 563, 527
- Gerritsen, J. 1997, Ph. D. Thesis, Kapteyn Astronomical University, Groningen
- Goldader, J. D., Joseph, R. D., Doyon, R., & Sanders, D. B. 1995, *ApJ*, 444, 97
- Graham, J. R., et al. 1990, *ApJ*, 354, L5
- Hibbard, J. E., & van Gorkom, J. H. 1996, *AJ*, 111, 655
- Hughes, D. H., et al. 1998, *Nature*, 394, 241
- Hutchings, J. B., & Neff S. G. 1992, *AJ*, 104, 1
- Hutchings, J. B., Holtzmann, J., Sparks, W. B., Morris, S. C., Hanisch, R. J., & Mo, J. 1994, *ApJ*, 429, L1
- Ishida, C. M. 2002, Ph. D. Thesis, University of Hawaii
- Jedrzejewski, R. 1987, *MNRAS*, 226, 747.
- Kawara, K., et al. 1998, *A&A*, 336, L9
- Kim, D.-C. 1995, Ph.D. Thesis, University of Hawaii
- Kim, D.-C., & Sanders, D. B. 1998, *ApJS*, 119, 41
- Kim, D.-C., Veilleux, S., & Sanders, D. B. 1998, *ApJ*, 508, 627
- Kim, D.-C., Veilleux, S., & Sanders, D. B. 2002, *ApJS*, in press (Paper I)
- Kormendy, J., & Bender, R. 1996, *ApJ*, 464, L119
- Kormendy, J., & Sanders, D. B. 1992, *ApJ*, 390, L53
- Lawrence, A., Rowan-Robinson, M., Leech, K., Jones, D. H. P., & Wall, J. V. 1989, *MNRAS*, 240, 329
- Leech, K. J., Rowan-Robinson, M., Lawrence, A., & Hughes, J. D. 1994, *MNRAS*, 267, 253
- Lipari, S., Colina, L., & Macchetto, D. 1994, *ApJ*, 427, 174
- Lutz, D., et al. 1998, *ApJ*, 505, L103
- Lutz, D., Veilleux, S., & Genzel, R. 1999, *ApJ*, 517, L13
- Majewski, S. R., Hereld, M., Koo, D. C., Illingworth, G. D., & Heckman, T. M. 1993, *ApJ*, 402, 125
- Márquez, I., et al. 2001, *A&A*, 371, 97
- Matsuhara, H., et al. 2000, *A&A*, 361, 407
- McLeod, K. K., & McLeod, B. A. 2001, *ApJ*, 546, 782
- McLeod, K. K., & Rieke, G. H. 1994a, *ApJ*, 420, 58
- McLeod, K. K., & Rieke, G. H. 1994b, *ApJ*, 431, 137
- McLeod, K. K., Rieke, G. H., & Storrie-Lombardi, L. J. 1999, *ApJ*, 511, L67
- McLure, R. J., et al. 1999, *MNRAS*, 308, 377
- Melnick, J., & Mirabel, I. F. 1990, *A&A*, 231, L19
- Mihos, J. C., & Hernquist, L. 1996, *ApJ*, 464, 641
- Mihos, J. C., Dubinski, J., & Hernquist, L. 1998, *ApJ*, 494, 183
- Moshir, M., et al. 1992, *Explanatory Supplement to the IRAS Faint Source Survey*, Version 2, JPL D-10015 8/92 (Pasadena: JPL) (FSC)
- Murphy, T. W., Jr., et al. 1996, *AJ*, 111, 1025
- Murphy, T. W., Jr., Soifer, B. T., Matthews, K., & Armus, L. 2001a, *ApJ*, 559, 201
- Murphy, T. W., Jr., Soifer, B. T., Matthews, K., Armus, L., & Kiger, J. R. 2001b, *AJ*, 121, 97
- Naab, T., & Burkert, A. 2001, in *ASP Conf. Ser. 230, Galaxy Disks and Disk Galaxies*, ed. J. G. Funes & E. M. Corsini (San Francisco: ASP), 451
- Pahre, M. A., de Carvalho, R. R., & Djorgovski, S. G. 1998, *AJ*, 116, 1606
- Percival, W. J., Miller, L., McLure, R. J., & Dunlop, J. S. 2001, *MNRAS*, 322, 843
- Puget, J. L., et al. 1999, *A&A*, 345, 29
- Regan, M. W., Vogel, S. N., & Teuben, P. J. 1995, *ApJ*, 449, 576
- Rigopoulou, D., et al. 1999, *AJ*, 118, 262
- Ryden, B. 1992, *ApJ*, 396, 445
- Sanders, D. B., & Mirabel, I. F. 1996, *ARA&A*, 34, 725
- Sanders, D. B., Soifer, B. T., Elias, J. H., Madore, B. F., Matthews, K., Neugebauer, G., & Scoville, N. Z. 1988a, *ApJ*, 325, 74
- Sanders, D. B., Soifer, B. T., Elias, J. H., Neugebauer, G., & Matthews, K. 1988b, *ApJ*, 328, L35
- Schweizer, F. 1982, *ApJ*, 252, 455
- Scoville, N. Z., et al. 2000, *AJ*, 119, 991
- Serjeant, S., et al. 2001, *MNRAS*, 322, 262
- Smail, I., Ivison, R. J., & Blain, A. W. 1997, *ApJ*, 490, L5
- Soifer, B. T., et al. 2000, *AJ*, 119, 509
- Soifer, B. T., et al. 2001, *AJ*, 122, 1213
- Stanford, S. A., & Bushouse, H. A. 1991, *ApJ*, 371, 92
- Stockton, A. 1999, *Galaxy Interactions at Low and High Redshift*, *Proceedings of IAU Symposium # 186*, held at Kyoto, Japan, 26-30 August, 1997. Edited by J. E. Barnes, and D. B. Sanders, 311
- Surace, J. A. 1998, Ph. D. Thesis, University of Hawaii
- Surace, J. A., & Sanders, D. B. 1999, *ApJ*, 512, 162
- Surace, J. A., & Sanders, D. B. 2000, *ApJ*, 120, 604
- Surace, J. A., Sanders, D. B., & Evans, A. S. 2000, *ApJ*, 529, 170
- Surace, J. A., Sanders, D. B., & Evans, A. S. 2001, *AJ*, 122, 2791
- Surace, J. A., Sanders, D. B., Vacca, D. B., Veilleux, S., & Mazzarella, J. M. 1998, *ApJ*, 492, 116
- Taylor, G. L., Dunlop, J. S., Hughes, D. H., & Robson, E. I. 1996, *MNRAS*, 283, 930
- Toomre, A. 1977, In *The Evolution of Galaxies and Stellar Populations*, eds. B. M. Tinsley, R. B. Larson, New Haven, CT: Yale Univ. Obs., 401
- Toomre, A., & Toomre, J. 1972, *ApJ*, 178, 623
- Tran, Q. D., et al. 2001, *ApJ*, 552, 527
- Tyson, J. A., Baum, W. A., & Kreidl, T. 1982, *ApJ*, 257, L1
- Veilleux, S. 2001, *proceedings from a conference on "QSO Hosts and their Environments"* held in Granada, Spain in January 2001, 165
- Veilleux, S., Kim, D.-C., & Sanders, D. B. 1999a, *ApJ*, 522, 113
- Veilleux, S., Kim, D.-C., Sanders, D. B., Mazzarella, J. M., & Soifer, B. T. 1995, *ApJS*, 98, 171
- Veilleux, S., Sanders, D. B., & Kim, D.-C. 1997, *ApJ*, 484, 92
- Veilleux, S., Sanders, D. B., & Kim, D.-C. 1999b, *ApJ*, 522, 139
- Walker, I. R., Mihos, J. C., & Hernquist, L. 1996, *ApJ*, 460, 121
- Whitmore, B. C., et al. 1999, *AJ*, 118, 1551
- Wright, G. S., James, P. A., Joseph, R. D., McLean, I. S. 1990, *Nature*, 344, 417
- Zhang, Q., Fall, S. M., & Whitmore, B. C. 2001, *ApJ*, 561, 727
- Zheng, Z., et al. 1999, *A&A*, 349, 735
- Zou, Z., Xia, X., Deng, Z., & Su, H. 1991, *MNRAS*, 252, 593

FIG. 1.— Color – magnitude diagrams of the 1-Jy sample. (a) Integrated R -band absolute magnitudes versus $R-K'$. (b) Integrated K' absolute magnitudes versus $R-K'$. (c) Nuclear (4-kpc diameter) R -band absolute magnitudes versus nuclear $R-K'$. (d) Nuclear (4-kpc diameter) K' absolute magnitudes versus nuclear $R-K'$. Nuclear quantities are measured within a diameter of 4 kpc.

FIG. 2.— Trends between the integrated R (left) and K' (right) absolute magnitudes and (a) – (b) the *IRAS* 25 $\mu\text{m}/60 \mu\text{m}$ colors; (c) – (d) the optical spectral types; (e) – (f) the *ISO* spectral types; (g) – (h) the infrared luminosities.

FIG. 3.— Trends between the integrated (left) and nuclear (4-kpc; right) $R-K'$ colors and (a) – (b) the optical spectral types; (c) – (d) the *IRAS* 25 $\mu\text{m}/60 \mu\text{m}$ colors. No trends are observed with the infrared luminosities, *IRAS* 60 $\mu\text{m}/100 \mu\text{m}$ colors and the strengths of the $H\beta$ and Mg Ib stellar features (not shown here).

FIG. 4.— Trends between the R (left) and K' (right) compactness values and (a) – (b) the optical spectral types; (c) – (d) the *IRAS* 25 $\mu\text{m}/60 \mu\text{m}$ colors; (e) – (f) the equivalent widths of the stellar Mg Ib feature.

FIG. 5.— Apparent nuclear separations in the 1-Jy sample of galaxies. The distribution is highly peaked at small values but also presents a significant tail at high values. The very uncertain separation measured in F11223–1244 (87.9 kpc) is not shown in this figure.

FIG. 6.— Trends between the apparent nuclear separations and (a) the optical spectral types; (b) the *IRAS* 25 $\mu\text{m}/60 \mu\text{m}$ colors. No trends are observed with the nuclear values of the equivalent widths of the $H\beta$ and Mg Ib stellar absorption features, two traditional indicators of the starburst age (not shown here).

FIG. 7.— Apparent nuclear separations as a function of infrared luminosities. The great majority of the extreme ULIGs with $\log [L_{\text{IR}}/L_{\odot}] > 10^{12.5} L_{\odot}$ are single-nucleus systems and therefore have $NS < 2.5$ kpc.

FIG. 8.— Total projected tail lengths as a function of (a) the optical spectral types; (b) the infrared luminosities; (c) the *IRAS* 25 $\mu\text{m}/60 \mu\text{m}$ colors; (d) the *IRAS* 60 $\mu\text{m}/100 \mu\text{m}$ colors; (e) the equivalent widths of the $H\beta$ stellar feature; (f) the equivalent widths of the Mg Ib stellar feature. No obvious correlations are observed with any of these parameters.

FIG. 9.— Interaction classes for the objects in the 1-Jy sample. See text in §3.4 for a description of each class. The five triplets in the sample are plotted separately on the left. The merger of two galaxies is expected to follow the sequence I \rightarrow V. Contrary to systems of lower infrared luminosities which often comprise two distinct galaxies (classes I, II and III), most (56%) of the objects in 1-Jy sample are single-nucleus systems and are therefore in the later stage of a merger (IV or V).

FIG. 10.— Positive trends between the interaction class and (a) the infrared luminosity, (b) the optical spectral type, and (c) the *IRAS* 25 $\mu\text{m}/60 \mu\text{m}$ color. No trends are observed with the *IRAS* 60 $\mu\text{m}/100 \mu\text{m}$ colors and the strengths of the $H\beta$ and Mg Ib stellar features (not shown here).

FIG. 11.— Observed surface brightness profiles of (left) R -band images and (right) K' images. These profiles have not been corrected for cosmological dimming. The profile of each image is plotted on two different radial scales: a linear scale and a $R^{1/4}$ scale. Solid lines in each of the panels are least-square exponential or de Vaucouleurs fits to the data. To avoid seeing effects, only the data outside of twice the radius of the seeing disk are considered in the fits. Arrows indicate the size of the seeing disk. The value of the reduced chi-square is indicated on the upper right hand corner of each panel. Values much larger than unity indicate poor fits, while values much less than unity indicate fits which are poorly constrained.

FIG. 12.— Fraction of (a) single-nucleus and (b) double-nucleus 1-Jy ULIGs with disk-like (D), elliptical-like (E), elliptical/disk-like (E/D) and ambiguous (A) radial profiles. E/D profiles are equally well fitted by an exponential or de Vaucouleurs function, while neither fits galaxies with “ambiguous” profiles. As expected, the fraction of ambiguous profiles is considerably larger among binary systems.

FIG. 13.— Trends between host galaxy profiles and (a) optical spectral types, (b) *ISO* spectral types, (c) *IRAS* 25 $\mu\text{m}/60 \mu\text{m}$ colors, and (d) interaction classes. Elliptical-like systems show a tendency to host warm AGN and to lie in advanced mergers. The nature of the host does not seem to depend strongly on the infrared luminosity, the 60 $\mu\text{m}/100 \mu\text{m}$ ratio, or the strengths of the stellar $H\beta$ and Mg Ib features (not shown here).

FIG. 14.— Absolute R (left) and K' (right) magnitudes of the host galaxies for individual objects in (a) – (b) double-nucleus systems and (c) – (d) single-nucleus systems. For comparison, the absolute magnitudes at R and K' of a L^* galaxy are -21.2 and -24.1 , respectively.

FIG. 15.— Trends between the R -band absolute magnitude of the host galaxies and (a) the infrared luminosities; (b) the *IRAS* 25 $\mu\text{m}/60 \mu\text{m}$ colors; (c) the optical spectral types. Luminous host galaxies show a tendency to host IR-luminous and warm AGNs. The tendency with infrared luminosity is due to distance-dependent effects.

FIG. 16.— Distribution of the host magnitude differences at (left) R and (right) K' among the binary systems (class III) of the 1-Jy sample. Notice the difference in the magnitude scale between the two figures. The magnitude difference is slightly larger at K' than at R , although most systems have a magnitude difference in both bands of less than 1.5 or, equivalently, a luminosity ratio of less than 4.

FIG. 17.— The nuclear (4-kpc diameter) $R-K'$ colors plotted against the colors of the host galaxies. HII galaxies, LINERs, Seyfert 2s and Seyfert 1s are represented as stars, open circles, filled circles, and filled squares, respectively. No significant correlation is observed between these two quantities, especially when considering only the objects with $(R-K')_{\text{host}} < 4$.

FIG. 18.— Seeing-deconvolved half-light radii, r_e , of the elliptical-like host galaxies in the 1-Jy sample measured at (a) R and (b) K' . The mean r_e of ULIGs at R (4.80 ± 1.37 kpc) is significantly smaller than the mean values measured by Dunlop et al. (2002) for the hosts of radio-quiet quasars (7.63 ± 1.11) and radio-loud quasars (7.82 ± 0.71 kpc), although there is some overlap. In contrast, the mean r_e of ULIGs at K' (3.48 ± 1.39 kpc) is nearly identical to that of the quasars measured in the H -band by McLeod & McLeod (2001; 3.39 ± 1.90). The origin of the discrepancy between the two quasar datasets is not known.

FIG. 19.— Surface brightnesses, μ_e , as a function of the half-light radii, r_e , measured at (a) R and (b) K' for the elliptical-like host galaxies in the 1-Jy sample. The surface brightnesses have been corrected for cosmological dimming and the half-light radii for seeing effects. The hosts of these ULIGs appear to be smaller and slightly brighter at R than the hosts of the radio-loud and radio-quiet quasars from the sample of Dunlop et al. (2002), but still follow with some scatter the $\mu_e - r_e$ relation of normal (inactive) ellipticals [represented by the dotted line in panel (a); Hamabe & Kormendy (1987) assuming $V-R = 0.5$ mag]. At K' , the interpretation is more difficult because data exist for a fewer number of ULIGs and no quasars. The dash line represents the fit of Hamabe & Kormendy (1987) assuming $V-K' = 3.7$ mag, while the dotted line is the best fit to the K -band data of Pahre (1999) for normal ellipticals. The hosts of Seyfert 1 ULIGs are noticeably brighter (especially at K') than normal galaxies; this may be due to positive residuals from the PSF subtraction. The solid line in Fig. 19b is the best fit through the ULIG data, excluding the Seyfert 1 galaxies.

FIG. 20.— Radial profiles of the axial ratio in the hosts of single-nucleus ULIGs. The arrow in each panel indicates $r = 3 \times r_e$.

FIG. 21.— Axial ratios measured at $3 \times r_e$ in single-nucleus ULIGs. The median and mean of this distribution are 0.77 and 0.75 ± 0.15 (1σ), respectively. These numbers are similar to those measured in normal ellipticals and in quasar hosts.

FIG. 22.— Radial profiles of the normalized R -band boxiness parameter, A_4/a , in the host galaxies of single-nucleus ULIGs. Note the large variations of A_4/a with radius in many of these objects. The arrows in each panel indicate $r = 2 \times r_e$ and $3 \times r_e$.

FIG. 23.— R -band boxiness values normalized to the semi-major axis at (a) $2 \times r_e$ and (b) $3 \times r_e$ for ULIGs with elliptical-like host galaxies. Both distributions are broader than that of normal ellipticals and peak near zero.

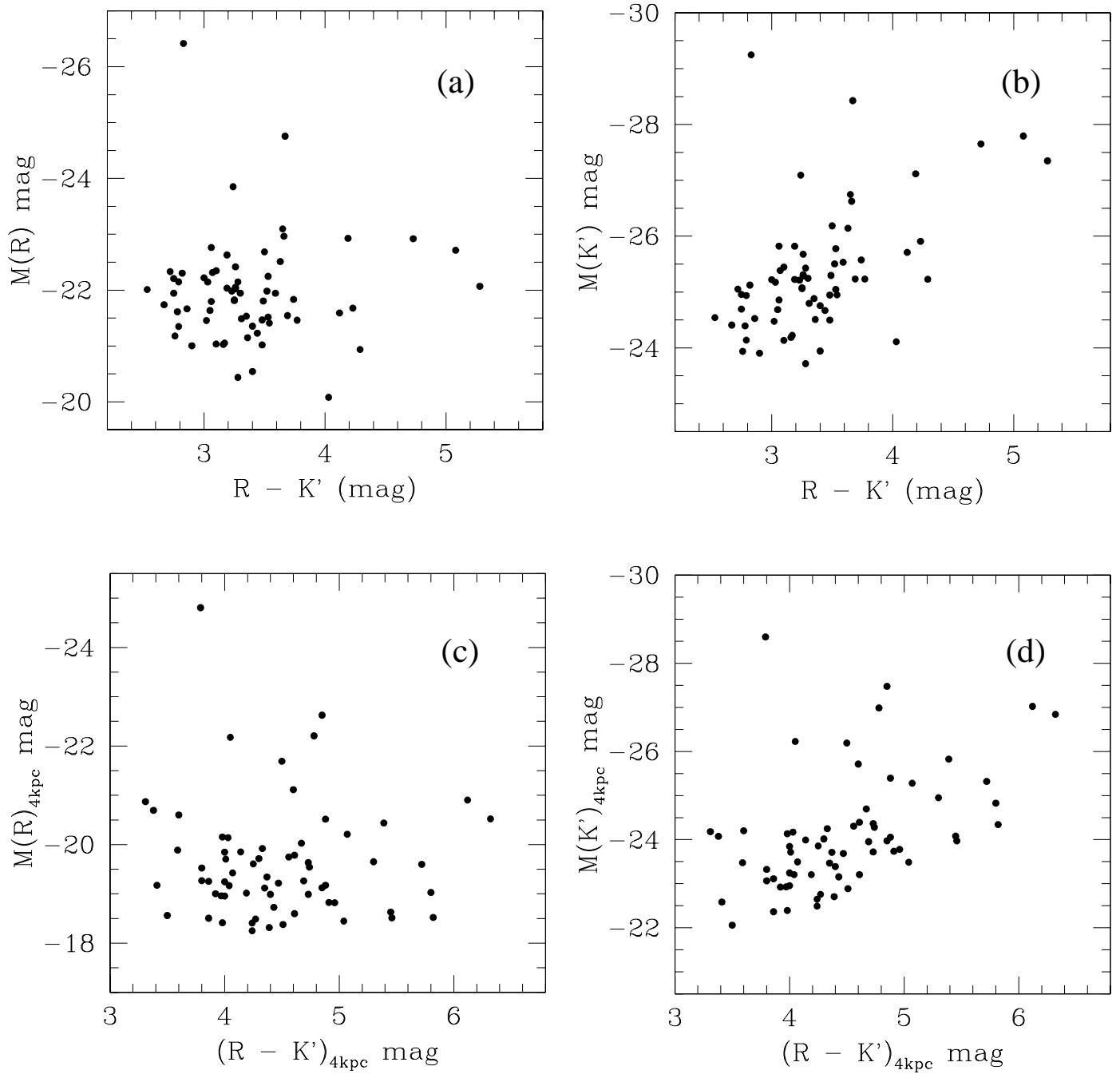


FIG. 1.—

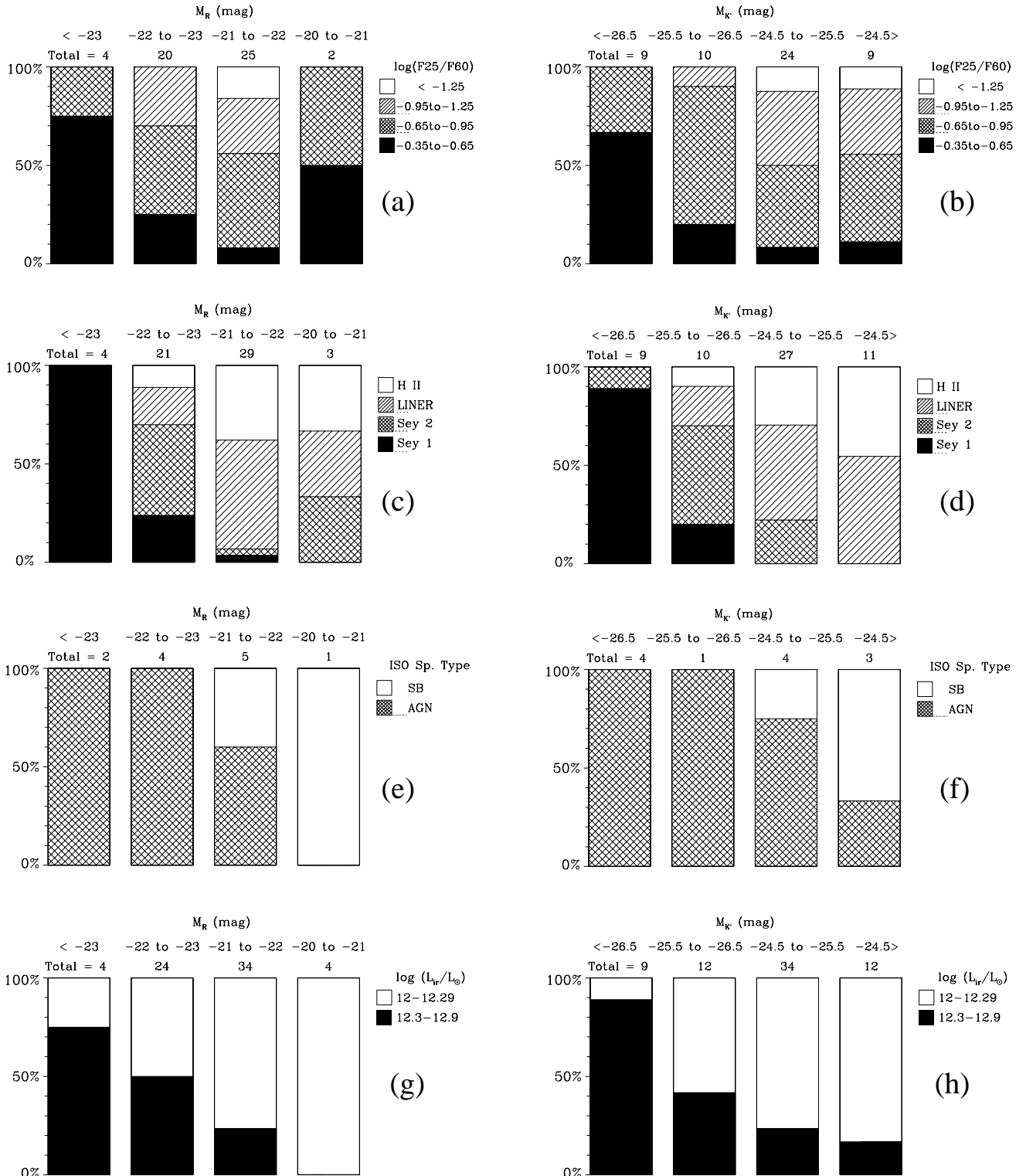


FIG. 2.—

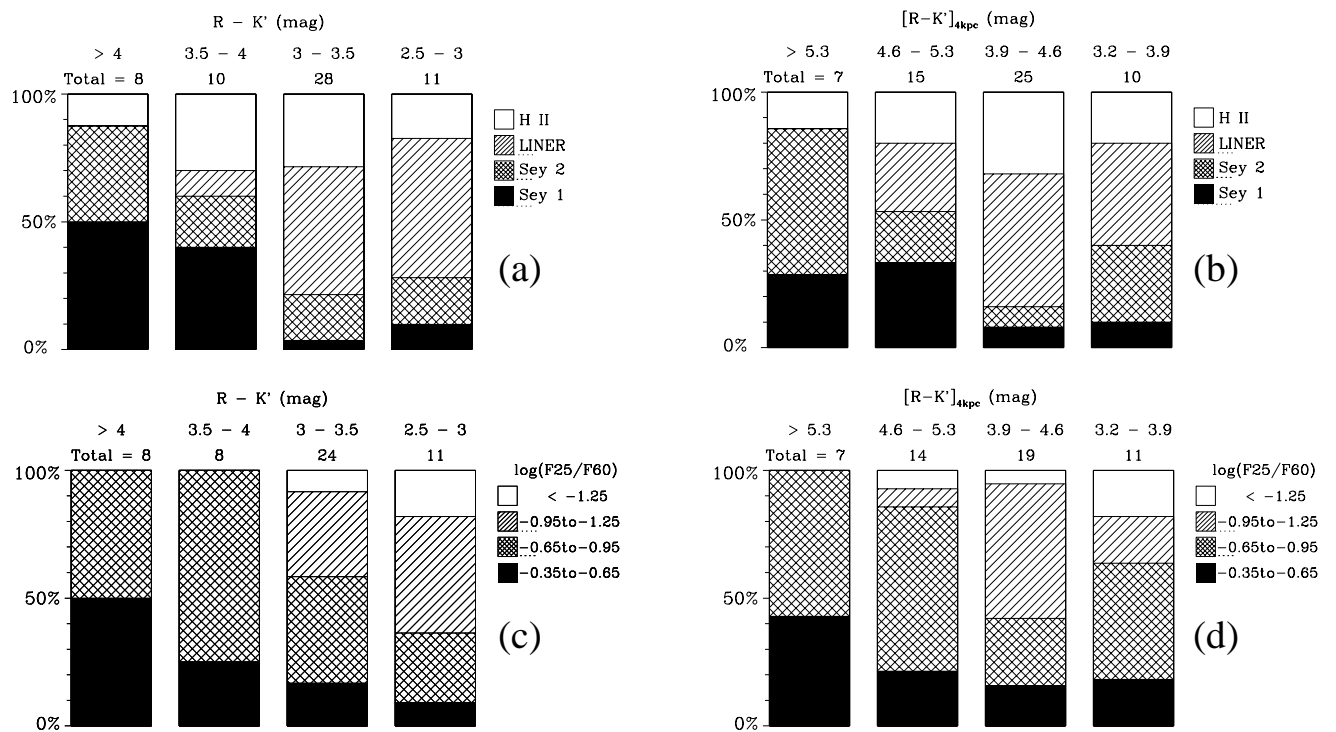


FIG. 3.—

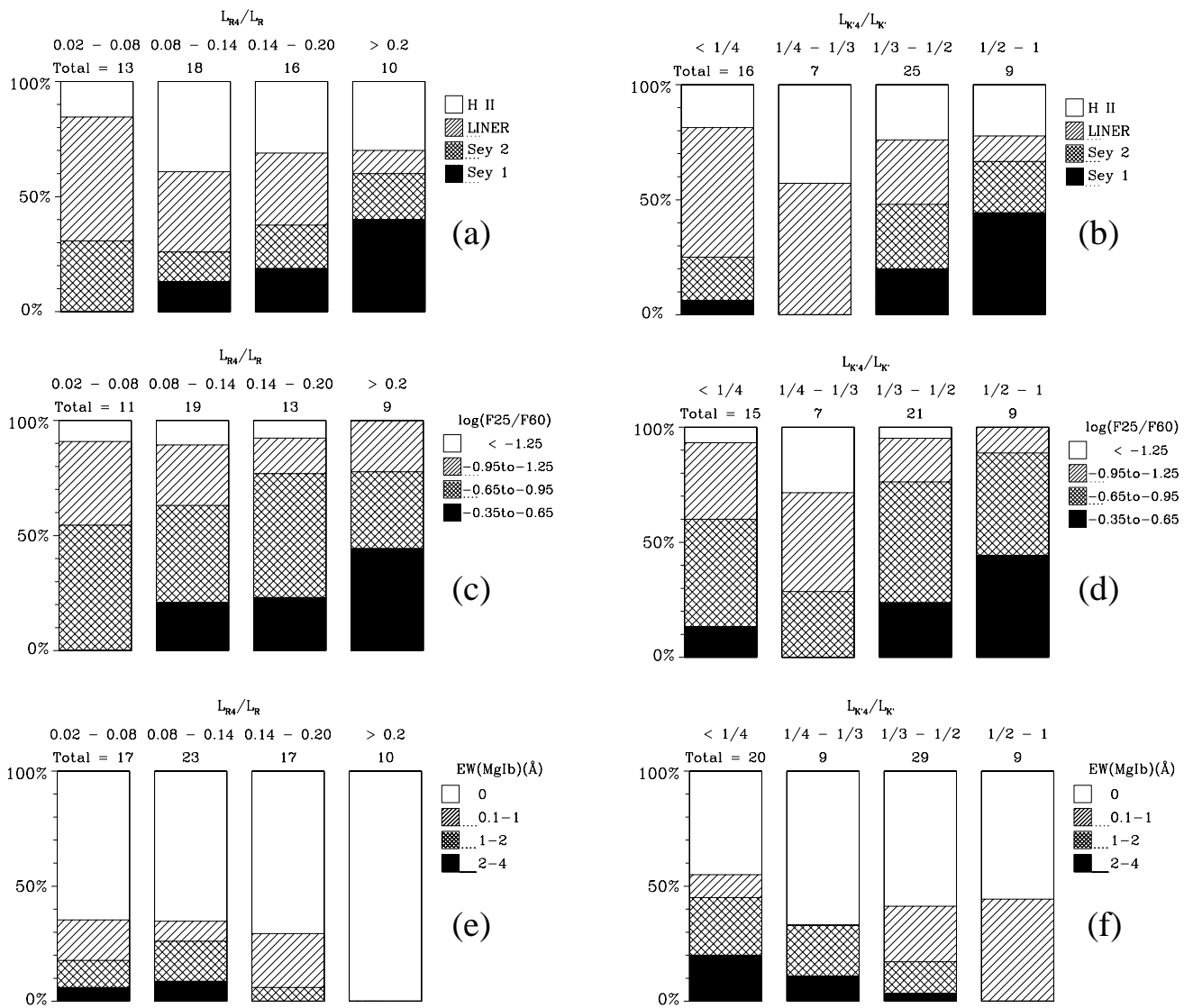


FIG. 4.—

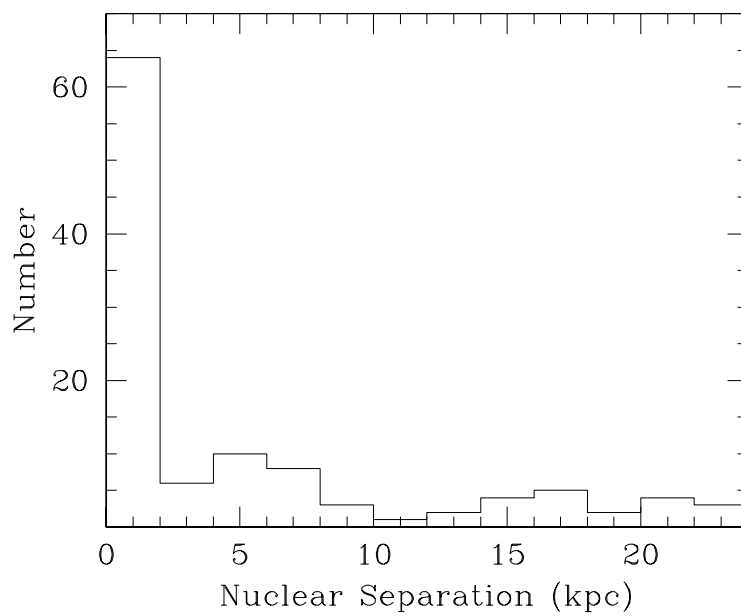


FIG. 5.—

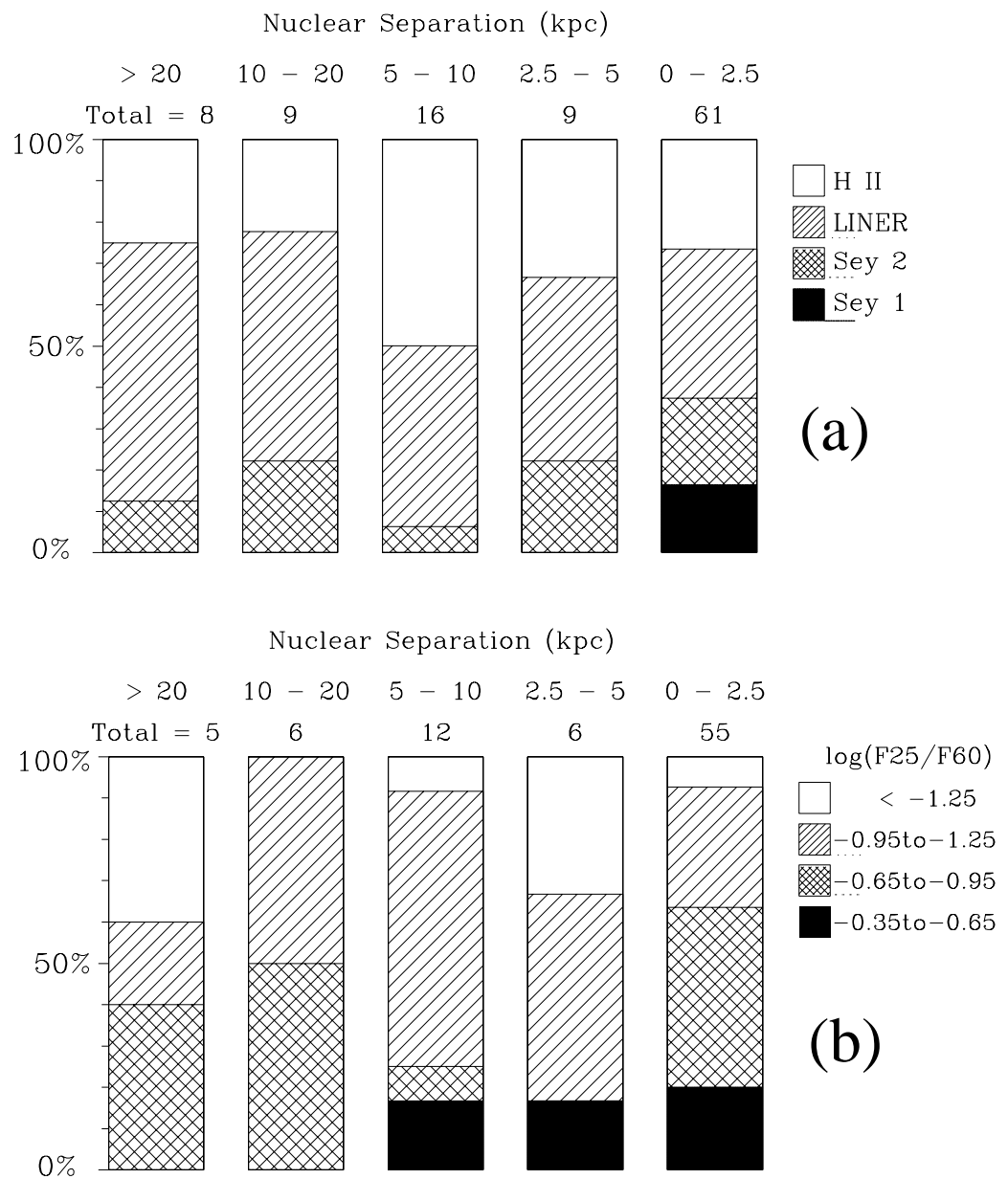


FIG. 6.—

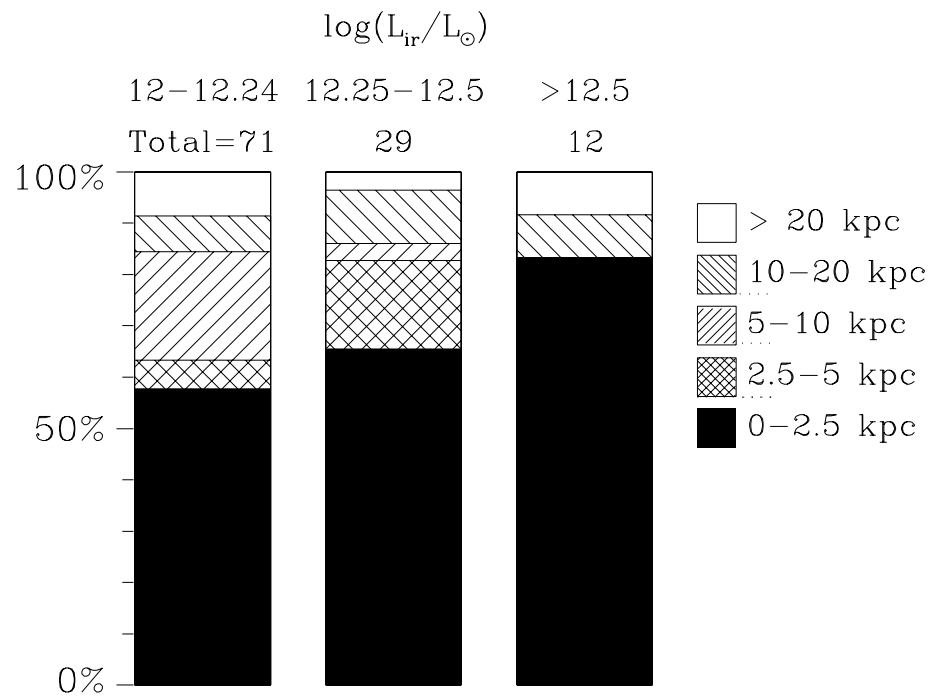


FIG. 7.—

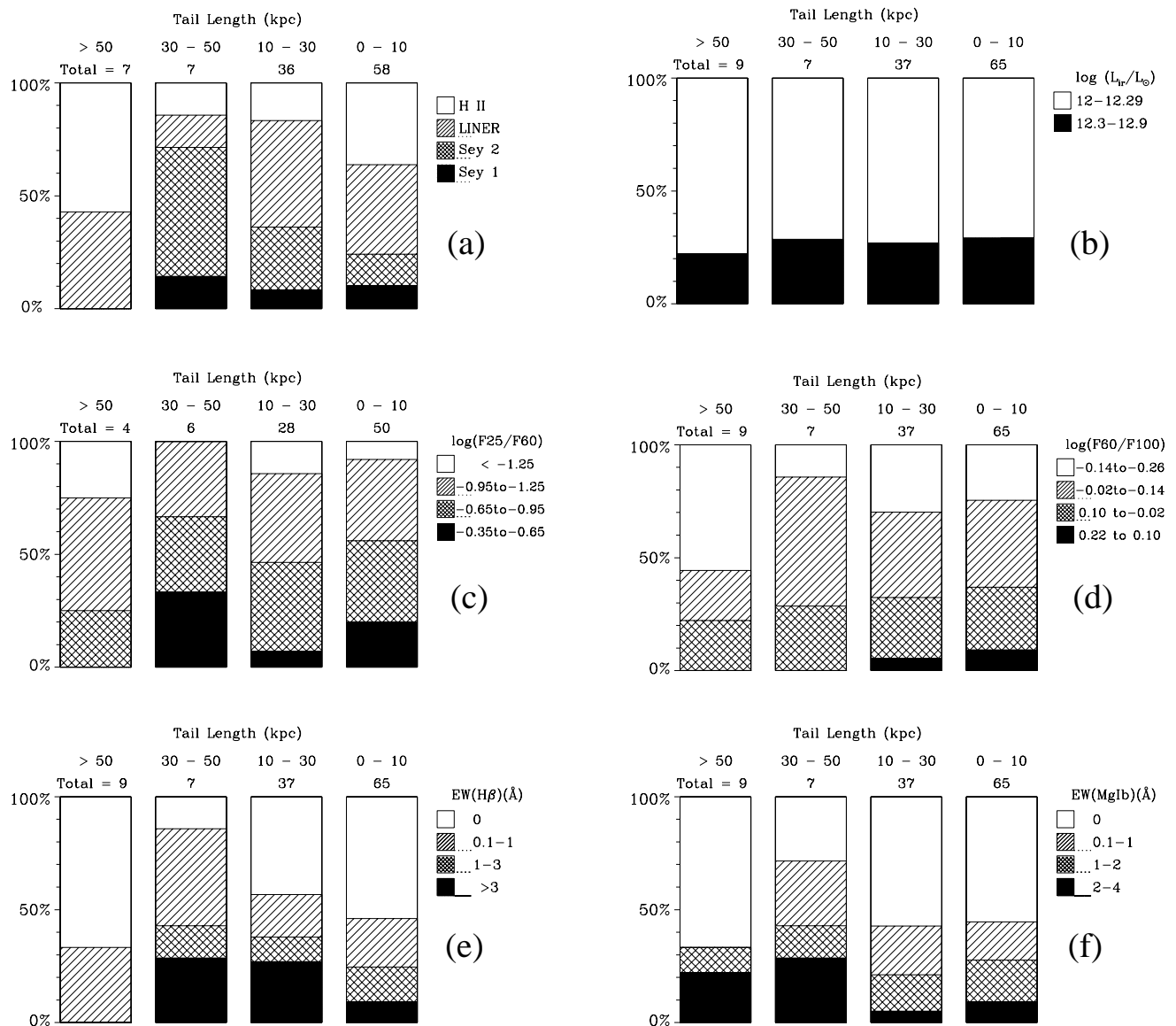


FIG. 8.—

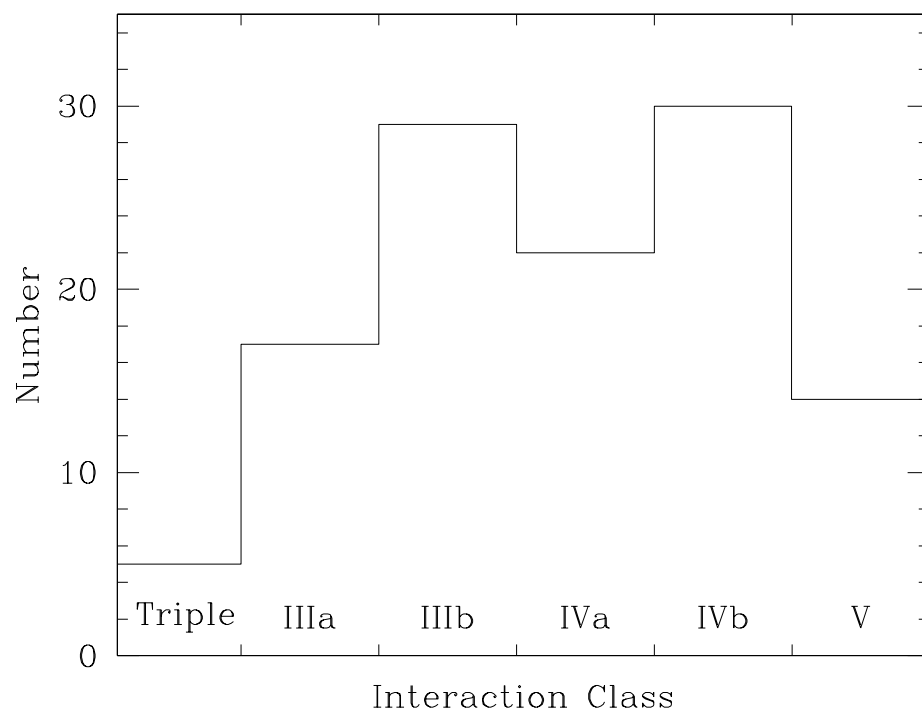


FIG. 9.—

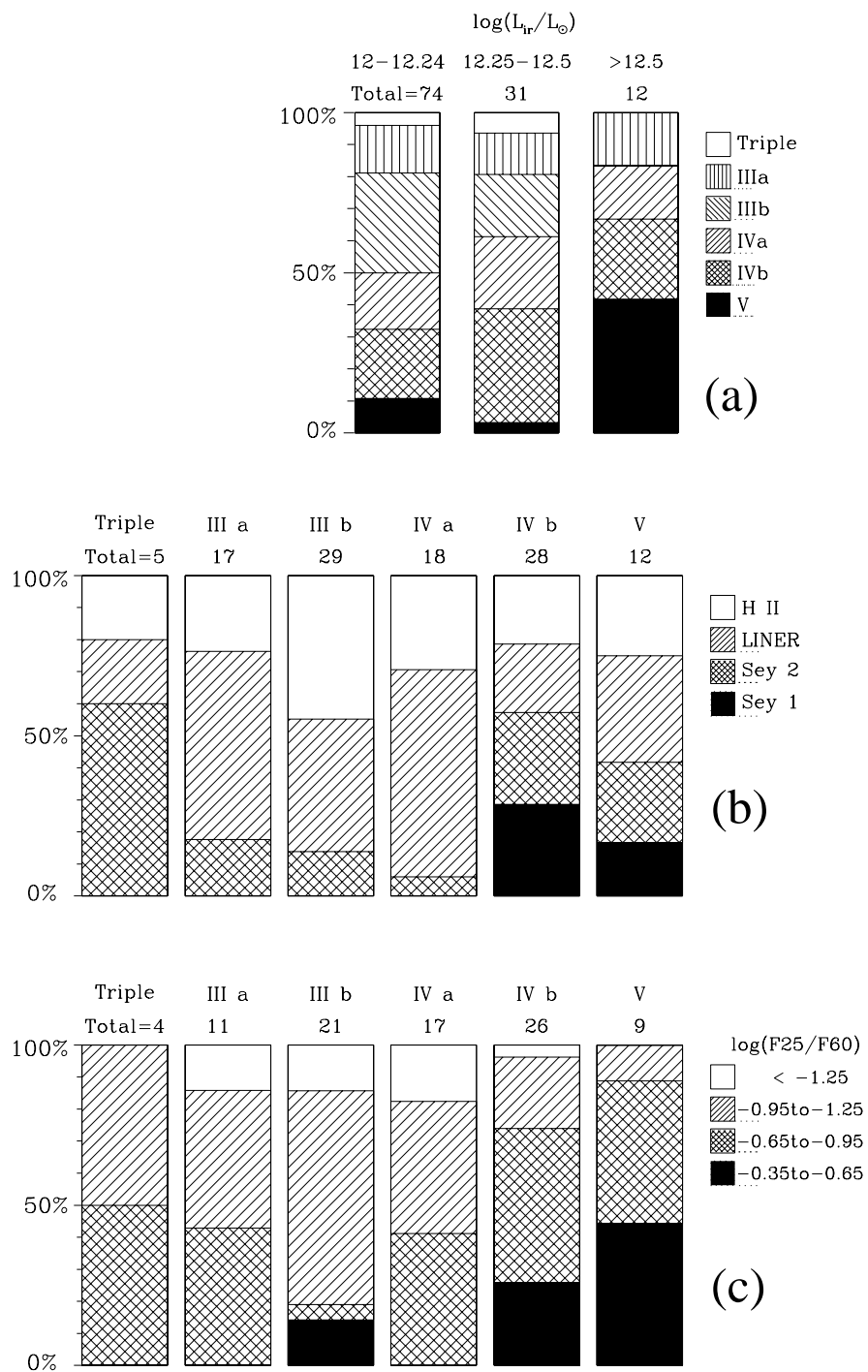


FIG. 10.—

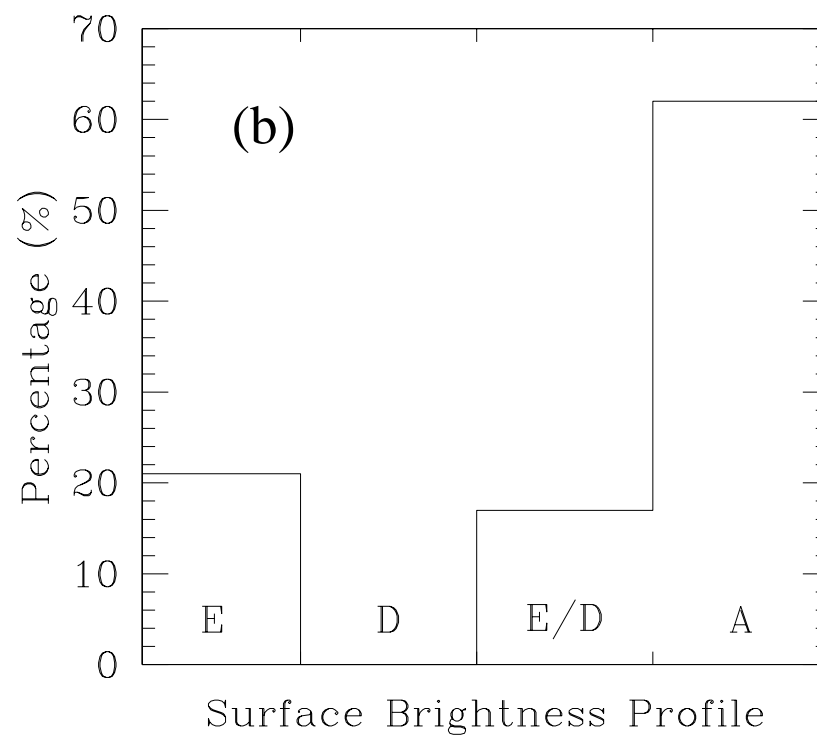
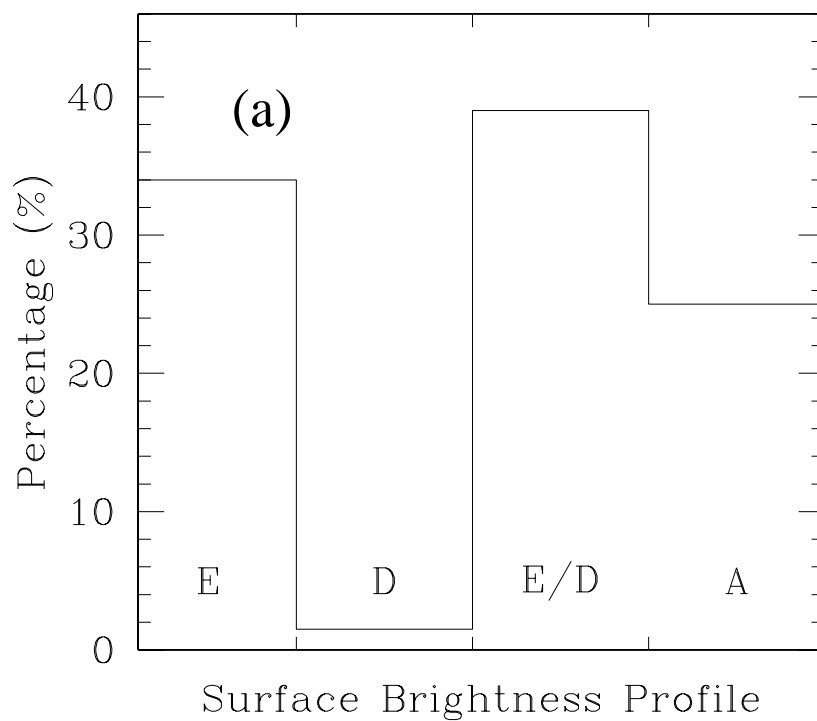


FIG. 12.—

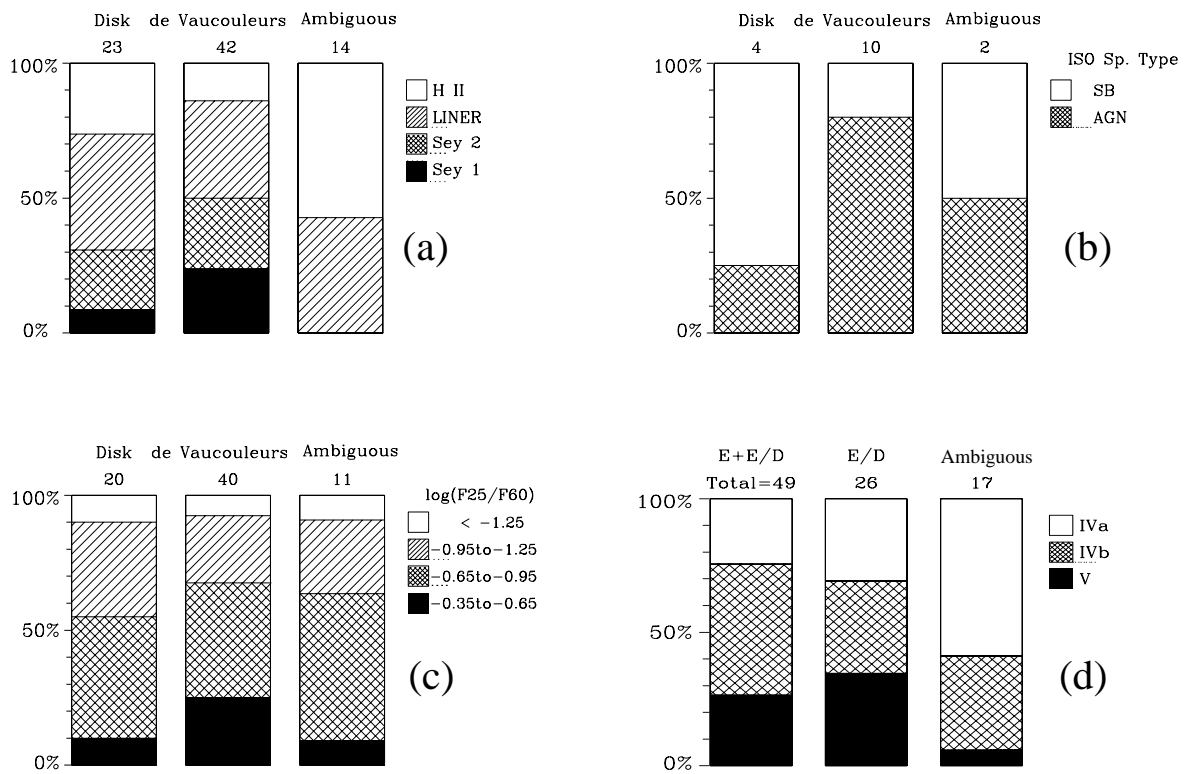


FIG. 13.—

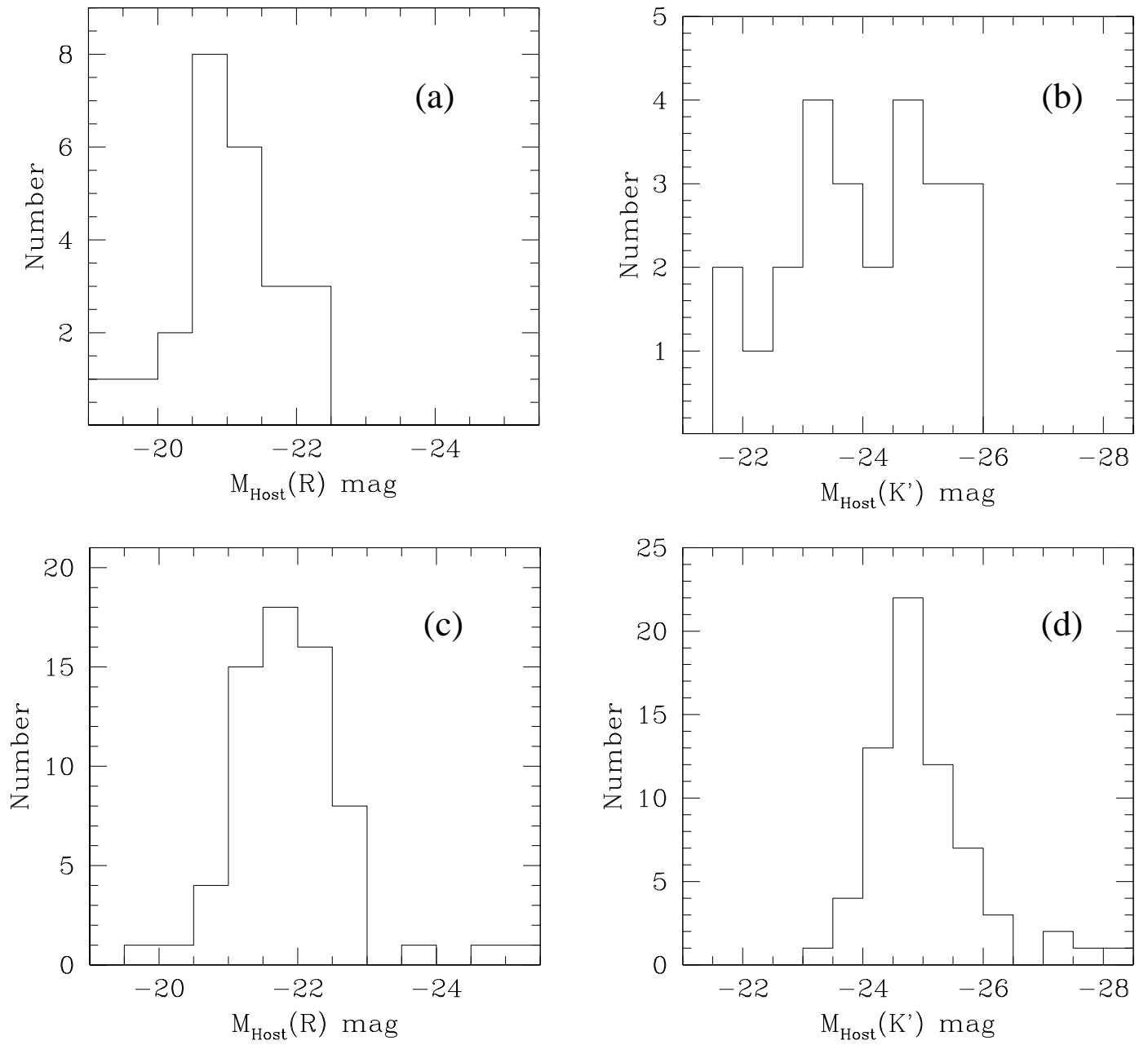


FIG. 14.—

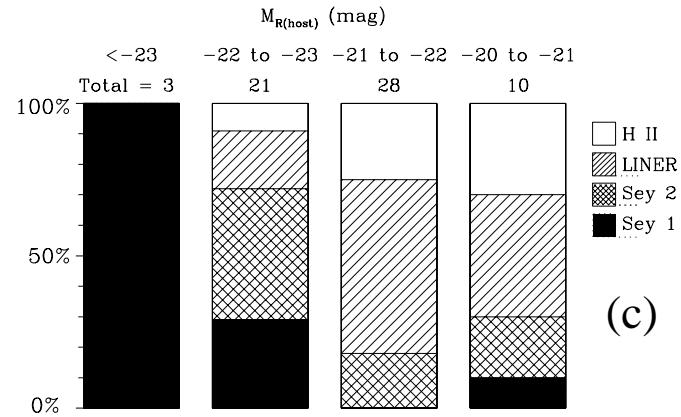
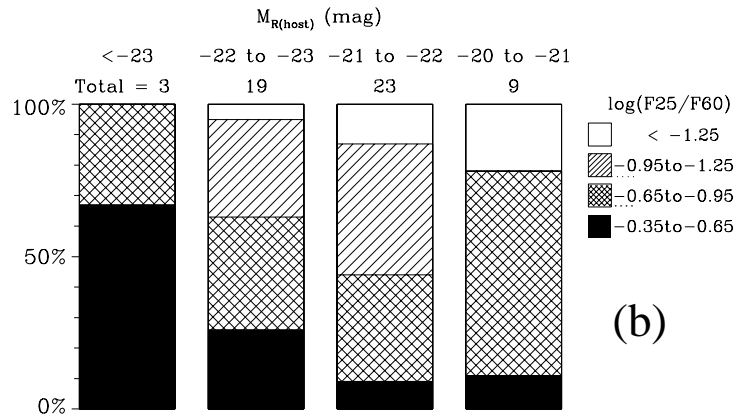
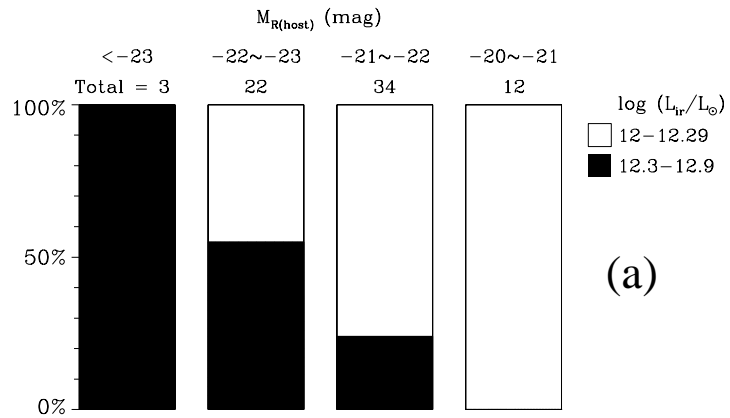


FIG. 15.—

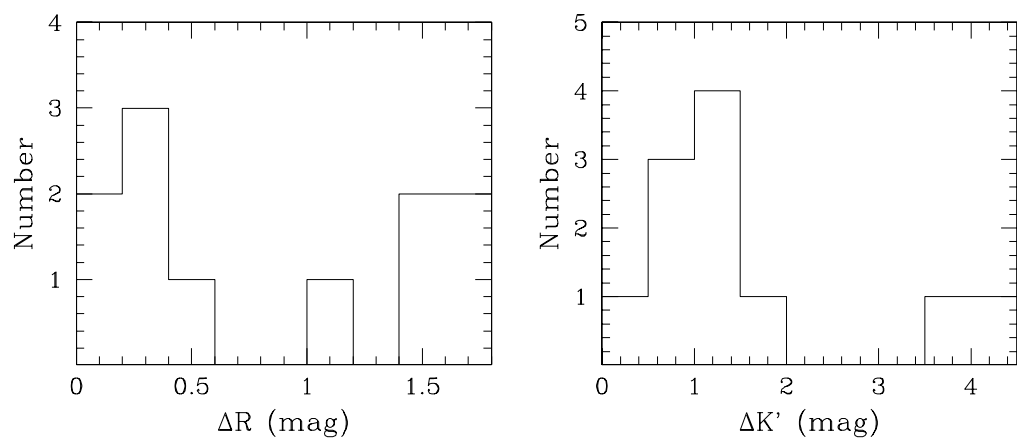


FIG. 16.—

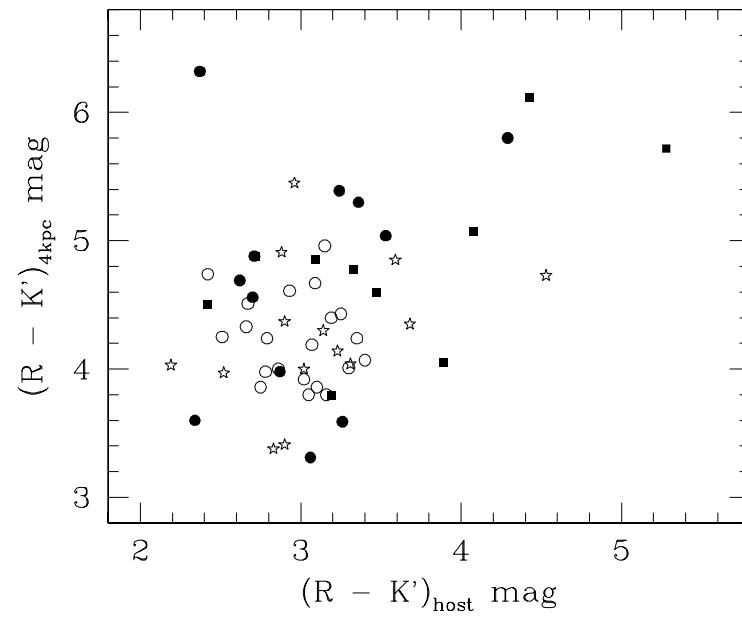


FIG. 17.—

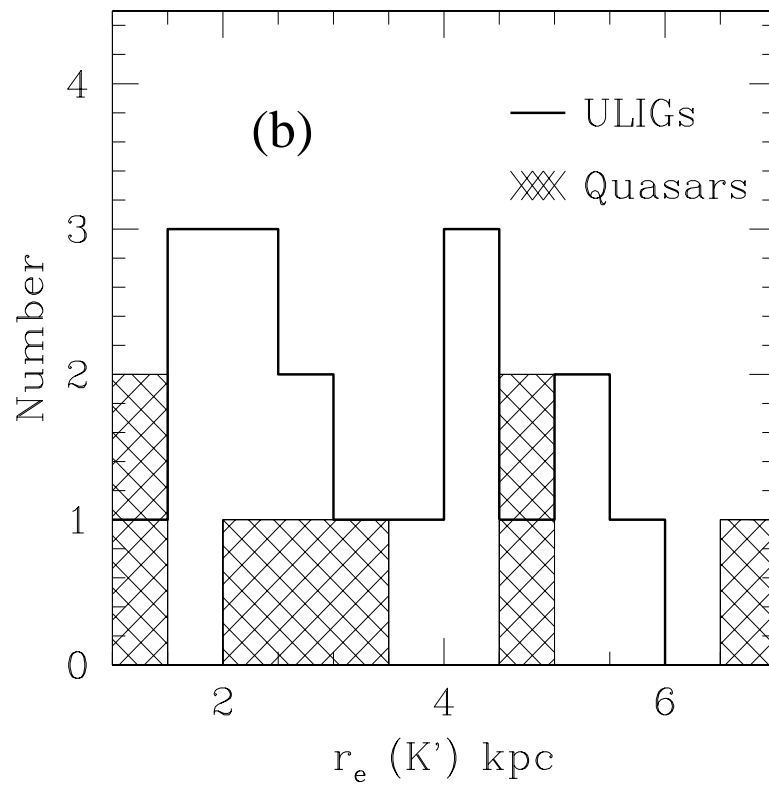
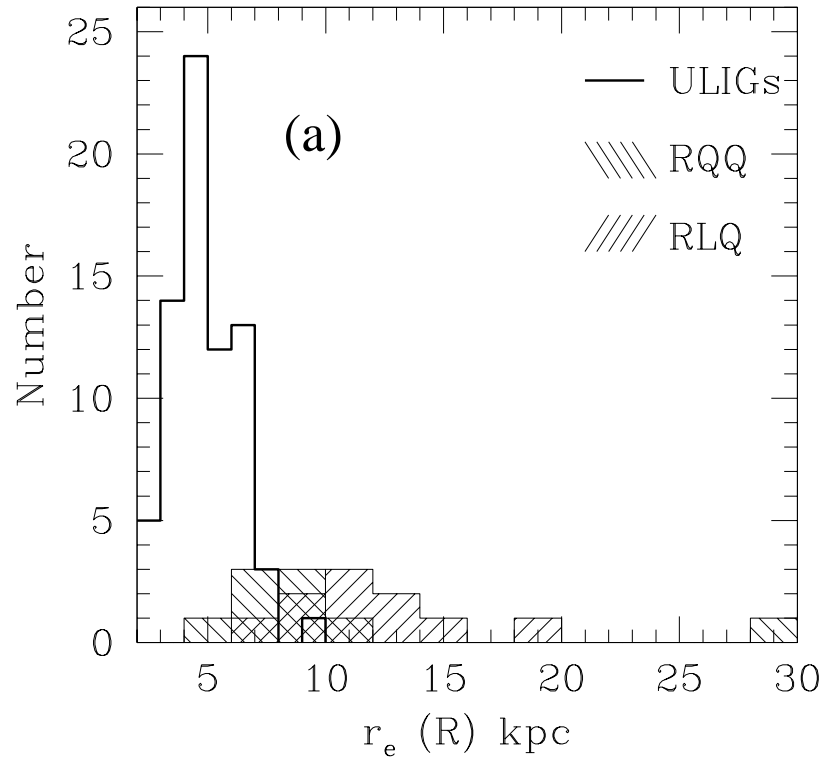


FIG. 18.—

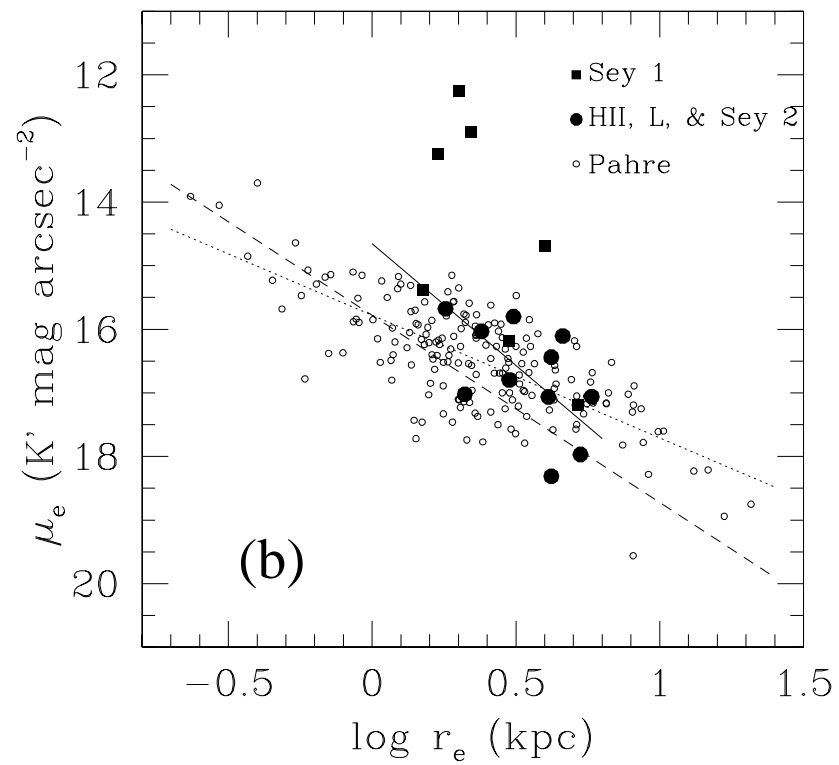
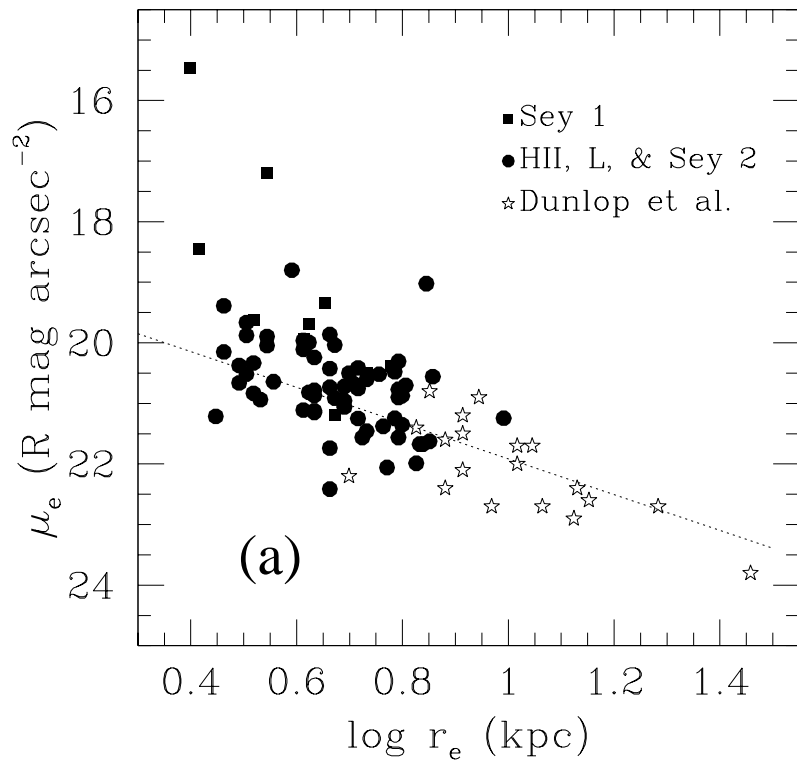


FIG. 19.—

FIG. 20.—

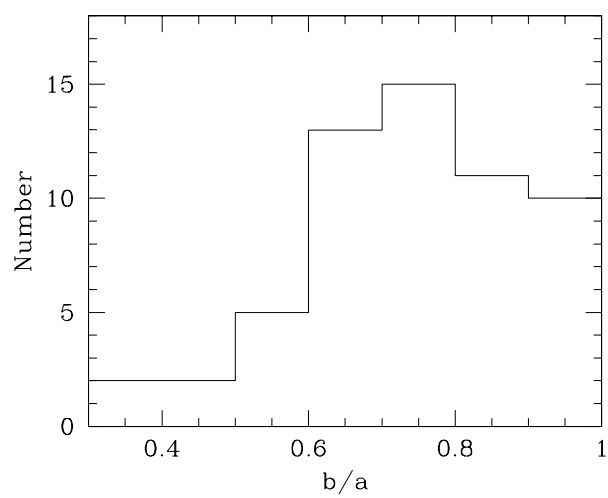


FIG. 21.—

FIG. 22.—

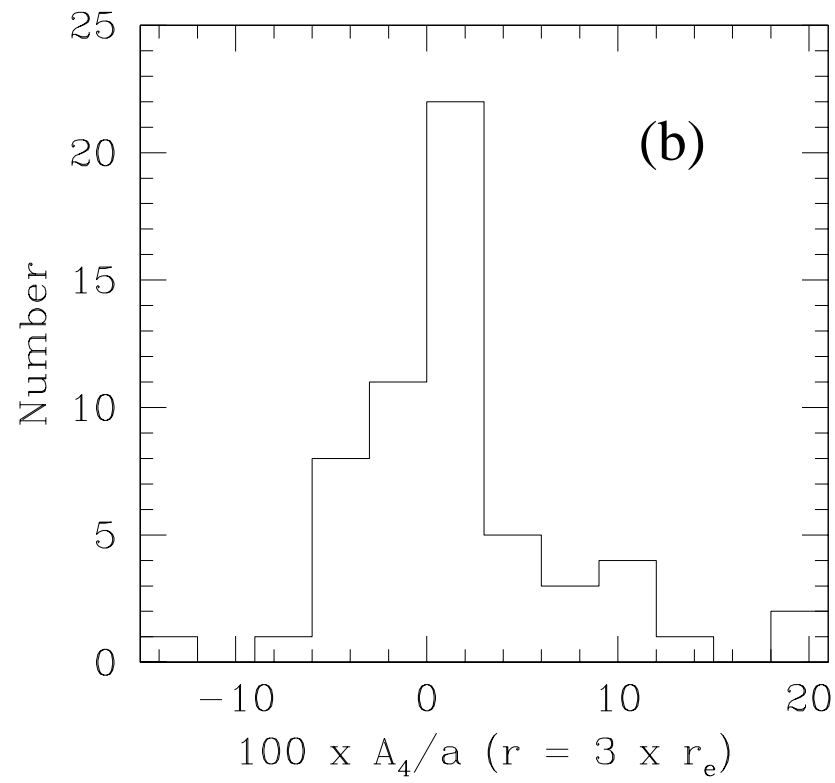
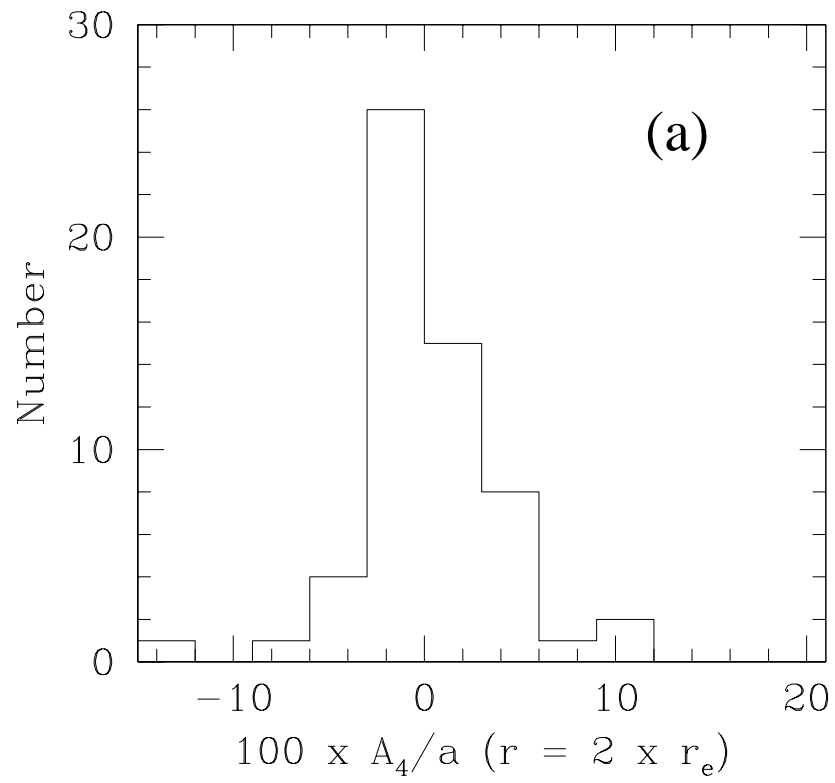


FIG. 23.—

This figure "fig11_3.jpg" is available in "jpg" format from:

<http://arxiv.org/ps/astro-ph/0207401v4>

This figure "fig20_3.jpg" is available in "jpg" format from:

<http://arxiv.org/ps/astro-ph/0207401v4>

This figure "fig22_3.jpg" is available in "jpg" format from:

<http://arxiv.org/ps/astro-ph/0207401v4>

TABLE 3
HOST GALAXY MAGNITUDES

Category (1)	$M_R(\text{host})$		$M_{K'}(\text{host})$		Redshift	
	Median (2)	Mean $\pm 1 \sigma$ (3)	Median (4)	Mean $\pm 1 \sigma$ (5)	Median (6)	Mean $\pm 1 \sigma$ (7)
All Doubles	-20.99	-21.02 \pm 0.76	-24.00	-23.98 \pm 1.25	0.135	0.136 \pm 0.038
All Singles	-21.77	-21.77 \pm 0.92	-24.81	-25.03 \pm 0.94	0.148	0.149 \pm 0.046
Singles, $L_{\text{IR}} > 10^{12.3} L_{\odot}$	-22.30	-22.47 \pm 0.99	-25.41	-25.68 \pm 1.12	0.179	0.183 \pm 0.053
Singles, $L_{\text{IR}} \leq 10^{12.3} L_{\odot}$	-21.53	-21.58 \pm 0.62	-24.67	-24.68 \pm 0.62	0.136	0.132 \pm 0.029
Singles, Seyfert 1s	-22.70	-22.99 \pm 1.29	-26.35	-25.58 \pm 1.08	0.155	0.145 \pm 0.048
Singles, Seyfert 2s	-22.33	-22.21 \pm 0.56	-25.23	-25.25 \pm 0.47	0.148	0.142 \pm 0.065
Singles, Seyfert 1s & 2s	-22.42	-22.58 \pm 1.03	-25.78	-25.89 \pm 1.05	0.149	0.143 \pm 0.056
Singles, Non-Seyferts	-21.61	-21.55 \pm 0.57	-24.66	-24.59 \pm 0.50	0.136	0.150 \pm 0.041
Singles, Warm: $f_{25}/f_{60} > 0.2$	-22.24	-22.36 \pm 1.28	-25.41	-25.68 \pm 1.21	0.148	0.139 \pm 0.042
Singles, Cool: $f_{25}/f_{60} \leq 0.2$	-21.74	-21.69 \pm 0.52	-24.68	-24.72 \pm 0.58	0.148	0.155 \pm 0.047

This figure "fig11_4.jpg" is available in "jpg" format from:

<http://arxiv.org/ps/astro-ph/0207401v4>

This figure "fig20_4.jpg" is available in "jpg" format from:

<http://arxiv.org/ps/astro-ph/0207401v4>

This figure "fig22_4.jpg" is available in "jpg" format from:

<http://arxiv.org/ps/astro-ph/0207401v4>

This figure "fig11_5.jpg" is available in "jpg" format from:

<http://arxiv.org/ps/astro-ph/0207401v4>

This figure "fig20_5.jpg" is available in "jpg" format from:

<http://arxiv.org/ps/astro-ph/0207401v4>

This figure "fig22_5.jpg" is available in "jpg" format from:

<http://arxiv.org/ps/astro-ph/0207401v4>

This figure "fig11_6.jpg" is available in "jpg" format from:

<http://arxiv.org/ps/astro-ph/0207401v4>

This figure "fig11_7.jpg" is available in "jpg" format from:

<http://arxiv.org/ps/astro-ph/0207401v4>

This figure "fig11_8.jpg" is available in "jpg" format from:

<http://arxiv.org/ps/astro-ph/0207401v4>

This figure "fig11_9.jpg" is available in "jpg" format from:

<http://arxiv.org/ps/astro-ph/0207401v4>

This figure "fig11_10.jpg" is available in "jpg" format from:

<http://arxiv.org/ps/astro-ph/0207401v4>

This figure "fig11_11.jpg" is available in "jpg" format from:

<http://arxiv.org/ps/astro-ph/0207401v4>

This figure "fig11_12.jpg" is available in "jpg" format from:

<http://arxiv.org/ps/astro-ph/0207401v4>

This figure "fig11_13.jpg" is available in "jpg" format from:

<http://arxiv.org/ps/astro-ph/0207401v4>

This figure "fig11_14.jpg" is available in "jpg" format from:

<http://arxiv.org/ps/astro-ph/0207401v4>

This figure "fig11_15.jpg" is available in "jpg" format from:

<http://arxiv.org/ps/astro-ph/0207401v4>

This figure "fig11_16.jpg" is available in "jpg" format from:

<http://arxiv.org/ps/astro-ph/0207401v4>

This figure "fig11_17.jpg" is available in "jpg" format from:

<http://arxiv.org/ps/astro-ph/0207401v4>

This figure "fig11_18.jpg" is available in "jpg" format from:

<http://arxiv.org/ps/astro-ph/0207401v4>

This figure "fig11_19.jpg" is available in "jpg" format from:

<http://arxiv.org/ps/astro-ph/0207401v4>

This figure "fig11_20.jpg" is available in "jpg" format from:

<http://arxiv.org/ps/astro-ph/0207401v4>

This figure "fig11_21.jpg" is available in "jpg" format from:

<http://arxiv.org/ps/astro-ph/0207401v4>

This figure "fig11_22.jpg" is available in "jpg" format from:

<http://arxiv.org/ps/astro-ph/0207401v4>

This figure "fig11_23.jpg" is available in "jpg" format from:

<http://arxiv.org/ps/astro-ph/0207401v4>

This figure "fig11_24.jpg" is available in "jpg" format from:

<http://arxiv.org/ps/astro-ph/0207401v4>

This figure "fig11_25.jpg" is available in "jpg" format from:

<http://arxiv.org/ps/astro-ph/0207401v4>

This figure "fig11_26.jpg" is available in "jpg" format from:

<http://arxiv.org/ps/astro-ph/0207401v4>